TRAUMATIC BRAIN INJURY MECHANISMS IN THE GÖTTINGEN MINIPIG IN RESPONSE TO TWO UNIQUE INPUT MODES

ELIZABETH MARY FIEVISOHN

Dissertation submitted to the faculty of the
Virginia Polytechnic Institute and State University
in partial fulfillment of the requirements for the degree of

Doctor of Philosophy
in
Biomedical Engineering

Warren N. Hardy, Chair
Pamela J. VandeVord
Stefan M. Duma
Matthew P. Galloway
Thomas A. Gennarelli

October 1st, 2015
Blacksburg, Virginia

Keywords: Traumatic Brain Injury, Göttingen minipig, Immunohistochemistry, Proton Magnetic Resonance Spectroscopy, Impact

TRAUMATIC BRAIN INJURY MECHANISMS IN THE GÖTTINGEN MINIPIG IN RESPONSE TO TWO UNIQUE INPUT MODES

Elizabeth Mary Fievisohn

ABSTRACT

Traumatic brain injury (TBI) continues to be a widespread problem in the United States with approximately 1.7 million occurrences annually[1]. Current automotive crash test standards use the Head Injury Criterion (HIC)[2] to assess head injury potential, but this metric does not relate an impact to underlying damage. For an injury metric to effectively predict TBI, it is crucial to relate level of impact to resulting injury. The research presented in this dissertation explains the development and repeatability of two novel injury devices, impact response characterization over the course of 24 hours in the Göttingen minipig and the relationships between metabolite changes, underlying disruption, and impact kinematics, and the characterization of impact response over the course of 72 hours. The translation-input and combined translation and rotation-input injury devices were shown to be repeatable, minimizing the number of animals needed for testing. Impact response over the course of 24 hours showed axonal disruption through immunostaining and proton magnetic resonance spectroscopy. The translation-input injury group metabolite analyses revealed the initial stages of glutamate excitotoxicity while the combined-input injury group showed a clear pathway for glutamate excitotoxicity. Numerous correlative relationships and potential underlying disruption predictors were found between metabolites, immunostaining, and kinematics. The most promising predictor combination for the translation-input injury device was N-acetylaspartylglutamate/Scyllo at 24 hours compared to 1 hour and linear speed for predicting underlying light neurofilament disruption. For the combined-input injury device, the strongest predictor combination was Glutamine/N-acetylaspartylglutamate at 24 hours compared to baseline and angular acceleration for predicting underlying light neurofilament disruption. Statistically significant predictors were found between Glutamate+Glutamine/Total Creatine at 24 hours compared to baseline and all kinematics and injury metrics with an angular component for predicting heavy neurofilament disruption. Analyses over the course of 72 hours revealed persistent axonal disruption and metabolite perturbations. Overall, this dissertation and the complementary parts of this project have many societal implications. Due to the high incidence of traumatic brain injury, there is a need for prevention, mitigation, and treatment strategies. Developing a new injury metric will help improve prevention strategies, especially in the automotive, sporting, and military environments.

[1] Faul, M., Xu, L., Wald, M. M., & Coronado, V. G. (2010). Traumatic Brain Injury in the United States. *Atlanta, GA: Centers for Disease Control and Prevention, National Center for Injury Prevention and Control*.

[2] Versace, J. (1971). A Review of the Severity Index. *SAE Technical Paper*. No. 710881

ACKNOWLEDGMENTS

There are many people that I would like to thank for their help and support over the years. First, I would like to thank my advisor, Warren Hardy, for entrusting me with this project and the countless opportunities to present my work. Your expertise and guidance has made me a better and more independent researcher.

I would like to acknowledge the advice and input of my committee members: Pamela VandeVord, Matthew Galloway, Stefan Duma, and Thomas Gennarelli. My research has benefited substantially from this unique and prestigious committee.

This research was supported in part by the National Highway Traffic Safety Administration. I would also like to thank the Wake Forest IACUC and ARP for their help. John Olson, Heather Sawyer, and Stephanie Rideout Danner, I could not have asked for a better team to work with and cannot thank you enough for your help during these experiments.

Special thanks to Alli Daniello, Ada Tsoi, Lianne Sandberg, and Stephanie Kusano for maintaining my sanity. I would like to thank my friends and colleagues in the Center for Injury Biomechanics and at Stony Brook University for their encouragement and support.

This work could not have been accomplished without the love and encouragement from my family. Finally, Josh, I can't even begin to thank you for being a constant source of love and positivity since high school. I could not have done this without you.

TABLE OF CONTENTS

LIST OF FIGURES

LIST OF TABLES

LIST OF ABBREVIATIONS

AIS	Abbreviated Injury Scale
ANOVA	analysis of variance
Asp	aspartate
ATD	anthropomorphic test device
β-APP	β-amyloid precursor protein
BrIC	brain injury criterion
CFC	channel frequency class
Cr	creatine
Cre	total creatine (creatine plus phosphocreatine)
CRLB	Cramér-Rao Lower Bound
CSDM	cumulative strain damage measure
CT	Computed Tomography
DAPI	4', 6-diamidino-2-phenylindole
DTI	diffusion tensor imaging
FITC	fluorescein isothiocyanate
fMRI	functional magnetic resonance imaging
FMVSS	federal motor vehicle safety standard
FP	fluid percussion
GABA	γ-aminobutyric acid
GCS	Glasgow Coma Scale
GCPII	Glutamate Carboxypeptidase II
GFAP	glial fibrillary acid protein
Gln	glutamine
Glu	glutamate
GPC	glycerophosphocholine
H&E	hematoxylin & Eosin
HIC	head injury criterion
HIP	head impact power
^{1}H-MRS	proton magnetic resonance spectroscopy
Iba-1	ionized calcium-binding adaptor molecule-1
Ins	myo-inositol
LSD	least significant difference
MPS	maximum principal strain
MRI	Magnetic resonance imaging
NAA	N-acetylaspartate
NAAG	N-acetylaspartylglutamate
NASS	National Automotive Sampling System
NF	neurofilament
PBS	phosphate-buffered saline

PCh	phosphocholine
PCr	phosphocreatine
R	Pearson Correlation Coefficient
Scyllo	scyllo-inositol
TBI	traumatic brain injury
WSTC	Wayne State Tolerance Curve

CHAPTER 1: INTRODUCTION

1.1 PREVALENCE

Traumatic brain injury (TBI) continues to be a serious problem in society with 1.7 million occurrences annually in the United States, accounting for 30.5% of all injury related deaths according to the Centers for Disease Control and Prevention. The leading causes of unintentional TBI are falls (35.2%), motor vehicle accidents (17.3%), being struck by/against an object (16.5%), and assault (10%; Faul et al., 2010), all of which can involve a non-penetrating impact-based event at the minor severity level. Motor vehicle accidents are the second leading cause of reported TBI (17.3%) and the leading cause of TBI-related deaths (31.8%; Faul et al., 2010). Specifically, in motor vehicle accidents, an analysis of data from the National Automotive Sampling System (NASS) from 1997-2006 showed that for belted occupants, 34.3% of severe head injuries were caused from frontal and 42.4% from nearside crashes (Yoganandan et al., 2011). In the year 2000, TBI cases were responsible for an estimated $60.4 billion in economic costs involved in fatal, hospitalized, and non-hospitalized events in the United States. This includes $51.2 million in productivity losses (Corrigan et al., 2010). Not only is the incidence and economic cost of TBI high, there have been no neuroprotective drug trials to survive past Phase III clinical trials (Narayan et al., 2002; Marklund et al., 2006; Margulies et al., 2009; Xiong et al., 2013). This chapter provides a brief review of the current techniques used to diagnose, prevent, and study TBI.

1.2 NEUROBIOLOGY

A basic overview of the neurobiology pertinent to this research is summarized in the following section. This summary was assembled from several sources: Atlas of Human Anatomy (Netter, 2011), Neuroanatomy Text and Atlas (Martin, 1996), Principles of Neural Science (Kandel et al., 2000), Fundamental Neuroscience (Squires et al., 2008), The Axon-Structure, Function, and Pathophysiology (Waxman et al., 1995), Basic Neurochemistry: Molecular, Cellular and Medical Aspects (Siegel et al., 1999), and Fletcher and Mullins (2010).

1.2.1 ANATOMY

The brain is located within the cranial vault of the skull, which consists of the frontal, ethmoid, sphenoid, occipital, two temporal, and two parietal bones. The cranial sutures are

interlocking lines of fusion (joints) – consisting of fibrous bands of tissue - that connect the skull bones. The coronal suture connects the frontal and the two parietal bones, the sagittal suture joins the two parietal bones, and the lambdoid suture connects the two parietal bones with the occipital bone. The bones of the skull have three layers. There is an outer table, diploë layer, and inner table (closest to the brain). The outer and inner tables are made of compact bone and the diploë layer consists of trabecular bone. The outer table is surrounded by a layer of connective tissue called the periosteum or pericranium. There is also a layer of periosteum lining the inner table, called the endocranium, which is fused to the underlying dura mater.

Inside the skull, the brain is covered by the meninges. Moving inward toward the brain, there are the dura, arachnoid, and pia mater. The dura includes the falx cerebri, which separates the left and right cerebral hemispheres, and the tentorium cerebelli, which separates the cerebrum and cerebellum. The arachnoid layer retains the cerebrospinal fluid. The pia mater follows the convolutions of the brain (gyri: folds in the cortex, and sulci: grooves in the cortex), but the dura and arachnoid do not.

The brain can be divided in to six regions: the cerebrum, diencephalon, cerebellum, midbrain, pons, and medulla. There are four ventricles that act as reservoirs for cerebrospinal fluid (CSF) and facilitate its circulation. The lateral and fourth ventricles contain a choroid plexus, which aid in production of CSF. The brain contains 12 cranial nerves and a network of arteries and veins.

The cerebrum contains the right and left cerebral hemispheres, corpus callosum, hippocampus, amygdala, and basal ganglia. The left and right hemispheres have four lobes named after the skull bones under which they are located. There are the frontal, temporal, parietal, and occipital lobes. This tissue is comprised of gray matter (mostly neuronal cell bodies) and white matter (axons). The frontal lobe controls motor behavior through the motor cortex (immediately rostral to the parietal lobe), emotions, and cognitive functions. The parietal lobe integrates sensory information from joints, muscles, and skin and helps perceive pain and touch. The temporal lobe is responsible for hearing as well as memory and emotions. Emotions are regulated in portions of the frontal, temporal, and parietal lobes. The occipital lobe is responsible for visual perception. Connecting the two hemispheres and inferior to the falx cerebri is the corpus callosum. The corpus callosum is made up of white matter that connects the right and left cerebral hemispheres. There are four parts of the corpus callosum: the rostrum, genu, body, and

splenium. In general, the corpus callosum is involved in integrating information and mediating complex behaviors of the brain with disconnection resulting in an inhibition in information processing speed and problem solving (Hinkley et al., 2012). The corpus callosum is a frequently injured region during brain trauma as part of a constellation of diffuse axonal injury. Adams et al. (1982) analyzed 45 cases and concluded that all cases displayed focal lesions in the corpus callosum and in the dorsolateral aspect of the rostral brainstem. The hippocampus is crucial during learning and memory and the amygdala is responsible for handling stressful situations and anxiety. The basal ganglia are an important collection of neurons that are responsible for many higher brain functions such as fine movement, emotion, and cognition.

The diencephalon is made up of the thalamus and hypothalamus. The thalamus is an important structure for transmitting information to the cerebral hemispheres. The hypothalamus maintains homeostasis by regulating processes such as sleep cycles and body temperature. The hypothalamus also controls hormone release from the pituitary gland.

The cerebellum (Figure 1.1) helps maintain balance and posture. An injured cerebellum can result in poor coordination and erratic limb movements.

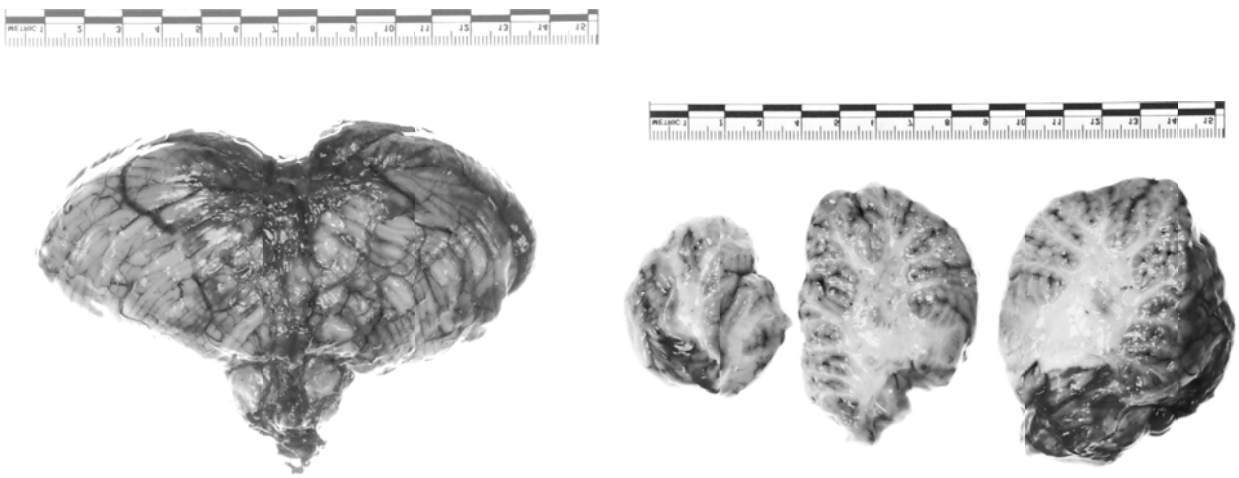

Figure 1.1: Human cadaver cerebellum (left) and one hemisphere cut in to sagittal sections (right).

The midbrain, pons, and medulla are part of the brainstem. The brainstem receives sensory information from the brain and controls the muscles of the head, regulates arousal, and transmits information back and forth between the brain and the spinal cord. Damage to the brainstem is life-threatening because the brainstem is involved with many involuntary actions

such as respiration and blood pressure regulation. Figure 1.2 displays important regions in the Göttingen minipig brain.

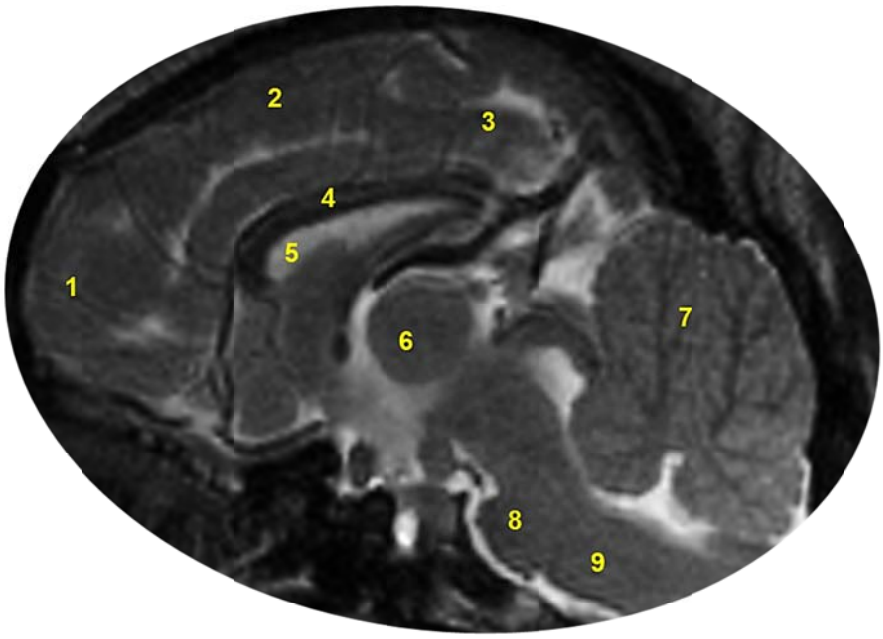

1: Frontal lobe
2: Parietal lobe
3: Occipital lobe
4: Corpus Callosum
5: Lateral Ventricle
6: Basal Ganglia
7: Cerebellum
8: Pons
9: Medulla

Figure 1.2: Important structures in the Göttingen minipig brain. T2-weighted MRI scan in the sagittal plane. CSF appears white.

On a microscopic level, neurons are responsible for signal conduction throughout the nervous system. They are made up of a cell body, dendrites (which receive signals from adjacent neurons), axon, and the pre-synaptic terminals. Neurons relay electrical signals to the next neuron by releasing neurotransmitters in to the synaptic cleft (region between pre-synaptic axon terminals and dendrites of adjacent neuron) for uptake. The myelin sheath wraps around the axon in a spiral pattern to insulate the axons, which facilitates electrical conduction. The myelin sheath is not continuous and breaks between the myelin are called nodes of Ranvier. The myelinated segments between the nodes of Ranvier are called internodes. The myelin loops transition from the internode to a small juxtaparanode region before terminating in the paranode leading to the unmyelinated node of Ranvier. These different regions of myelin loops have specific adhesion molecules to the axon membrane. The properties of the axonal membrane are described in detail by Poliak and Peles (2003), Peles and Salzar (2000), and Arroyo and Scherer (2000). Myelin is

made up of 70% lipid and 30% protein. The main proteins that make up myelin in the central nervous system are proteolipid protein (50%) and myelin basic protein (30%). The major lipids that constitute myelin are cholesterol, galactolipids, and phospholipids.

The axon cytoskeleton is made up of microtubules, microfilaments, and neurofilaments. Microtubules extend the length of the axon (from soma to terminal) and act as a track for organelles and proteins driven by molecular motors. The kinesin family of motor proteins is responsible for the majority of membrane-bound organelle movement in the anterograde direction during fast axonal transport. The dynein family of motor proteins implements the majority of fast axonal transport in the retrograde direction. Microtubules are made up of 13 protofilaments in a tubular arrangement with an outside diameter of 25-28 nm. Microfilaments are 3-5 nm in diameter and are concentrated in the periphery of the axon. Neurofilaments are a type of intermediate filament. Neurofilaments are made up of a triplet protein of light (60-70 kDa), medium (130-170 kDa), and heavy (180 to 200 kDa) subunits. There are on average 3-10 times more neurofilaments in the axon than microtubules. The medium and heavy neurofilaments have sidearms, which limit the axonal packing density and play a role in determining the axon caliber. Neurofilament compaction has been identified after brain injury and is caused by the shortening of these sidearms thereby decreasing the axon diameter (Pettus et al., 1994; Pettus and Povlishock, 1996). Another marker commonly used to assess axonal integrity is β-amyloid precursor protein (β-APP). This protein is normally found in the axon and is carried through anterograde transport. Increased β-APP inside the axon indicates impaired anterograde transport during TBI (Stone et al., 2001; Stone et al., 2004). Another marker for neuron health is caspase-3. Caspase-3 is a mediator of programmed cell death that is upregulated to initiate apoptosis after an injury (Porter et al., 1999; Sajja et al., 2012).

Other cell types that are found in the brain are ependymal cells, oligodendrocytes, microglia, and astrocytes. Ependymal cells line the ventricles in the brain. Oligodendrocytes are responsible for insulating axons in the central nervous system by forming the myelin sheath. On average, each oligodendrocyte is connected to 15 axonal internodes. Microglial cells are immune system-derived phagocytes, which become activated during injury, disease, or infection. Activated microglial cells retract cytoplasmic processes, actively proliferate, and release inflammatory factors (Polivok et al., 2005). Immunostaining with ionized calcium-binding adaptor molecule-1 (Iba-1) is useful in visualizing microglia because this stain allows for

visualization of active processes, thus facilitating identification of active and resting states (Kettenmann et al., 2011). Astrocytes are responsible for maintaining the extracellular environment. They can take up excess potassium, for example, or excess neurotransmitters from synaptic zones. Astrocytes are made up of 8-10 nm diameter filaments of glial fibrillary acid protein (GFAP), which are upregulated in reactive astrocytes. Reactive astrocytes also proliferate, migrate, and have an irregular nucleus (Polikov et al., 2005). Gennarelli (1996), Maxwell et al. (1997), Gennarelli et al. (1998), and Kou and VandeVord (2014) provide thorough reviews of the pathophysiology of traumatic axonal injury at the cellular level.

1.3 DEFINITION AND DIAGNOSIS

TBI encompasses many different types of brain injuries including penetrating and non-penetrating brain injuries (Faul et al., 2010). Non-penetrating injuries are further characterized in to focal injuries such as contusions and intracranial hemorrhages (Adams et al., 1983) or diffuse damage such as diffuse axonal injury. TBI can also be thought of in terms of damage that occurs at the moment of injury (primary) and damage that develops and progresses over time (secondary) (Adams et al., 1983).

Clinically, TBI severity is assessed using the Glasgow coma scale (GCS). The GCS is a metric based on consciousness for which numbers are assigned for eye opening response, verbal response, and motor response. The maximum (least injured) score is 15 and the lowest is 3. Severe head injury is classified as a score of 8 or less. Moderate injury is a score from 9-12 and a minor head injury is a score of 13-15 (Teasdale and Jennett, 1974; Teasdale and Jennett, 1976). Some classify a score of 13 as moderate as opposed to mild injury because of the risk for complications (Maas et al., 2008; Matis and Birbilis, 2008). It has been shown that patients with the same GCS score can have many different injuries and markedly different outcomes (Gennarelli et al., 1982a). The abbreviated injury scale (AIS), is used by health organizations for clinical trauma management, motor vehicle accident investigators, and researchers to categorize the threat-to-life. The scale ranges from 0 (no injury) to 6 (maximal, currently untreatable injury) (Gennarelli and Wodzin, 2005). An example of a minor brain injury (AIS 1) is a mild concussion with no loss of consciousness. The GCS and the AIS scale give an initial assessment of the injury, but do not evaluate symptoms or predict prognosis. Common immediate symptoms of minor TBI include loss of consciousness, poor balance, headaches, and problems with

coordination (Paniak et al., 2002). Long-term symptoms including depression, anxiety, lower sleep quality, working memory impairment, and impaired information processing speed can persist even one year after injury (Dean et al., 2013).

Neuropsychological assessment also provides insight in to the extent of TBI with the aim of identifying areas of deficits. After an injury, the common domains assessed include memory function, intellectual function, processing speed, psychomotor speed, language, attention, and executive function (Tsaousides and Gordon, 2009). The most popular neuropsychological battery is the Halstead-Reitan Neuropsychological Battery, which includes a tactual performance, finger oscillation, category, seashore rhythm, aphasia screening, speech sounds perception, sensory-perceptual, strength of grip, and tactile form recognition tests (Podell et al., 2010). Numerous neuropsychological tests exist, but many are used together to evaluate specific domains. Once the deficits are identified, there are various training programs that have been developed to retrain and provide compensatory strategies to dealing with cognitive impairments (Tsaousides and Gordon, 2009).

Imaging is another technique that is frequently used to assess brain injury. Computed tomography (CT) is usually the first imaging procedure carried out on TBI patients. This imaging can quickly identify significant pathologies such as skull fracture and hemorrhaging (Bigler and Maxwell, 2011). Both CT and magnetic resonance imaging (MRI) are used to assess gross damage such as hemorrhages and lesions. However, CT tends to underestimate focal lesions (Mittl et al., 1994) and Lee et al. (2008) did not find correlation between CT or 3T MRI findings and cognitive impairment in patients with minor TBI, citing the need to investigate improved imaging techniques. According to a report to Congress (Gerberding and Binder, 2003), focus is shifting from severe TBI to minor TBI. Mild TBI accounts for at least 75% of all TBI in the U.S., but the consequences frequently are not mild. More complex imaging methods are being investigated as potentially better measures of TBI severity and injury persistence or recovery over time, especially during minor TBI. Some of these techniques include diffusion tensor imaging (DTI), functional magnetic resonance imaging (fMRI), and proton magnetic resonance spectroscopy (^{1}H-MRS) (Hunter et al., 2012). DTI evaluates anisotropy in water diffusion along white matter tracts in the brain. Post-injury changes in diffusion anisotropy in the brain are a subject of study (Basser et al., 1994; Bassar and Pierpaoli, 1996; Arfanakis et al., 2002), as is the predictive nature of these changes with respect to clinical outcome after severe

TBI (Sidaros et al., 2008). Tractography can be used to further evaluate DTI images so that white matter connectivity can be described (Nucifora et al., 2007). fMRI identifies areas of activation in the brain during certain tasks. This mainly has been used to observe deficits over time and the effectiveness of rehabilitation strategies (Cazalis et al., 2006; Sanchez-Carrion et al., 2008). ^{1}H-MRS quantifies chemical shifts within a specified volume (voxel) that correspond to metabolite concentrations (Brooks et al., 2001). These concentrations give insight in to the state of the brain either from a specific disorder or from an injury (Moore and Galloway, 2002), and have been used to study TBI both clinically and in animal research (Brooks et al., 2001). ^{1}H-MRS has the potential to diagnose injury severity by identifying important biochemical changes within the brain, but more work needs to be done to look at regional differences in the brain (Hunter et al., 2012), and to confirm that metabolite changes found after TBI insults in animal models are observed clinically. Overall, complex imaging modalities can give insight in to the effects of TBI, but more research needs to be done to relate findings to underlying injury and to be able to predict outcome.

1.4 HEAD INJURY CRITERION

The development of strategies for preventing TBI is related to available injury metrics. The current automotive standard for evaluating head injury potential is the Head Injury Criterion (HIC). This metric is used in regulatory testing of motor vehicles as part of the Federal Motor Vehicle Safety Standards (FMVSS). For frontal collision occupant crash protection under FMVSS 208, the Hybrid III 50th percentile male and the Hybrid III 5th percentile female anthropomorphic test devices (ATD) are regulated. The resultant linear acceleration at the center of gravity of the head is used to assess the potential for head injury (Eqn. 1.1).

$$\mathrm{HIC} = \left[\frac{1}{t_2 - t_1}\int_{t_1}^{t_2} a\, dt\right]^{2.5}(t_2 - t_1), \qquad \text{(Eqn. 1.1)}$$

Where a is the resultant linear acceleration measured at the center of gravity of the head and t is time.

The resultant linear acceleration range is chosen to maximize the function (supremum). The calculated HIC value shall not exceed 700 within a 15 ms interval (also referred to as HIC_{15}). This corresponds to a 5% risk of attaining an AIS 4+ injury according to the injury assessment reference values (Mertz et al., 2003). Examples of AIS 4+ head injuries include

diffuse axonal injury involving a loss of consciousness for longer than 6 hours, subdural hematomas involving more than 25 cc of blood, or multiple large cerebral contusions (Gennarelli and Wodzin, 2005).

The current HIC is based on the Wayne State Tolerance Curve (WSTC). The WSTC derives from an acceleration-time tolerance curve described by Gurdjian et al. (1966). This tolerance curve resulted from a combination of concussive data from applying pressure to the dural sac of anesthetized dogs and linear skull fracture data from cadavers (Gurdjian et al., 1961; Gurdjian et al., 1964; Gurdjian et al., 1966). Ono et al. (1980) performed cadaver and monkey experiments, providing additional data for impacts lasting longer than 10 ms. This was known as the Japan Head Tolerance Curve. In 1966, Gadd plotted the WSTC on a log-log scale producing a straight-line. Gadd also suggested integrating acceleration over the entire pulse area to incorporate different impulse shapes. The Gadd severity index weighted the acceleration by raising it to the power of the slope of the straight line fit and based on the log-log plot of the WSTC, suggested value of 2.5 with a suggested threshold of 1000 (Gadd, 1966). Versace (1971) proposed the current HIC. This standard is shown by Eqn. 1.1. HIC is calculated using resultant linear acceleration, but this acceleration arises from both linear and angular accelerations applied at the center of gravity of the head. Eppinger (1981) provides a physical interpretation of HIC as the "rate of change of kinetic energy modulated by the square root of the averaged acceleration over the time interval".

Motor vehicle accidents still contribute to a large percentage of TBI every year. HIC_{15} is not a requirement in side impact crash testing and HIC_{36} has only recently been added or will be added (2014-2016) for certain side impact tests (FMVSS 214) even though this type of collision contributes to a high number of severe head injuries (42.4% of AIS 4+ injuries in near side versus 34.3% in frontal; Yoganandan et al., 2011). In addition, the HIC thresholds adopted for infants, children, and small females (some are still not in regulation) were scaled from the threshold for the average mid-size male and the child restraint regulation uses a threshold of 1000 for HIC_{36} for the 3 and 6 year old (FMVSS 213; Mertz et al., 2003). A HIC_{36} of 1000 corresponds to a 16% risk for a mid-size male to sustain a life-threatening brain injury (Prasad and Mertz, 1985). These are not proven estimates of the likelihood these populations will sustain life-threatening head injuries. However, currently a better approach does not exist, especially since there is not an injury metric that relates an impact to underlying damage. An improved

injury metric will give insight in to the best predictors for underlying damage and could lead to a more appropriate approximation for these populations.

There are clear shortcomings in the ability of the federal standard to prevent head injury. This could be related to an inability of the regulatory tests to control for the types of head injury experienced in the field (i.e. the test doesn't adequately reflect reality), or an inability of the metric to predict injury adequately. It is likely that there is some combination of these limitations involved.

King et al. (2003) explains the uncertainty regarding the ability of HIC to predict injury and questions which parameter should govern a head injury criterion. Currently, different hypotheses are based on input parameters, including linear and angular acceleration, but it was proposed that brain response parameters such as strain, strain rate, and the product thereof should replace the current input acceleration limits. Of course, such parameters cannot be evaluated using ATDs, or crash dummies.

Many different injury metrics have been proposed as being better predictors of head injuries. Three metrics to note include the brain injury criterion or BrIC, the head impact power or HIP, and the concussion correlate or CC.

The kinematic brain injury criterion (BrIC) was developed by Takhounts et al. (2013) (there was a previous version by Takhounts et al., 2011). BrIC is described by Eqn. 1.2.

$$\mathrm{BrIC} = \sqrt{\left(\frac{\omega_x}{\omega_{xC}}\right)^2 + \left(\frac{\omega_y}{\omega_{yC}}\right)^2 + \left(\frac{\omega_z}{\omega_{zC}}\right)^2}, \qquad \text{(Eqn. 1.2)}$$

Where ω_x, ω_y, and ω_z are the maximum angular speeds in x, y, or z respectively, and ω_{xC}, ω_{yC}, and ω_{zC} are the critical angular velocities in their respective directions.

BrIC was developed based on angular speeds and values for the critical angular speeds were determined such that a BrIC=1 corresponded to a 50% probability of an AIS 4+ injury according to the cumulative strain damage measure (CSDM) (Bandak and Eppinger, 1994) and the maximum principal strain (MPS) (Mao et al., 2013). These critical angular velocities (average of CSDM and MPS) are ω_x=66.25 rad/s, ω_y=56.45 rad/s, and ω_z=42.87 rad/s. BrIC was developed based on historically available injury data in an effort to better relate kinematics to injury. However, these data are limited.

The head impact power (HIP) was put forth by Newman et al. (2000). It was suggested that the magnitude of the rate of change in kinetic energy would correlate to head injury severity/probability. This 6 degree of freedom injury criterion is derived from the general expression for the rate of change of translational and rotational kinetic energy for a rigid body (Eqn. 1.3)

$$\mathrm{HIP} = 4.50\mathrm{a}_x \int \mathrm{a}_x dt + 4.50 a_y \int \mathrm{a}_y dt + 4.50\mathrm{a}_z \int \mathrm{a}_z dt + 0.016\alpha_x \int a_x dt + 0.024 a_y \int a_y dt + 0.022 a_z \int a_z dt, \quad \text{(Eqn. 1.3)}$$

Where a is linear acceleration (m/s^2), mass of the human head is 4.50 kg, mass moment of inertia in x, y, and z is 0.016, 0.024, and 0.022 Nms^2, respectively.

Reconstructions from professional football players who may have sustained a concussion were used to evaluate the probability of concussion based on HIP. HIP of 12.8 kW was said to correspond to 50% probability of minor TBI (Newman et al., 2000).

Rowson et al. (2013) developed a concussion risk curve derived from data collected from instrumented football players. This data set included 60,011 impacts with 37 diagnosed concussions. Laituri et al. (2015) took the basis of this logistic risk curve (Eqn. 1.4) and called it the concussion correlate (CC). CC displayed the best fidelity from the aggregate perspective of field data and was second to HIC when looking from a point-estimate perspective. However, concussion diagnosis is based on symptoms; therefore the exact underlying damage is unknown. In addition, football players do not represent the entire population and this concussion risk curve could benefit from additional data.

$$\mathrm{CC} = \beta_0 + \beta_1 \mathrm{a}_{\mathrm{res}} + \beta_2 \alpha_{\mathrm{res}} + \beta_3 \mathrm{a}_{\mathrm{res}} \alpha_{\mathrm{res}}, \quad \text{(Eqn. 1.4)}$$

Where $\beta_0, \beta_1, \beta_2, \beta_3$ are coefficients of logit and are -10.2, $4.33e^{-2}$, $8.73e^{-4}$, and $-9.20e^{-7}$, respectively, a_{res} is the peak resultant translational acceleration (G), and α_{res} is the peak resultant rotational acceleration (rad/s^2).

Unfortunately, without *in vivo* research that directly relates an impact to underlying damage in a clinically-relevant way, the theories regarding which parameter/injury metric is the most relevant remains speculation.

1.5 INJURY MODELS

A large body of research has been dedicated to replicating the clinical pathology of TBI using experiments *in vivo* in an effort to make prevention and intervention strategies more effective. The most prevalent injury models include fluid percussion, inertial rotation, controlled cortical impact or rigid indentation, and weight-drop or impact acceleration. A brief review of each method is provided below. Hardy et al. (1994), Cernak et al. (2005), and Xiong et al. (2013) provide additional reviews of head injury models.

1.5.1 FLUID PERCUSSION

The fluid percussion (FP) injury model was developed by Lindgren and Rinder (1966). Injury is caused by applying a fluid pressure pulse to the intact dura. First, a craniotomy is done to expose the dura of the animal and to cement a plastic cap in place. To induce injury, a weighted pendulum is released from a desired height and strikes a piston. This piston is connected to a reservoir of sterile saline that releases a fluid pressure pulse on to the exposed dura. Craniotomy positions are varied to induce either midline or lateral FP injury (McIntosh et al., 1987; McIntosh et al., 1989). Changing the craniotomy position for lateral FP injury will result in different locations and degrees of tissue damage (Vink et al., 2001; Floyd et al., 2002). Initially, this type of apparatus allowed for little biomechanical control, with the only adjustable parameter being the weight drop height, leaving the contact speed and tissue deformation unknown (Lighthall et al., 1989). Different groups have modified the device to increase control over the fluid volume and to remove air bubbles within the saline reservoir (Stalhammer et al., 1987; Yamaki et al., 1994). Recently, the micro-FP device has been developed, which is a pneumatically-driven device to control the impact pressure and dwell time (Kabadi et al., 2010). The FP device was originally designed for use in rabbits (Lindgren and Rinder, 1966; Lindgren and Rinder, 1969), but has been modified to be used in cats (Sullivan et al., 1976; Povlishock et al., 1978), rats (Dixon et al., 1987; McIntosh et al., 1987), and mice (Carbonell et al., 1998; Spain et al., 2010).

This type of injury mimics many human brain injury pathologies such as hemorrhaging and axonal damage (Dixon et al., 1987; Povlishock et al., 1983; McIntosh et al., 1989). However, this injury results in a high mortality rate due to the disproportional involvement of the brainstem (Cernak et al., 2005) and is more indicative of a penetrating injury.

1.5.2 INERTIAL ROTATION

The inertial rotation device was developed based on a hypothesis put forth by Holbourn (1945), that brain damage was most likely produced by head rotation, not translation. Higgins and Schmall (1967) developed a device that imparts pure-rotation without head impact. To induce injury, the animal is attached to a helmet. This helmet is connected to a linkage system that is attached to a pneumatic actuator. This system turns linear displacement of the actuator in to rotation of the head (Gennarelli et al., 1979). The head is moved rapidly through a prescribed degree arc in a biphasic acceleration-deceleration wave (Higgins and Schmall, 1967). Injury has been produced by sagittal, coronal, and axial rotation (Gennarelli et al., 1982b). This device was originally used in non-human primates (Higgins and Schmall, 1967; Unterharnscheidt and Higgins, 1969) and has been modified to produce injury in miniature swine (Ross et al., 1994; Kimura et al., 1996; Smith et al., 1998).

This device produces clinical brain injury pathologies. Gennarelli et al. (1982b) was able to produce coma, and axonal injury in the corpus callosum and white matter in non-human primates. There was axonal injury present without contusions or intracerebral hemorrhages. The most common pattern of injury was axonal damage in the white matter and focal lesions in the corpus callosum and superior cerebellar peduncles. Out of the three directions of rotation studied, coronal rotation produced the most severe abnormalities and correlated highly with prolonged traumatic coma. Sagittal rotation produced the least injury. Ross et al. (1994) did not replicate injuries in the corpus callosum in the Hanford minipigs compared to the primate model and attributed this difference to the lack of a pronounced falx cerebri, affecting the biomechanical response of the brain during the injury event.

Lighthall et al. (1989) discusses the inertial rotation device and its limitations. Except for skull fracture, this pure rotation injury model produces almost all types of primary head injury (Gennarelli, 1983). Even though this injury device causes a wide spectrum of injuries in the non-human primate, interpretation of the biomechanics and its relationship to injury outcome is obfuscated by the two-phase acceleration-deceleration pulse. Also, it is thought that diffuse axonal injury is produced by inertial forces, but it is the driving contact forces that generate the levels of acceleration required to induce diffuse axonal injury (Smith and Meaney, 2000). Ommaya and Hirsch (1971) state that twice the input would be needed to generate the same

injuries with just pure rotation. Overall, this injury method replicates clinical pathologies, but is not indicative of practical input modes.

1.5.3 Controlled Cortical Impact

The controlled cortical impact device was developed by Lighthall (1988) as an experimental model that allowed independent control of contact velocity and impact depth. This device is a pneumatic impactor with a small-bore, stroke-constrained pneumatic cylinder (5-cm stroke). A craniotomy is needed to impact the intact dura directly. Controlled cortical impact has been studied in ferrets (Lighthall, 1988; Lighthall, 1990), rats (Dixon et al., 1991; Hamm et al., 1992; Palmer et al., 1993), mice (Smith et al., 1995; Fox et al., 1998; Hannay et al., 1999), and pigs (Alessandri et al., 2003; Manley et al., 2006).

This device has produced many different clinical pathologies associated with brain trauma such as cerebral contusions, hemorrhages, hematomas, and diffuse injury in ferrets (Lighthall, 1988), and hippocampal neuronal loss and axonal injury in the corpus callosum of mice (Smith et al., 1995). Controlled cortical impact allows for control over biomechanical parameters associated with the injury and does reproduce clinical pathologies. But it involves a craniotomy, thus it does not produce injury in a way that is characteristic of impact.

1.5.4 Weight-Drop

Denny-Brown and Russell (1941) established the first controlled non-penetrating head impact device. This device consisted of a pendulum designed to impact the occipito-parietal region of the skull of dogs, cats, and monkeys. Feeney et al. (1981) developed a weight-drop model used to directly injure the dura in rats. Marmarou et al. (1994) developed an impact acceleration model that has been studied frequently as it produces a non-penetrating impact-based injury (Cernak et al., 2005). A brass weight is dropped down a Plexiglas tube striking a stainless steel disk covering the rodent skull (Marmarou et al., 1994). The rodents are rested on a foam bed during the injury event. Graded injury can be produced by varying the weights (Ucar et al., 2006) and the drop height (Marmarou et al., 1994). Foda et al. (1994) reported widespread injury of neurons, axons, and microvasculature. Axonal injury was present in the corpus callosum, internal capsule, cerebral and cerebellar peduncles, and in the brainstem.

The Denny-Brown and Russell device has been used in cats, dogs, and monkeys (Denny-Brown and Russell, 1941; Walker et al., 1944; Groat et al., 1945). The Marmarou weight-drop

model has been used in rats (Marmarou et al., 1994; Heath and Vink, 1995; Povlishock et al., 1997) and mice (Chen et al., 1996).

The Marmarou weight-drop model does replicate clinical pathologies in a non-penetrating, impact-based model, however the device does not allow for direct measurement of the impact kinematics. Recently, work at Wayne State University measured impact kinematics during these impacts (Li et al., 2011). Positive correlation was found between β-APP accumulations in the corpus callosum and linear head acceleration and also surface righting time in rats. In the corpus callosum, the combination of linear acceleration and time-to-surface-righting were the best predictors of axonal damage. Power was the best predictor when combining the corpus callosum and pyramidal tract axonal damage (Li et al., 2011b). The Marmarou model is limited in that it has been used only in rodents, produces a high variability in the injury severity attributed to radial movement of the weight during its descent through the polymer tube (Cernak et al., 2005; Xiong et al., 2013), and has the possibility of producing a second impact from the weight rebounding and then falling back down on to the animal (Cernak et al., 2005), although this can be prevented.

Overall, the previously used injury models have limitations that might explain why there are still many unknowns surrounding TBI. Clinically, non-penetrating, impact-based injuries cause the majority of TBI (Faul et al., 2010). In addition, research has shown that head injury is unlikely without an impact (McLean, 1995). The Marmarou model does produce a clinically-relevant injury, but there is a need for a repeatable injury model that can be used in a higher-order animal.

1.6 ANIMAL MODELS

When choosing an animal model, the overall research goal needs to be considered. The lack of success of the popularly used injury models to lead to drug treatments spurred evaluation of previously used animal models. Many TBI studies used rodent models because their small size and relatively inexpensive cost allow for more studies to be performed (Povlishock et al., 1994). However, when comparing the rodent to the human brain, there are important dissimilarities. Other than obvious size differences, the rodent brain is lissencephalic, meaning that there are no gyri or sulci. The rodent brainstem exits the brain axially, whereas the human brainstem exits at an angle. In addition, the rodent brain has a considerably lower white matter to gray matter ratio

(Swanson, 1995). Gennarelli (1994) stresses the importance of gyral complexity and craniospinal angle to mimicking human behavioral, neurochemical, metabolic, and pathologic responses to brain injury. In addition to rodent models, other studies have used dogs (Denny-Brown and Russell, 1941), rabbits (Lindgren and Rinder, 1966), ferrets (Lighthall, 1988), cats (Povlishock et al., 1978), non-human primates (Higgins and Schmall, 1967), and minipigs (Ross et al., 1994) to study TBI. Previously used minipig models, such as the Hanford minipig, do not have a pronounced falx cerebri, which affects the mechanical response of the brain (Ross et al., 1994; Meaney et al., 1995). Importantly, this brain structure has been shown to play a role in how the brain moves inside the skull during an impact to cadavers (Hardy et al., 2007). The animal model chosen for this research was the Göttingen minipig. The Göttingen minipig does have a pronounced falx cerebri, gyrencephalic brain, and a brainstem that exits at an angle (Fievisohn et al., 2012).

Developing an injury metric that relates impact to underlying damage requires an animal model. This means that scaling from an animal to a human is necessary. For example, when looking at brain mass, the rodent brain would have to be scaled by a factor of approximately 837, whereas the Göttingen minipig brain would only have to be scaled by a factor of 24 (Herculano-Housel, 2009). Other factors such as brain length and the ratio of white matter to gray matter also make the rodent an undesirable model. Using a higher order animal model is necessary in terms of overall morphological similarities, but also when considering scaling concerns. Figure 1.3 shows a rat, Göttingen minipig, and a human cadaveric brain side-by-side for comparison.

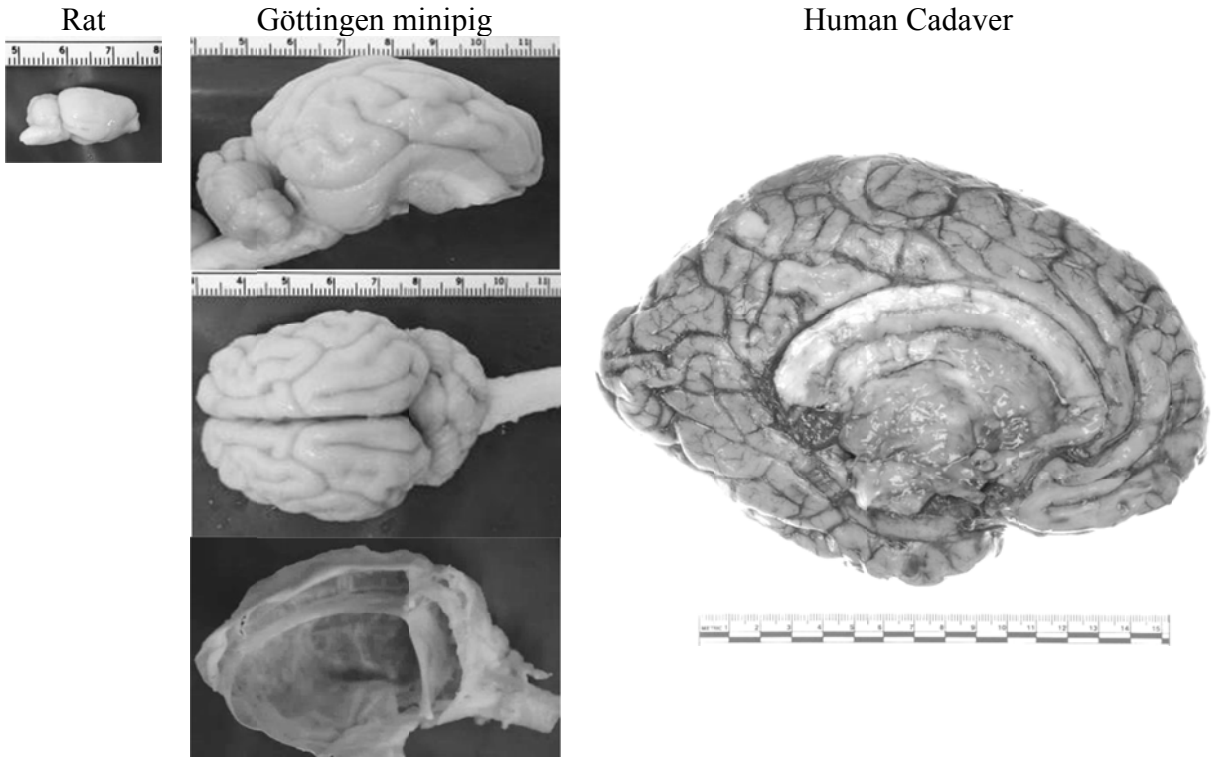

Figure 1.3: Sprague-Dawley rat, Göttingen minipig, and Human cadaver brain.

1.7 RESEARCH OBJECTIVES

The objective of this research was to take the initial steps toward developing an injury metric that relates impact kinematics to underlying damage while addressing some of the limitations of previous injury and animal models as already discussed. The focus of this research was to develop two novel injury devices and characterize impact response *in vivo* using a gyrencephalic animal model.

This research has four primary components, which are described in subsequent chapters:

1. Development and demonstration of the repeatability of two novel injury devices,
2. Impact response characterization over the course of 24 hours using these two devices in a Göttingen minipig model *in vivo* using immunohistochemistry and proton magnetic resonance spectroscopy,
3. Identification of correlative relationships and potential predictors between underlying damage, metabolite changes, and impact kinematics,
4. Pilot study of impact response over the course of 72 hours to determine if there is recovery or persistence.

CHAPTER 2: DEVELOPMENT AND REPEATABILITY OF TWO UNIQUE TRAUMATIC BRAIN INJURY DEVICES

2.1 DEVICE DESCRIPTIONS

Two devices have been developed to produce impact TBI in the Göttingen minipig. One device is a translation-input injury device and the other is a combined translation and rotation-input injury device. The animals are secured to the devices in the supine position. Both devices involve a platform that is dropped to produce injury (rapid deceleration) when it contacts brass tubing used to tune the impact profile. The animals are positioned on top of the platforms.

Appendix A contains technical drawings of parts that were machined to size. All materials are multipurpose 6061 aluminum unless otherwise specified. Appendix B contains a table with materials and dimensions for each device.

2.1.1 TRANSLATION-INPUT INJURY DEVICE

The translation-input injury device is shown in Figure 2.1. It produces a translation-only injury by restricting motion to one plane (a linear drop). This is accomplished by constraining the motion of an animal platform via linear rails. The bottom of the platform impacts brass tubing causing rapid deceleration of the device/animal. The platform dimensions are approximately 66 x 76 x 196 cm. The device consists of five primary components: the linear rail frame, steel support blocks, aluminum block/brass tubing, animal platform, and winch attachment.

Figure 2.1: Translation-input injury device.

A: Animal platform; B: Winch; C: Brass Tubing; D: Linear Rails; E: Steel Blocks.

Linear rail frame: The linear rail frame guides the platform, restricting movement to one direction. This structure consists of two halves (on either side of the animal platform) that bolt to a baseplate. Each half consists of a set of two I-beams that are joined at the bottom and the top with 90° angle. The bottom angle also attaches these I-beams to the baseplate. U-channel spans each set of I-beams for support. Across the top aluminum angle, two stainless steel threaded rods connect the halves. The two sets of 90° angle, the U-channel, and the threaded rods are used to adjust and keep the I-beams aligned to minimize binding. Each I-beam (four total) is used to anchor a linear rail assembly, which consists of a rail support and a precision case-hardened steel shaft.

Steel support blocks: The purpose of the steel support blocks is to hold the device in place during an impact event, but also to provide a foundation for the brass tubing. Each block consists of a stack of four hot rolled steel plates separated by leather sheets. The blocks sit on top of the baseplate. Between the bottom plates and the baseplate are vibration damping pads. The

blocks overhang the baseplate. Delrin® slabs are used to support the overhanging portion of the support blocks. Threaded rods insert through the leather sheets and thread in through the top three blocks, and half-way through the bottom block to secure them together.

Aluminum block/brass tubing: The aluminum blocks provide a means to position and fasten the brass tubing, which facilitates adjustment of the impact profiles in a repeatable fashion. The aluminum blocks are attached to the top of each steel support block via an aluminum plate interface. V-shaped channels are cut in the top of each block, and eyebolts are fastened to each side. A carriage bolt is passed through the brass tubing and kept in place via connections to the eyebolts. Two threaded rods passed through each steel support block (plate stack) are used to fasten the aluminum block assemblies to the baseplate. Figure 2.2 shows the aluminum block/brass tubing on top of a steel support block.

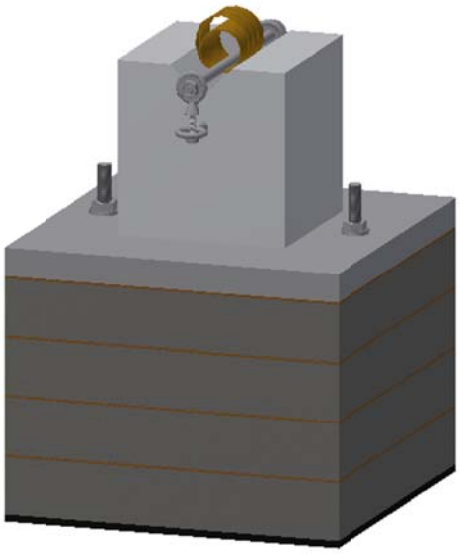

Figure 2.2: Aluminum block with brass tubing secured to a stack of steel blocks.

Animal platform: The animal platform holds the animal in place and slides along the linear rail structure. The platform rides between the two halves of the linear rail fixture via linear bushings (pillow blocks). Silicone lubricant coats the rails to reduce friction. The platform consists of a plate bolted to two pieces of rectangular tube. Two stainless steel impact cubes are bolted to the underside of the plate at opposite ends. One of these impact cubes is fixed to the animal head, and hosts the instrumentation to record the impact. Both of the steel cubes strike brass tubing, which rapidly decelerates the platform, causing injury to the animal. Having

symmetry limits the amount of rotation that occurs during the event. The platform accommodates an aluminum head restraint that is fitted to the animal.

Winch attachment: A winch is used to lift the device up to the desired drop height. To support the winch, two U-channels are attached to the top aluminum angle of each half of the linear rail frame with another U-channel, to which the winch is mounted, spanning between them. These U-channels accommodate higher drop heights.

The animal attaches to the platform in the supine position. The winch hoists the platform up to a desired height and synthetic string spans between the winch strap and a strap wrapped around the platform. This string is cut to drop the animal/platform.

2.1.2 Combined Translation and Rotation-Input Injury Device

The combined translation and rotation-input injury device is shown in Figure 2.3. The overall dimensions are approximately 183 x 30 x 147 cm. It is a two-segment compound pendulum that rapidly decelerates when impacting brass tubing, after Parnaik et al. (2004). The device has been broken down in to five primary components: support structure, aluminum block/brass tubing, aluminum hinges, aluminum platforms, and winch attachment.

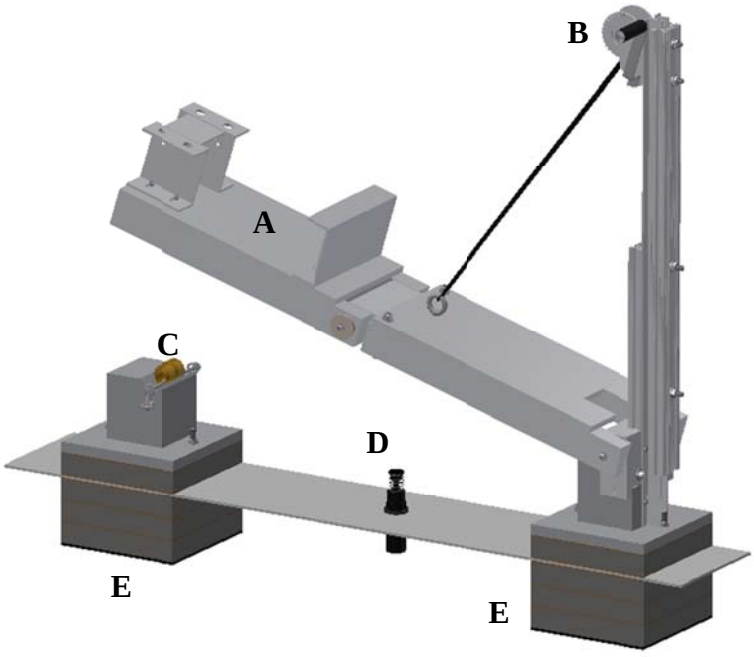

Figure 2.3: Combined translation and rotation-input injury device.

A: Animal platform; B: Winch; C: Brass Tubing; D: Damper; E: Steel Blocks.

Support structure: The support structure allows the device to stand on its own and holds the apparatus in place during an impact event. This support structure includes two blocks consisting of a stack of four hot rolled steel plates separated by leather sheets. Threaded rods insert through the top three plates of each block, and thread in half-way through the bottom plates to tie each stack together. Between the bottom plates and the ground is a sheet of vibration damping pad. Between the top and second plates is a flat stock steel plate that spans both steel blocks. There is a heavy-duty shock absorber on this steel plate to arrest the device after an impact.

Aluminum platforms: Two aluminum platforms are connected to each other by a hinge, and one of the platforms (the "base platform") is connected to the base of the device by a second hinge. The platform farthest from the base is the one to which the animal attaches (the "animal platform"). Each platform consists primarily of a plate and a set of two rectangular tubes. On each set of rectangular tubes, a 3.8-cm diameter bore was made in the end to accommodate stainless-steel hinge pins. Four aluminum plugs are fitted in to the ends of each tube to aid in the hinge pins for both platforms. On the base platform, aluminum blocks inserted in the rectangular tubing reinforce the interface between the hinge and the base platform.

A steel impact cube is bolted in to the underside of the animal platform. The animal head is attached to the plate of this platform using a bolt passed through the impact cube. This bolt threads in to a stainless steel slug attached to the animal skull. The impact cube strikes brass tubing, causing the rapid deceleration of the device and animal. The impact cube also hosts the instrumentation used to characterize the impact. On the top of the animal platform, two hole-patterns allow a hindquarter restraint and head restraint to be fitted to each animal to prevent decoupling.

Aluminum block/brass tubing: On one of the steel blocks, an aluminum block is attached to the top of the stack using the threaded rods that tie the stack together. The top of the aluminum block has a V-shaped channel used to position and fasten the brass tubing. Two sets of eyebolts are used to tighten a carriage bolt in place through the brass tubing. This keeps the brass tubing secured and in position during impact.

Aluminum hinges: The other steel block supports an aluminum assembly that serves as the base hinge for the two aluminum platforms. One section of the assembly has a 5.1-cm

diameter hole to accommodate two bronze sleeves that serve as bearings for 3.8-cm diameter stainless steel shaft (hinge pin). This hinge connects the base platform to the rest of the fixture, allowing the compound animal/base platform pendulum to rotate as one unit when initially dropped.

A second hinge connects the animal platform to the base platform. This hinge also consists of a 5.1-cm diameter bore that accommodates a stainless steel pin. Bronze sleeves are used as hinge bearings. A stainless steel stop prevents the angle between the platforms from exceeding 180 degrees.

Winch attachment: A reinforced mast made from aluminum angle supports a winch, which lifts the platforms up to the desired drop height. The mast is bolted to the base hinge. An eyebolt on the base platform allows the winch strap to directly connect to the device.

Similar to the translation-input injury device, synthetic string is looped between the winch strap and eyebolt to prepare for an impact event. The string is cut to release the device. When released, the aluminum platforms are kept at a constant angle (180 degrees) by wedging a small piece of copper tube between them at the hinge. Abrupt deceleration occurs when the steel impact cube bolted to the underside of the animal platform contacts brass tubing. At impact, the copper tube crushes, allowing the aluminum platforms to rotate with respect to each another. This action serves to lengthen the time of rotational motion, and increases the change in angular speed by affecting a change in the direction of motion during impact. At the end of the event, overall motion is stopped by a damper that sits on the steel plate of the support structure beneath the body of the hinge between the two platforms.

2.1.3 Animal Surgical Preparation

The animals are rigidly attached to the devices to facilitate measurement of the kinematics applied to the head. Strong coupling ensures that the kinematics measured by the instrumentation on the impact block and those imparted to the head are identical. This is accomplished by performing surgical head preparation as described by Fievisohn et al. (2012).

First, a cruciate incision is made in the scalp and the skin is reflected. Six small segments of periosteum are dissected to allow for custom expandable bone screws (Figure 2.4), which do not penetrate the inner table of the skull, to be inserted along the edges of the parietal bone (between the nuchal crest and the coronal suture). These custom bone screws exert outward

pressure when a smaller bolt threads in to a larger bolt. A dental dam is used as a barrier between the skull and Bosworth Trim® dental cement (Bosworth® Company, Skokie, Illinois). The dental cement connects the bone screws to a cylindrical steel slug. This steel slug bolts in to the injury device through a steel cube, creating a rigid connection between the animal and the device (Figure 2.5). This steel cube also hosts the instrumentation to record the impact kinematics.

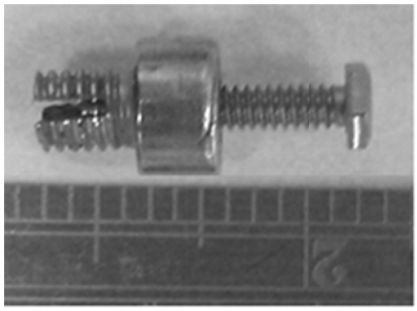

Figure 2.4: Custom expandable bone screw.

Figure 2.5: Slug (left), bone screws cemented to the skull (middle), and animal bolted in place (right).

A restraint system (Figure 2.6) further prevents any undesired decoupling or injury. There is an aluminum head restraint and hindquarter restraint (combined-input device only). Canvas wraps around the minipig abdomen and is tightened with straps. Importantly, a rigid piece of foam is placed underneath the neck to prevent neck flexion and associated brainstem injury.

Figure 2.6: Animal restrained in the translation-input (left) and combined-input injury device (right).

2.1.4 INSTRUMENTATION

Instrumentation in the impact cube consists of two linear accelerometers (7264-2000TZ-360), one angular accelerometer (7302BM4) (Meggitt Sensing Systems, San Juan Capistrano, CA), and one angular rate sensor (ARS PRO, DTS, Seal Beach, CA) (Figure 2.7). A TDAS Pro system records data at 20 kHz (DTS, Seal Beach, CA). Each channel is antialias filtered using a -3-dB point of 4300 Hz and an 8-pole Butterworth profile. High-speed video is used for overall observation.

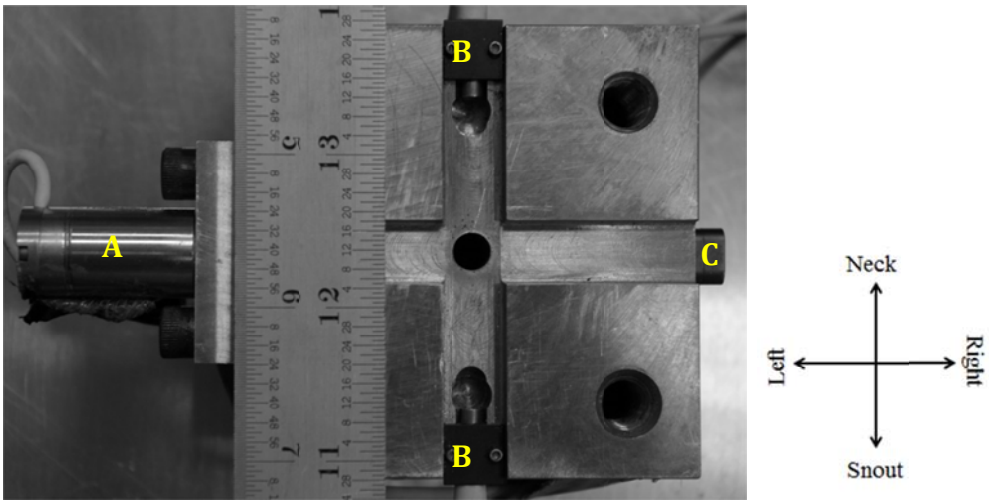

Figure 2.7: Instrumented steel cube (pig in supine position).

Angular accelerometer (A), linear accelerometers (B), angular rate sensor (C). Top (side toward animal head) shown.

The kinematics parameters of interest include linear acceleration, linear speed, angular acceleration, and angular speed. Linear acceleration is calculated by averaging the outputs of the two linear accelerometers, which are equidistant from the center of the slug in the median plane. Linear acceleration is integrated to get linear speed. Angular acceleration is calculated by taking the difference between the two linear acceleration measurements and dividing by the distance between the accelerometer seismic masses. Finally, angular speed is taken from the angular rate sensor when available or by integrating the angular acceleration. These signals are filtered using channel frequency class (CFC) 1000 Hz for linear and angular acceleration and 180 Hz for linear and angular speed, according to the SAE J211 standard (Society of Automotive Engineers, 2007).

2.2 REPEATABILITY TESTS

To test the repeatability of the two devices, Göttingen minipig carcasses were used (one for each device) and prepared identically as explained previously.

Five tests were conducted using the translation-input injury device. The carcass was dropped from a height of 55.9 cm as measured from the top of the aluminum block to the bottom edge of the plate of the animal platform. Two combinations of butted and nested brass tubes having varying diameter, wall thickness, and length, were used to program the deceleration pulses. These tube combinations are described in Table 2.1.

Four tests were conducted using the combined-input injury device. The minipig carcass was dropped from an angle of 15° from horizontal on to the brass tubing combinations described in Table 2.1.

Table 2.1: Brass tubing used for each injury device.

	Diameter (cm)	Thickness (cm)	Length (cm)	Quantity
Translation-input device (2 sets)	5.08	0.081	1.27	2
	5.08	0.165	1.27	1
	3.81	0.081	5.08	1
Combined-input device	5.08	0.081	2.54	2
	5.08	0.165	1.27	1
	3.81	0.081	7.62	1

Linear acceleration, linear speed, angular acceleration, and angular speed from the five trials of the translation-input injury device and the four trials of the combined-input injury device were analyzed using CORA v.3.6.1 (CORrelation and Analysis; Partnership for Dummy Technology and Biomechanics, Ingolstadt, Germany) (Gehre et al., 2009). This software was developed to provide an objective way to compare data. For example, this type of analysis could be used to determine if an ATD is characteristic of post-mortem human surrogate responses for the same test. This software compares curves using a corridor rating and a cross correlation rating. To evaluate device repeatability, only the cross correlation rating was used. The cross correlation rating is calculated by shifting the reference curve by a time step along the full time interval. At each increment, the cross-correlation value is calculated. At the maximum cross-correlation value, the phase shift, size, and progression (shape) values are quantified to get the overall cross correlation rating. The results range between 0 and 1, with 1 being a perfect match. All CORA recommended parameters were used to compare curves between 0 and 50 ms, using the first test as the standard for each device.

2.2.1 RESULTS

2.2.1.1 Translation-Input Injury Device

Plots of filtered linear acceleration, linear speed, angular acceleration, and angular speed for the repeated tests are shown in Figure 2.8. The CORA analyses resulted in a score of 0.978 for the linear acceleration traces and 0.980 for the linear speed. Angular acceleration and speed resulted in scores of 0.377 and 0.497, respectively.

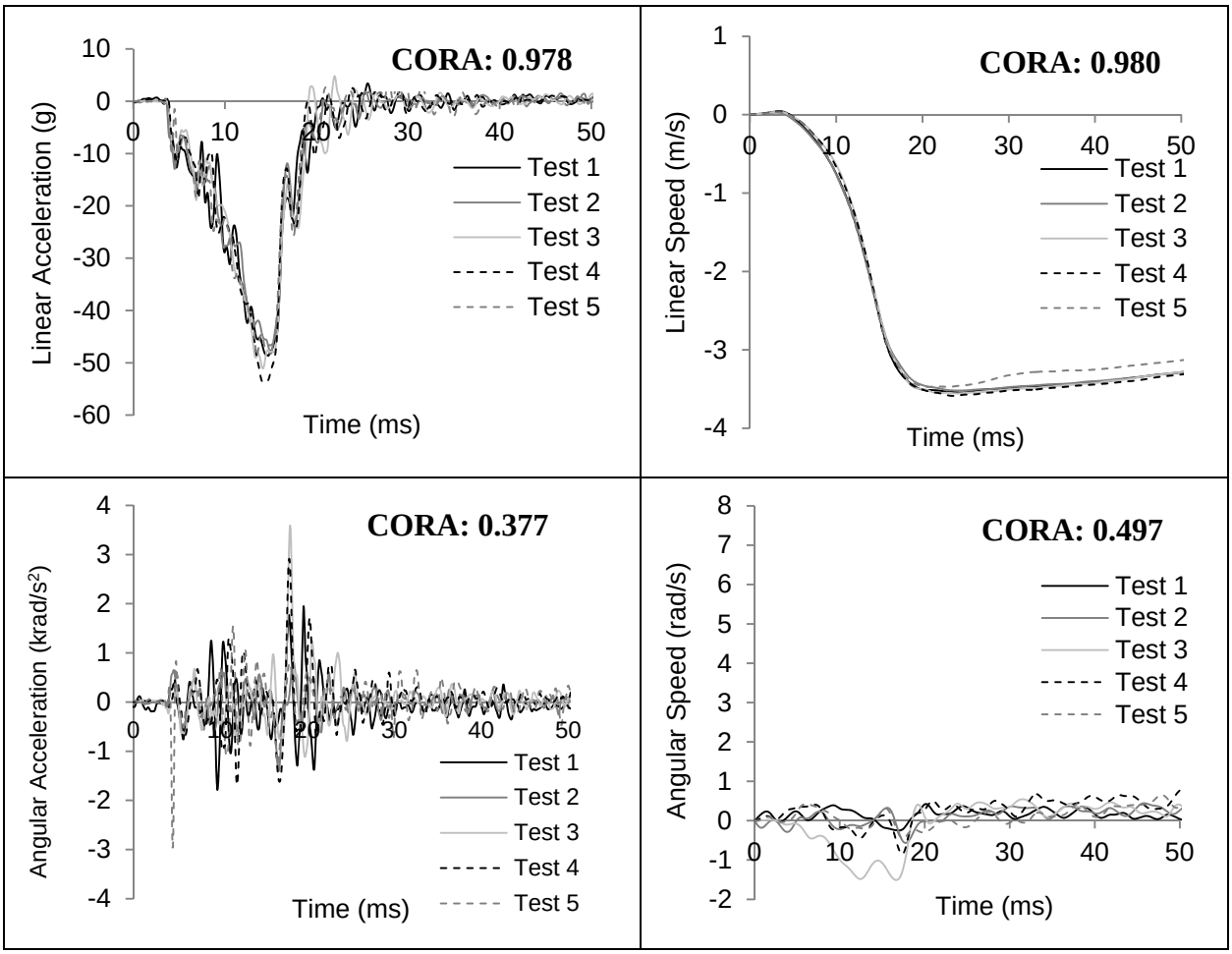

Figure 2.8: Kinematics traces from five tests with the translation-input injury device.

2.2.1.2 Combined Translation and Rotation-Input Injury Device

Plots of the filtered linear acceleration, linear speed, angular acceleration, and angular speed for the repeated tests are shown in Figure 2.9. The CORA analyses resulted in a score of 0.994 for the linear acceleration traces, 0.997 for the linear speed, 0.893 for the angular acceleration comparisons, and 0.999 for the angular speed comparisons.

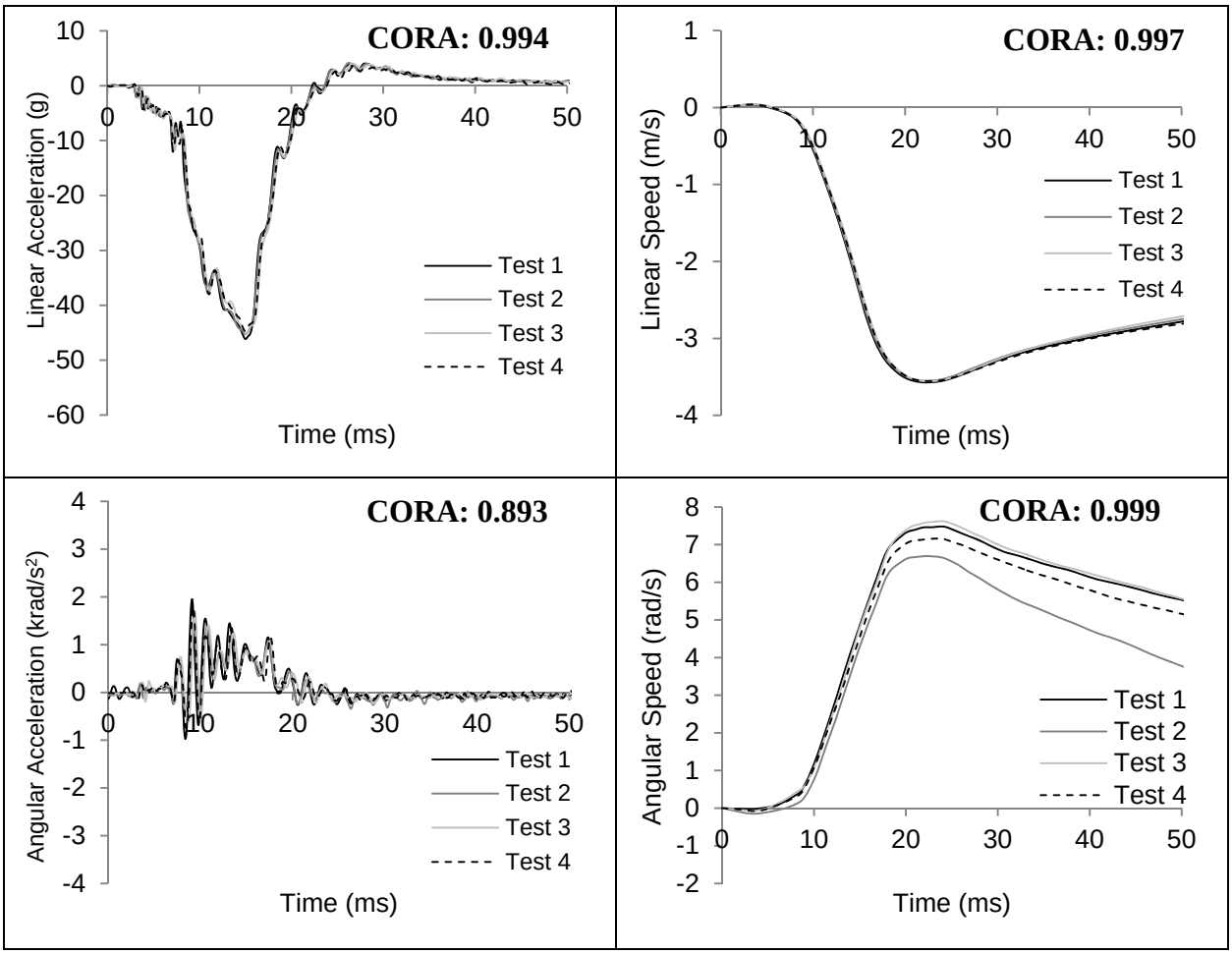

Figure 2.9: Kinematics traces from four tests with the combined-input injury device.

2.2.2 DISCUSSION

A repeatability analysis was conducted to evaluate two unique injury devices. Limitations include multiple testing on a single day and thus analyses could benefit from conducting tests on different days and also from moving the devices to a different location to assess reproducibility.

CORA software also has some limitations. It was developed to provide an objective way to compare curves. The parameters can be adjusted according to application, but this also means that the parameters could be altered to produce different results. This takes away from the goal of objectivity. In addition, the global meaning of the score is unknown. There is not a standard CORA rating to define similar versus different curves. However, this rating does provide a numerical value to comparing curves instead of a qualitative assessment.

Two unique devices were fabricated to induce non-penetrating impact-based injuries in the Göttingen minipig. The translation-input injury device produced repeatable tests with CORA

ratings for the linear acceleration and linear speed above 0.97. The angular acceleration and angular speed had much lower CORA scores between 0.3 and 0.5. However, the angular kinematics were low enough to essentially have the characteristics of noise, thus large CORA scores were not expected. This reinforces the fact that angular motion is minimal (e.g. angular speed falls between ± 2 rad/s). The combined translation and rotation-input injury device produced repeatable tests, with all of the CORA ratings above 0.89 out of 1. This level of repeatability helps to minimize the number of animals required for testing, as the bulk of the experimental variability stems from the animals.

CHAPTER 3: *IN VIVO* RESEARCH METHODS

The following chapter describes the *in vivo* research methods used to achieve the results expressed in the remaining chapters.

3.1 ANIMAL PREPARATION AND IMPACT EVENT

Female Göttingen minipigs (Marshall BioResources, North Rose, NY, USA) averaging 22.03±1.39 weeks old, having approximately 10-kg mass, were impacted using either the translation-input injury device or the combined translation and rotation-input injury device to induce impact-TBI. Sham animals were treated identically except for the impact event. Table 3.1 describes experimental groups based on impact mode and survival time. All animal protocols were approved by the Wake Forest University Baptist Medical Center's Animal Care and Use Committee (A10-151, A12-113, and A13-152).

Table 3.1: Experimental groups sizes (n).

Group	Survival Time		
	1 hour	24 hour	72 hour
Translation-input injury	0	11	2
Combined-input injury	3	10	2
Sham	0	3	0

Animals were sedated with an oral dose of midazolam (1 mg/kg). Isoflurane was used for anesthesia (3-5% induction, 2-3.5% maintenance). Animals were intubated and ventilated throughout. Intravenous fluids were delivered through one of the auricular veins for all surgical, impact, and imaging procedures.

All animals (including shams) underwent sterile surgical head preparation. The incision site was shaved and scrubbed three times, alternating 70% isopropyl alcohol with betadine prep pads. Bupivacaine (0.25%) was given subcutaneously around the incision site serving as a local anesthetic and buprenorphine (0.05 mg/kg) was given intramuscularly for analgesia. A cruciate incision was made in the scalp and the skin reflected. Six small segments of periosteum were removed to allow for custom expandable bone screws (described previously), which do not penetrate the inner table, to be inserted in to crown of the skull along the margins of the parietal bones between the nuchal crest and the coronal suture. A sterile dental dam was used to create a

barrier between the skull and Bosworth Trim® dental cement (Bosworth® Company, Skokie, IL, USA). The dental cement was used to connect the bone screws to a cylindrical steel slug (2.5-cm diameter, 2.5-cm long). This steel slug is fixed to the injury devices via a bolt passed through the impact (instrumentation) block and animal platform. The surgical procedures were identical for both experimental and sham animals.

Animals were attached to the injury devices as described previously. In addition to the kinematics parameters that were collected, HIC, BrIC, HIP, and CC were calculated (Eqn. 3.1, 3.2, 3.3,and 3.4 respectively). Only parameters in the median plane were used because the impacts were constrained to this plane. For calculating HIP, the entire equation was used for the combined-input group and only the translational components in the equation were used for the translation-input group (the angular acceleration term was ignored; Eqn. 3.3). The average critical angular velocity in the median plane was scaled from Takhounts et al. (2013). Based on the principles of equal stress/velocity scaling, the critical velocity in y of 56.45 rad/s for humans is 163.27 rad/s for the Göttingen minipig. For calculating HIP, the pig head mass was estimated to be 1.27 kg and the mass moment of inertia in y was 0.002615 Nms^2. Peak linear and angular accelerations were scaled based on the principles of equal stress/velocity for calculation of the CC (Eqn. 3.4). For the translation-only impacts, the angular acceleration terms in the CC equation were ignored.

$$\mathrm{HIC}_{15} = \left[\frac{1}{t_2 - t_1}\int_{t_1}^{t_2} a\,dt\right]^{2.5}(t_2 - t_1), \qquad \text{(Eqn. 3.1)}$$

Where a is the resultant linear acceleration measured at the center of gravity of the head.

$$\mathrm{BrIC} = \frac{\omega_y}{\omega_{yC}}, \qquad \text{(Eqn. 3.2)}$$

Where ω_y is the maximum angular velocity in y and ω_{yC} is the critical angular velocity in y.

$$\mathrm{HIP} = ma_y \int a_y dt + I_y \alpha_y \int \alpha_y dt, \qquad \text{(Eqn. 3.3)}$$

Where:

m = mass of the pig head

a_y = linear acceleration in y

α_y = angular acceleration in y

I_y = mass moment of inertia in y

$$CC = \beta_0 + \beta_1 a_{res} + \beta_2 \alpha_{res} + \beta_3 a_{res} \alpha_{res}, \quad \text{(Eqn. 3.4)}$$

Where:

$\beta_0, \beta_1, \beta_2, \beta_3$ are coefficients of logit and are -10.2, $4.33e^{-2}$, $8.73e^{-4}$, and $-9.20e^{-7}$, respectively

a_{res}=peak resultant translational acceleration (G)

α_{res}=peak resultant rotational acceleration (rad/s^2)

After the impact event, the steel slug, dental cement, and bone screws were removed and the scalp incision was sutured before post-impact scanning. Animals that survived until a 24-hour post-impact scan were aroused after the immediate post-impact scan and were monitored overnight. Buprenorphine was administered every 8-12 hours (0.05 mg/kg). Animal preparation for scanning was identical to that described above starting with sedation with midazolam, etc. For animals that survived until a 72-hour post-impact scan, the cycle of animal monitoring and administering buprenorphine continued until the 72-h scan.

3.2 ^{1}H-MAGNETIC RESONANCE SPECTROSCOPY

A 7T Bruker Biospin MR scanner (Bruker Biospin, Billerica, MA, USA) in the Radiology Department at the Wake Forest University Baptist Medical Center was used to perform ^{1}H-MRS scans using a custom two-channel quadrature radiofrequency coil (Doty Scientific, Columbia, SC, USA). This custom coil accounted for the large tissue volume of the minipig head, and was designed to be short enough to allow proper positioning of the minipig brain at the isocenter. Metabolites were measured within a 216-mm^3 voxel placed in the genu of the corpus callosum (Figure 3.1). Two spectra were acquired from every ^{1}H-MRS voxel. The first spectrum was taken without water suppression and was used as a reference (32 signal averages). The second spectrum was the metabolite spectrum with water suppression (1600 signal averages). ^{1}H-MRS scans were taken at baseline, 1 hour, 24 hours, and up to 72 hours after impact.

After the scans were acquired, LCModel software (Version 6.3; Stephen Provencher Inc. Oakville, Ontario, CA) was used to resolve and quantify the metabolites in to concentrations (mM) with an associated goodness of fit, calculated as Cramér-Rao Lower Bound (CRLB). Water-scaling (factor that scales metabolite values based on the estimated concentration of the water peak in the voxel compared to the unsuppressed water signal) was used to obtain

institutional concentrations for metabolites including alanine, aspartate (Asp), creatine (Cr), phosphocreatine (PCr), γ-aminobutyric acid (GABA), glucose, glutamine (Gln), glutamate (Glu), glycerophosphocholine (GPC), phosphocholine (PCh), myo-inositol (Ins), lactate, N-acetylaspartate (NAA), N-acetylaspartylglutamate (NAAG), scyllo-inositol (Scyllo), taurine, and combinations of more than one metabolite such as GPC+PCh (Cho or cholines), NAA+NAAG, Cr+PCr (Cre), and Glu+Gln. The concentrations were corrected for the amount of white matter present in the voxel. Two of the animals had ^{1}H-MRS scans with only 1080 signal averages instead of 1600, which was corrected for in the water-scaling of the data.

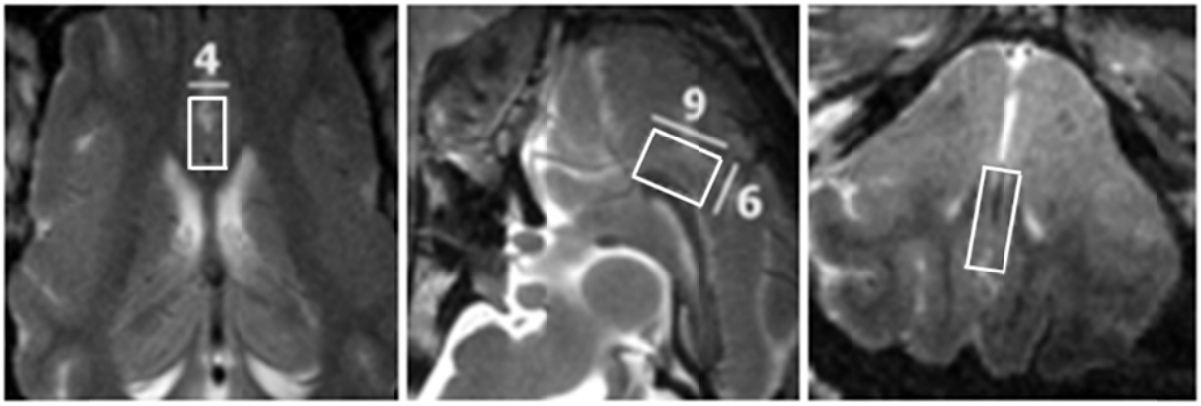

Figure 3.1: ^{1}H-MRS voxel in the genu of the corpus callosum.

3.3 IMMUNOHISTOCHEMISTRY

After the final post-impact scan was completed, the animals underwent perfusion to flush the vasculature with heparinized saline and then 4% paraformaldehyde for brain fixation. As soon as the perfusion was started, the animals were euthanized (150-200 mg/kg of sodium pentobarbital in Beuthanasia-D). The Virginia Tech Animal Laboratory Services at the Virginia-Maryland College of Veterinary Medicine embedded sections containing the genu of the corpus callosum (Figure 3.2) in paraffin and sectioned them at approximately 4 μm.

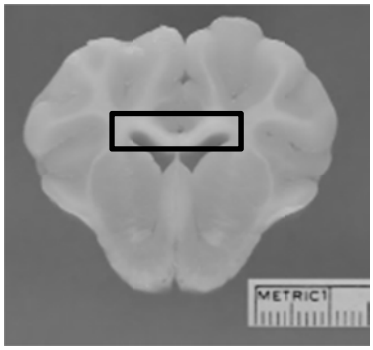

Figure 3.2: Coronal section of a pig brain with a box around the genu of the corpus callosum.

Underlying brain pathology was characterized using immunofluorescent staining, which identified axon cytoskeleton damage by highlighting light and heavy neurofilament (NF) chains, astrocyte activation by binding with glial fibrillary acid protein (GFAP), apoptosis by labeling with cleaved caspase-3, complete axonal disruption by labeling beta-amyloid precursor protein (β-APP), and microglial activation with ionized calcium-binding adaptor molecule-1 (Iba-1).

3.3.1 IMMUNOFLUORESCENT STAINING PROTOCOL

3.3.1.1 Deparaffinization, Rehydation, and Antigen Retrieval Protocol

Slides containing sections of genu were first deparaffinized in xylene twice for five minutes, then immersed in 100% ethanol twice for three minutes and in 95% ethanol for one minute. Next, slides were rinsed in distilled water and placed in a microwavable vessel containing sodium citrate buffer for antigen retrieval. The vessel was heated until the solution boiled and then for an additional 20 minutes. Slides were cooled with running distilled water for 10 minutes.

3.3.1.2 Staining Protocol

For immunostaining, the slides were washed thoroughly in phosphate-buffered saline (PBS) three times for five minutes each. Then, the slides were incubated in blocking buffer for one hour. Primary antibody solution was added for two stains per set of slides as shown in Table 3.2. The slides stayed in primary antibody solution overnight at 4°C. Next, the slides were rinsed in PBS three times for five minutes each. Subsequently, secondary antibody was added using a concentration of 1:100 to fluorescently label one stain in the set with fluorescein isothiocyanate (FITC) or a green color (FITC-AffiniPure Donkey Anti-Mouse IgG, Jackson

ImmunoResearch Laboratories Inc, West Grove, PA, USA; or Donkey anti-Goat IgG-FITC, sc-2024, Santa Cruz Biotechnology, Inc., Dallas, TX, USA), and the other stain in the set with Alexa Fluor or a red color (Alexa Fluor 555 Donkey Anti-Rabbit IgG, Life Technologies™, Grand Island, NY, USA). After the slides were incubated at room temperature in secondary antibody for 1.5 hours, the slides were washed in PBS three times for five minutes each. The slides were dried before SlowFade® Gold anti-fade reagent with DAPI (Life Technologies™, Grand Island, NY, USA) was used to label cell bodies with DAPI (4', 6-diamidino-2-phenylindole) or a blue color. Finally, coverslips were applied.

Table 3.2: Primary antibodies used for immunohistochemistry.

Set	Description	Antibody	Company	Color	Dilution
1	Light NF	Anti-68 kDa light NF	Abcam®	FITC	1:100
	Heavy NF	Anti-200 kDa heavy NF	Abcam®	Alexa Fluor	1:100
2	Astrocyte Activation	Anti-GFAP	Abcam®	FITC	1:100
	Programmed Cell Death	Anti-Caspase-3	Abcam®	Alexa Fluor	1:100
3	Microglia Activation	Anti-Iba-1	Abcam®	FITC	1:100
	Axonal swelling	Anti-Amyloid Precursor Protein	Life Technologies™	Alexa Fluor	1:100

3.3.2 IMAGE ANALYSES

Images were taken with a Zeiss Axiovert 40 CFL (Carl Zeiss Microscopy, Oberkochen, Germany). Three to five images were taken in the genu of the corpus callosum, which was assumed to represent the distribution of stain throughout the entire region. The images were taken using 20x magnification.

An image analysis technique was developed to address different exposure times and contrast for images taken between microscope bulbs. This technique also accounted for variation between different batches of antibodies. The process required that seven pixels be selected ranging from high to low intensity within the stained portions of the image. The highest and lowest values of red, green, and blue values were taken from these points and used to evaluate all pixels within the image. If a pixel fell within these ranges, then the pixel intensity was changed to blue. If the pixel does not meet these criteria, then it was changed to black. This essentially marked all of the pixels that were stained. A custom macro was developed for use in ImageJ (NIH, Bethesda, MD, USA). Two slides were stained per animal and the stained pixel

percentages were averaged. An example of a GFAP stained image and the corresponding processed image are shown in Figure 3.3.

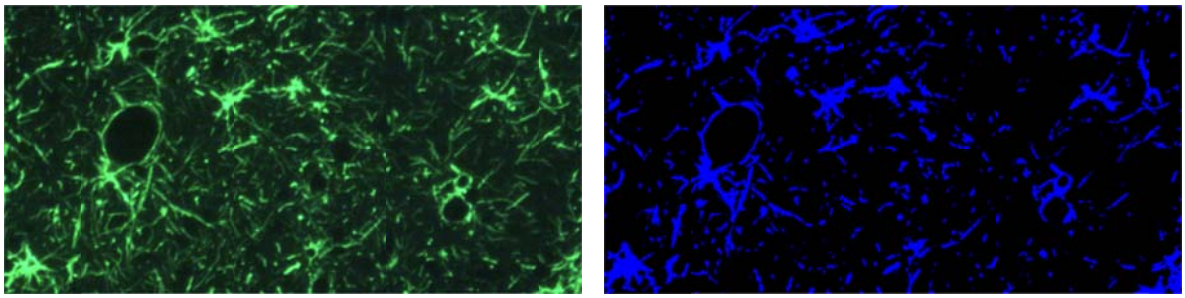

Figure 3.3: GFAP stained original image (left) and the corresponding processed image (right).

3.4 STATISTICAL ANALYSES

3.4.1 ^{1}H-MRS

Only metabolite values with a CRLB of less than 50 were included. Outlier analyses were completed in SPSS Statistics 17.0 (SPSS Inc., Chicago, IL, USA) and data points that were more than three times the interquartile range were excluded from further analyses. The baseline scan from one animal of the combined-input injury device group was excluded because the LCModel software did not produce a good visual curve fit and the baseline concentrations did not fall within the rest of the dataset. Data were excluded if the paired metabolite was not resolved also. For example, if NAA could not be resolved from NAAG, only NAA+NAAG was analyzed. The metabolite concentration time points included varying sample sizes. For the translation-input injury device group, one animal did not have a 24-hour metabolite scan, ten animals survived 24 hours after impact, and two survived 72 hours after impact. For the combined-input injury device group, three animals survived only 1 hour after impact and therefore did not have 24-hour data for comparison. Ten animals survived 24 hours after impact, but two of them did not have useable metabolite scans, and two survived 72 hours. Table 3.3 shows the animals included in the metabolite analyses (not including the values triaged through the exclusion criterion described above).

Metabolite concentrations were compared using repeated measures analysis of variance (ANOVA) with least significant difference (LSD) post-hoc test, which simplified to paired Student's t-tests for missing time points, to evaluate differences between baseline, 1-hour, and 24-hour metabolite concentrations. The 72-hour survival animal metabolite concentrations were

used for extra data points for the baseline, 1-hour, and 24-hour time point. Both pure metabolite concentrations and ratios between them were compared. For example Glu values between time points were compared, but also the ratio of Gln to Glu (Gln/Glu), as these can give insight in to the injury cascades. A p-value less than 0.05 was considered statistically significant.

Table 3.3: Number of animals included in the ^{1}H-MRS analyses per time point.

Group	Time point		
	Baseline	1 hour	24 hour
Translation	13	13	12
Combined	13	13	10

3.4.2 IMMUNOHISTOCHEMISTRY

Two-tailed Student's t-tests were used to compare sham animal average stained pixel percentages (n=3) to all 24-hour impact average stained pixel percentages within each experimental group (n=11 for translation-input, n=10 for combined-input). A p-value less than 0.05 was considered statistically significant. There were not enough animals in the 1-hour or the 72-hour time point experimental groups to allow for statistical comparisons, therefore only the 24-hour time point was evaluated.

3.5 LINEAR REGRESSION ANALYSES

Correlations between significant ($p<0.05$) and trending ($p<0.1$) metabolite changes from the 24-h impact characterization, statistically significant immunohistochemistry results, and kinematics were calculated using SPSS Statistics 17.0 (SPSS Inc., Chicago, IL, USA) to find relationships between neurochemical responses, underlying damage, and kinematics. Kinematics parameters included linear and angular acceleration, linear and angular speed, HIC, BrIC, HIP, and CC. For metabolite relationships found between a kinematics and a staining parameter, multiple linear regressions with ANOVAs were conducted to determine if the metabolite and kinematics changes could be used to predict the immunostaining parameter. A p-value of less than 0.05 was considered statistically significant.

3.6 72-HOUR ANIMAL ANALYSES

There were only two 72-hour survival animals impacted with each injury device, thus no statistical comparisons could be made. Trends in the metabolite concentrations are represented as

the individual animals' concentrations in relation to the averages of the baseline, 1-h, and 24-h time points.

CHAPTER 4: IMPACT RESPONSE CHARACTERIZATION OVER THE COURSE OF 24 HOURS

The results and discussion presented here represent the metabolic changes over the course of 24 hours and the underlying disruption quantified in animals that survived 24 hours.

4.1 TRANSLATION-INPUT INJURY

4.1.1 RESULTS

4.1.1.1 Experimental Groups, Kinematics, and Gross Findings

Eleven animals that were impacted using translation-input injury device survived 24 hours. The 72-hour (n=2) survival animals were also included in the metabolite analyses. Linear acceleration ranged between 27.5-70.2 g and linear speed ranged between 2.7-3.5 m/s. The impact kinematics are catalogued in Table 4.1. Kinematics traces are provided in Appendix C. Raw data are presented in Appendix D. Error from integrating the linear acceleration to get linear speed is tabulated in Appendix E. A sequence of still images from a translation-input impact event is shown in Figure 4.1.

Three of the translation-input injury group animals sustained distributed cortical contusions. These animals were impacted at average linear acceleration of 66.5±6.0 g and linear speed of 3.4±0.1 m/s. Figure 4.2 shows images of the brains with contusions (red discoloration) marked by arrows, and Hematoxylin & Eosin (H&E) stained cortical sections (10x) with arrows indicating pooled blood in the cerebral vasculature. H&E staining marks the nuclei blue and eosinophilic marks structures in various shades of red, pink, and orange. For example, the red blood cells are marked in bright red.

Table 4.1*: *Impact kinematics for the translation-input injury group animals.

Translation-Input Injury				
Pig #	Survival Time Duration (h)	Linear Acceleration Magnitude (g)	Linear Acceleration Duration (ms)	Impact Speed Magnitude (m/s)
1	24	55.8	17.5	3.0
2	24	27.5	23.0	2.9
3	24	61.1	13.1	3.5
4	24	66.1	13.1	3.4
5	24	39.4	19.4	2.7
6	24	38.4	17.9	2.7
7	24	43.3	17.5	2.8
8	24	70.2	13.4	3.4
9	24	69.8	13.0	3.5
10	24	59.6	14.2	3.3
11	24	62.1	13.7	3.4
12	72	67.9	13.7	3.5
13	72	66.0	14.1	3.4
	Average±SD	55.9±14.0	15.6±3.1	3.2±0.3

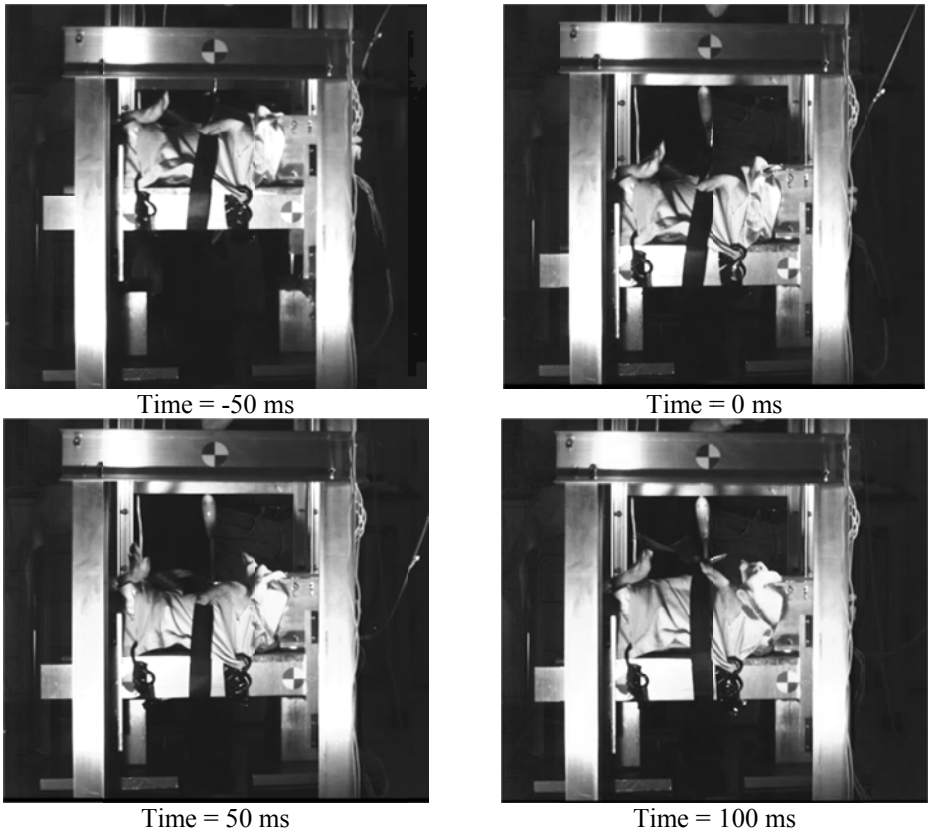

Figure 4.1: Still sequence from a translation-input impact event.

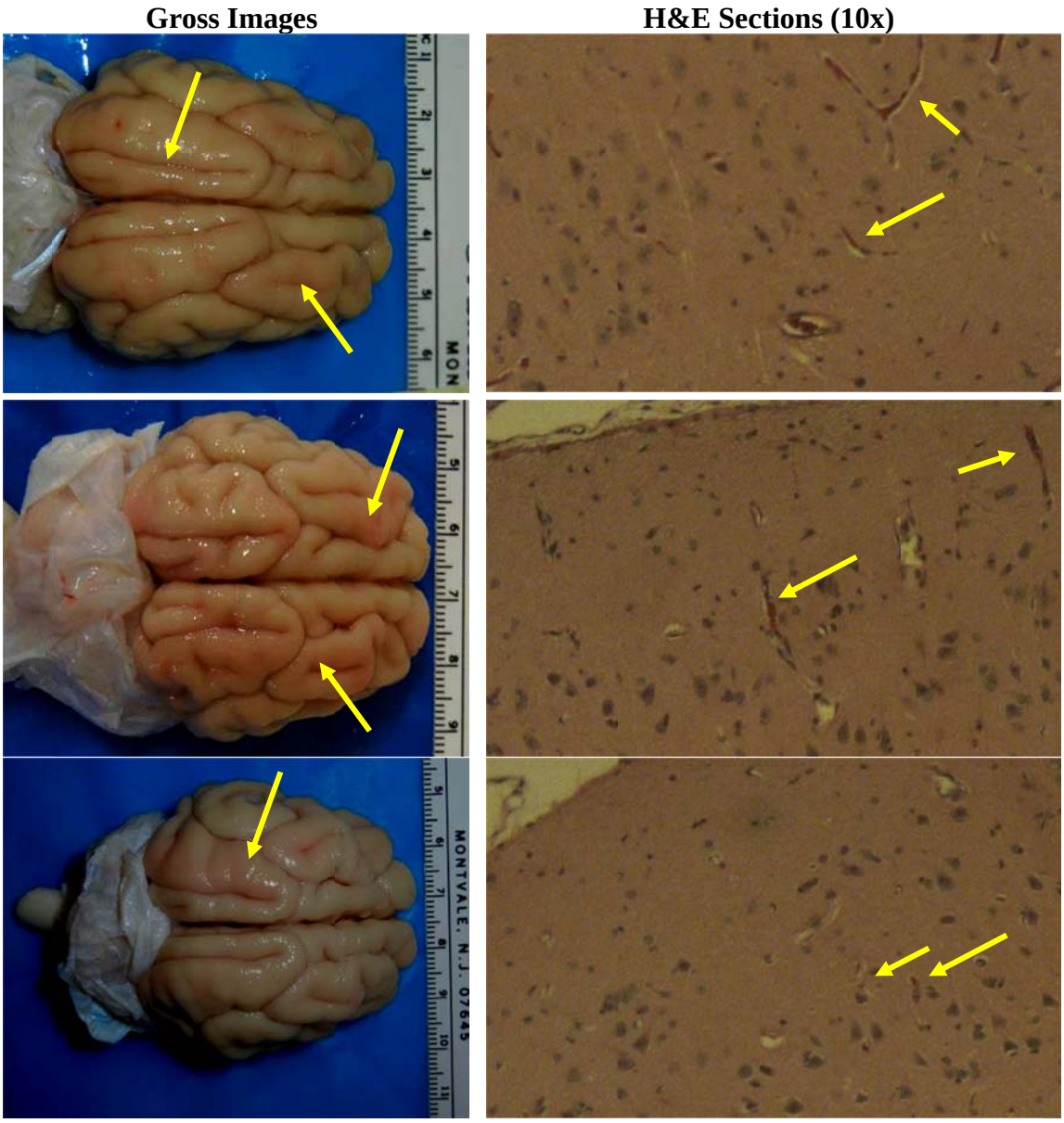

Figure 4.2: Brains with contusions (left) and H&E stained sections (right). Arrows mark contused areas (left) and pooled blood in the vasculature (right).

4.1.1.2 ^{1}H-MRS

One-hour post-impact scans were taken an average of 68±8 minutes. The next day scans were taken an average of 24 hours, 20±27 minutes after impact. Comparisons among ^{1}H-MRS metabolite concentrations show 20 significant relationships between baseline, 1 hour, and 24 hours after impact, as listed in Table 4.2. The bolded percentages are those that are common between the two experimental groups. Some of the metabolites were not resolved and therefore

could not be compared statistically. These included alanine, aspartate, GABA, glucose, lactate, taurine, Cr, PCr, GPC, and PCh.

Table 4.2: Translation-input injury group significant metabolic differences[1].

	Translation-Input Injury		
	1 h/ base	24 h/ base	24 h/ 1 h
Gln	22.3*	35.4**	
Glu	**14.0**		**25.9***
Scyllo			28.4
Cho		20.3*	**14.9***
Glu+Gln		**29.1****	**14.2***
NAAG/Scyllo			-16.6*
Gln/Ins	20.1		
Gln/Glu	27.1		
Gln/Glu+Gln	12.9*		
Glu/Glu+Gln	-7.3*		
NAA/Cho	**14.0****		**-13.3****
Cho/NAA+NAAG	**-6.7**	6.6*	**13.4****
Cho/Glu+Gln	**-7.9***		
Gln/Cho	**25.0****		
Glu/NAA	**-11.8***		**14.9***
Glu/NAA+NAAG			**10.7**
NAA/Glu+Gln			**-10.9***
NAA+NAAG/Glu+Gln			-6.4
Gln/Cre	17.6	**25.8**	
Cho/Cre			**11.6***

****p<0.05, **p<0.01, Unlabeled values have a p<0.1***

[1]The labels 1h/base, 24h/base, and 24h/1h indicate changes in the 1 h time point relative to the baseline, 24 h time point relative to the baseline, and 24 h time point relative to the 1 h time point.

4.1.1.3 Immunohistochemistry

For the immunohistochemical staining, the translation-input injury group at 24 h after impact displayed significant increases of 16.6±7.5% and 8.3±5.5% in light and heavy neurofilament, respectively, relative to the sham controls ($p<0.05$) (Figure 4.3). There were no significant differences found between experimental animals and sham animals for GFAP, cleaved caspase-3, or Iba-1. The β-APP staining revealed that there were no axonal swellings or complete axonal disconnections present in any of the animals.

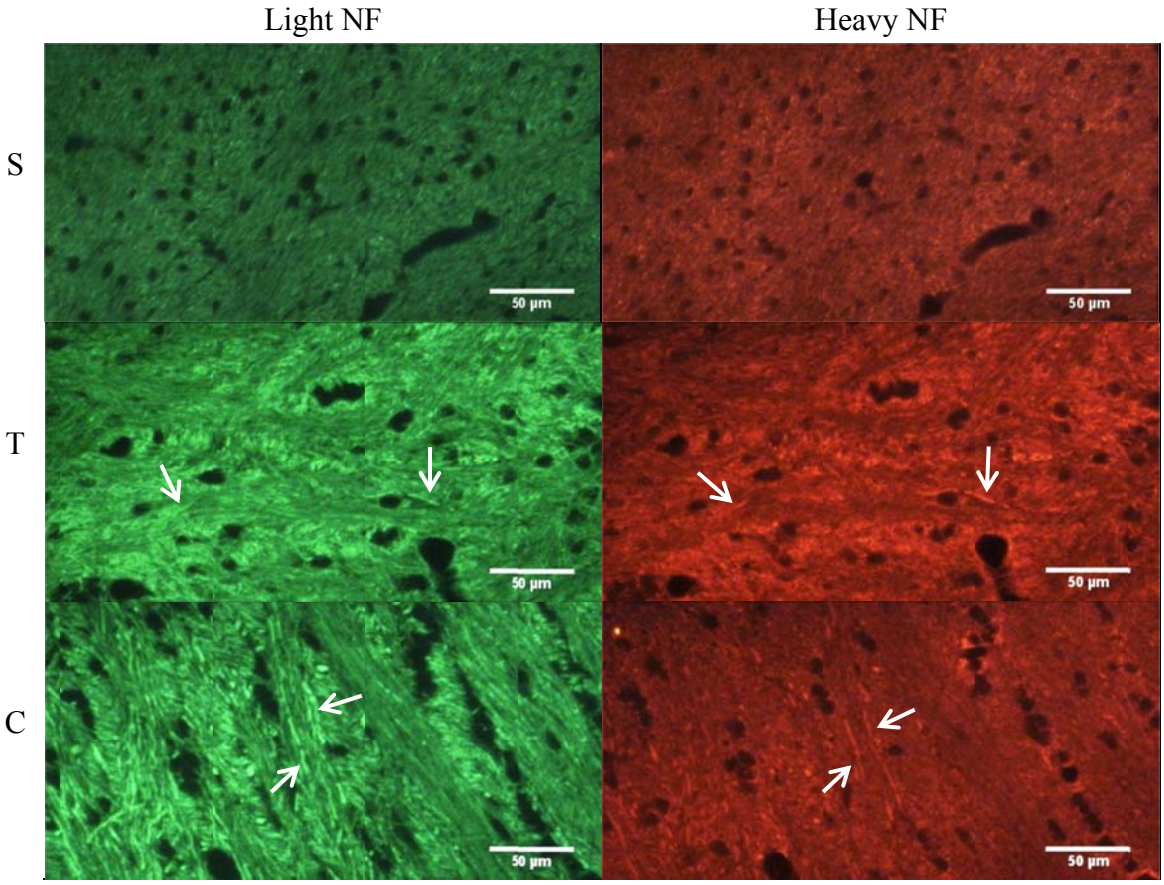

Figure 4.3: Immunostained sham (S), translation-input (T), and combined-input injury group animal (C).
A few of the highlighted NF chains are shown by arrows.

4.2 COMBINED-INPUT INJURY

4.2.1 RESULTS

4.2.1.1 Experimental Groups and Kinematics

Ten animals that were impacted using the combined translation and rotation-input injury device survived 24 hours after impact. The 1-hour (n=3) and 72-hour (n=2) survival animals were also included in the metabolite analyses.

For the combined-input injury group, animals were impacted using linear acceleration ranging between 40.0-106.5 g, linear speed ranging between 2.6-4.4 m/s, angular acceleration ranging between 1,014.5-4,492.6 rad/s^2, and angular speed ranging between 7.2-10.8 rad/s. The impact kinematics are cataloged in Table 4.3. Kinematics traces are provided in Appendix C. Raw data are presented in Appendix D. Error from integrating the linear acceleration to get linear

speed is tabulated in Appendix E. A sequence of still images from a combined-input impact event is shown in Figure 4.4.

Table 4.3: Impact kinematics for the combined-input injury group animals.

Combined-Input Injury							
Pig #	Survival Time (h)	Linear Acceleration		Impact Speed	Angular Acceleration	Angular Speed	
		Magnitude (g)	Duration (ms)	Magnitude (m/s)	Magnitude (rad/s^2)	Magnitude (rad/s)	Duration (ms)
1	24	40.1	19.9	2.6	1783.8	7.6	145.0
2	24	76.9	13.9	4.3	2524.0	10.3	122.2
3	24	95.9	13.6	4.2	3814.9	10.8	124.7
4	1	90.5	13.7	4.1	3005.7	10.8	106.4
5	24	60.4	16.2	3.6	1443.1	9.1	105.0
6	24	90.1	13.2	4.4	3324.9	10.5	111.6
7	24	62.4	14.6	3.7	1584.4	9.0	113.8
8	1	60.6	14.8	3.5	1699.7	9.1	112.6
9	1	41.2	16.2	2.7	1630.8	7.3	143.3
10	24	40.6	16.0	2.8	1474.8	7.2	133.5
11	24	56.4	14.5	3.5	2134.6	8.7	115.5
12	24	41.8	15.7	2.8	1760.5	7.4	146.0
13	24	57.1	15.2	3.5	1014.5	9.0	120.4
14	72	106.5	12.7	4.2	3180.9	10.6	116.1
15	72	101.6	13.4	4.1	4492.6	10.2	116.8
Average±SD		68.1±23.6	14.9±1.8	3.6±0.6	2324.6±1015.6	9.2±1.3	122.2±13.6

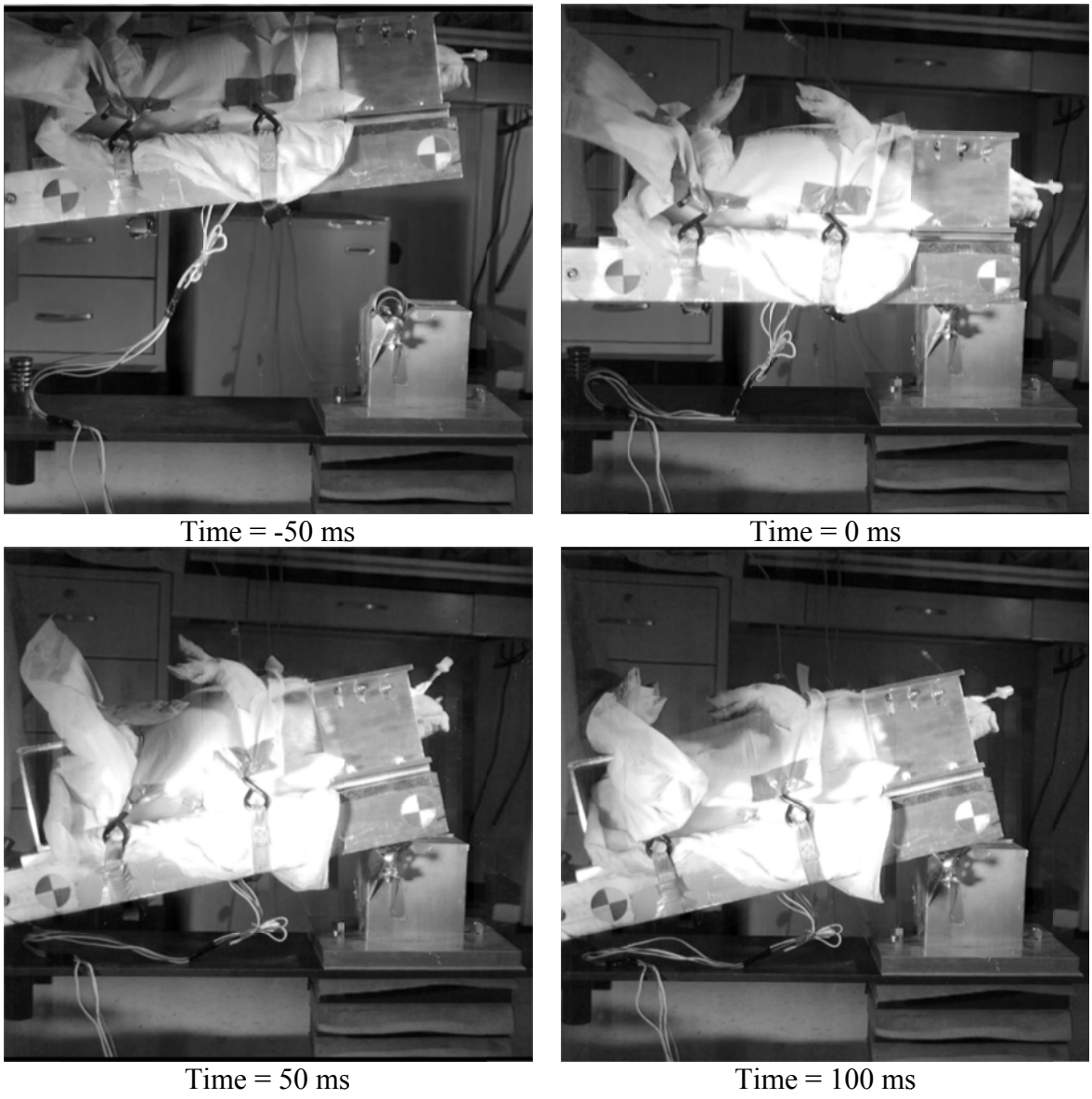

Figure 4.4: Stills from a combined-input impact event.

4.2.1.2 ^{1}H-MRS

The one-hour post-impact scans were taken an average 71±19 minutes. The next day scans were taken an average 24 hours, 49±36 minutes after impact.

Comparisons between ^{1}H-MRS scans show 36 significant relationships between baseline, 1 hour and 24 hours post-impact, as listed in Table 4.4. The bolded percentages are those that are common between the two experimental groups. Some of the metabolites were not resolved and

could not be compared statistically. These included alanine, Cr, PCr, GABA, GPC, PCh, glucose, lactate, and taurine.

Table 4.4: Combined-input injury group significant metabolic differences.

	Combined-Input Injury		
	1 h/ base	24 h/ base	24 h/ 1 h
Asp			24.0
Glu		**41.5****	**30.2***
NAA	14.1*		
Cho	-7.7*		**13.2***
Glu+Gln		**25.2***	**18.2**
Gln/Glu+Gln		-9.7*	-10.9
Gln/Glu		-14.9	
Glu/Glu+Gln		10.5*	14.3
NAA/NAAG	70.5		
NAAG/NAA+NAAG	-19.2		
NAA/NAA+NAAG	10.6		
Ins/Cho			-21.7*
Cho/Cre	-8.6		**17.1***
Gln/Ins		29.5	
Glu/Ins		55.2**	46.7**
Ins/Glu+Gln		-21.6*	
Glu/Scyllo	-15.0		
NAA/Cre	18.4		
NAAG/Cre			30.2
Asp/Cre			30.7*
Asp/Ins		37.4	44.1**
Ins/NAAG	87.9*	20.6	-19.2
Gln/Cre		**17.2***	
Glu/Cre		40.0**	34.0**
Glu+Gln/Cre		23.5**	23.4**
Gln/Cho	**26.6***		
Glu/Cho	16.5*	37.6*	
Cho/Glu+Gln	**-14.3****	-12.3*	
Asp/Gln	-19.5		
Gln/NAAG		43.9*	
Glu/NAA	**-13.3****		**38.3***
Glu/NAAG		59.6**	
Glu/NAA+NAAG		38.3**	**31.0***
NAA/Glu+Gln	13.5*		**-11.0**
NAAG/Glu+Gln		-26.4	
NAA+NAAG/Glu+Gln		-13.1*	
NAA/Cho	**26.7****		**-14.8**
NAAG/Cho		-18.3	
Cho/NAA+NAAG	**-10.5***		**13.1**

*p<0.05, **p<0.01, Unlabeled values have a p<0.1

[1]The labels 1h/base, 24h/base, and 24h/1h indicate changes in the 1 h time point relative to the baseline, 24 h time point relative to the baseline, and 24 h time point relative to the 1 h time point.

4.2.1.3 Immunohistochemistry

The combined translation and rotation-input injury group at 24 h after impact displayed significant increases of 14.4±6.5% and 19.3±11.1% in light and heavy neurofilament, respectively, relative to the sham controls ($p<0.05$) (Figure 4.3). There were no significant differences found between experimental animals and sham animals for GFAP, cleaved caspase-3, or Iba-1. The β-APP staining revealed that there were no axonal swellings or complete axonal disconnections present in any of the animals.

At 1 hour after impact, even though there were not enough animals to perform statistical analyses, the immunohistochemistry results did show both light and heavy neurofilament disruption (Figure 4.5).

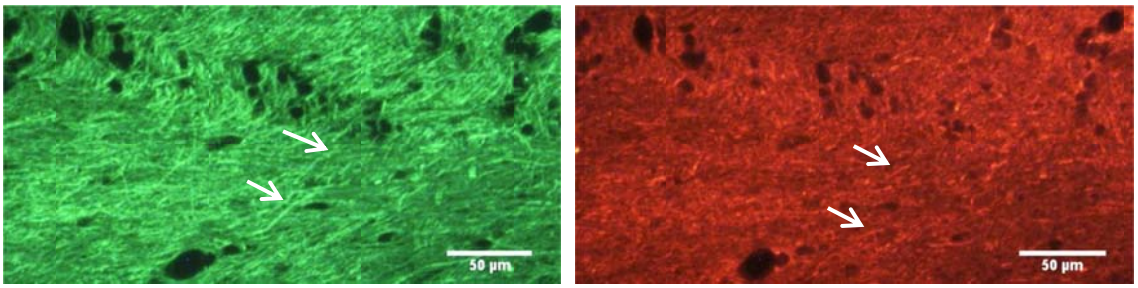

Figure 4.5: Immunostained images of a combined-input injury group animal at 1 h after impact with light (left) and heavy (right) NF chains.
A few of these highlighted chains are shown by arrows.

4.3 DISCUSSION

4.3.1 TRANSLATION-INPUT INJURY

The translation-input injury device produces an impact restricted to one direction with negligible rotation. Based on gross examination of the impacted brains, the threshold for developing cortical contusion is near linear acceleration of 60-70 g and linear speed of 3.3-3.5 m/s in the minipig. Further testing is needed to corroborate this observation.

The impact caused 20 significant metabolite changes in the genu of the corpus callosum. Overall, the impact response suggests the initial stages of glutamate excitotoxicity and membrane disruption.

Significant increases in glutamine at 1 hour and 24 hours after impact compared to baseline could be due to an energy crisis (insufficient amounts of ATP) related to an increase in glutamate. Glutamate excitotoxicity is a pathology implicated in numerous neurodegenerative

diseases such as TBI, epilepsy, and Parkinson's disease (Mehta et al., 2013). A relative abundance of glutamate in the extracellular space can provoke a toxic response. Overstimulation of glutamate receptors can lead to excess accumulation of intracellular calcium. This can ultimately trigger pathways that lead to neuronal death (Mark et al., 2001). Typically after glutamate has accomplished its role as an excitatory neurotransmitter, it is taken up by glial cells and inactivated using the enzyme glutaminase and ATP to store glutamate as glutamine until needed. This current study observed a significant increase in glutamate at 24 hours compared to 1 hour after impact, which indicates that there was an increase in glutamate that is initially subdued by converting it to glutamine. Also, at 24 hours compared to 1 hour, there is not a significant change in glutamine suggesting that there might be signs of glutamate excitotoxicity at longer time points. An increase in glutamine has been observed by Harris et al. (2012) in the contused cortex and hippocampal region (also contains corpus callosum and dorsal-most thalamic nuclei) of rats exposed to controlled cortical impact injury at approximately 1 hour and 24 hours after injury. Also, Lei et al. (2009) studied ischemic injury in rats and found increases in glutamine in the left striatum at 3, 8, and 24 hours after injury, and suggested that this increase might reflect astrocytes working to convert glutamate to glutamine to prevent an excitotoxic response.

There was also a significant increase in cholines at 24 hours compared to baseline and 24 hours compared to 1 hour after impact. Cholines are considered a biomarker for membrane phospholipid turnover (Moore and Galloway, 2002) indicating membrane disruption. Other studies have found increases in cholines in TBI patients. For example, Shutter et al. (2004) conducted ^{1}H-MRS scans in patients with TBI and found increases in cholines in gray and white matter, but also observed that it was an indicator of injury and is predictive of poor outcomes if measured early after injury (6-12 months).

4.3.2 COMBINED-INPUT INJURY

The combined translation and rotation-input injury device did not produce any gross signs of damage. The combined-input injury group did exhibit an underlying response, characterized by 36 significant metabolite changes over the course of 24 hours. Overall, the results are indicative of glutamate excitotoxicity and membrane disruption.

The significant increases in glutamate at 24 hours compared to baseline and relative to 1 hour indicate glutamate excitotoxicity. This is further supported by an observed decrease in the ratio of Gln/Glu at 24 hours compared to baseline ($p=0.058$). Ramonet et al. (2004) described the adaptation of this ratio as crucial in reducing glutamate excitotoxicity and avoiding neuronal death. The metabolite data point to the specific pathway responsible for this excess glutamate. There was a significant increase in NAA initially (1 hour compared to baseline) with an observed increase in the ratio of NAA/NAAG ($p=0.07$). There was also significant increase in the ratio of Glu/NAAG at 24 hours compared to baseline. The increased amount of glutamate and NAA could be caused by the hydrolysis of NAAG by the enzyme glutamate carboxypeptidase II (GCPII) as described by Figure 4.6 (Fievisohn et al., 2014; Neale et al., 2005). NAAG breakdown inhibition has been the interest of many studies and has been shown to reduce ischemic brain injury (Slusher et al., 1999). There was also an observed increase in aspartate at 24 hours compared to 1 hour after impact ($p=0.09$). This suggests that NAA is being broken down to acetate and aspartate. Acetate is known to be used in myelin lipid synthesis (Moffett et al., 2007). This agrees with the fluctuations in cholines (initial decrease at 1h/b, but subsequent elevation at 24h/1h), which is considered a biomarker for membrane phospholipid turnover (Moore and Galloway, 2002) indicating a membrane disruption. Further, there are ratios between Ins, NAA, and cholines that change, which also could point to membrane disruption as all of these are known to contribute to the myelin sheath (Ross and Bluml., 2001; Chakraborty et al., 2001).

Pascual et al. (2007) observed an increase in NAA and glutamate in rats injured using the Marmarou weight-drop model. In addition, the fluctuation in cholines with an initial decrease, but subsequent elevation has been also described by Schuhmann et al. (2003) and Harris et al. (2012) in controlled cortical impact injury within one week in the cortex of rats and contribute these changes to membrane disruption.

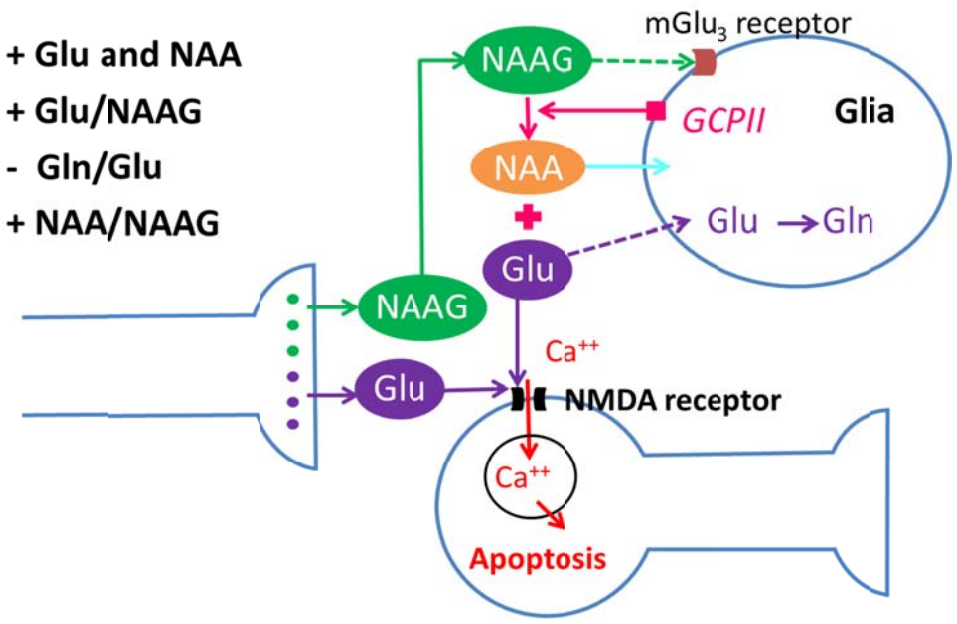

Figure 4.6: Glutamate excitotoxicity pathway.

Interactions between NAAG, NAA, and Glu after Neale et al., 2005 (with permission from Elsevier: Appendix F) and Fievisohn et al., 2014. NAAG pathway that activates $mGlu_3$ receptors on glial cells thereby inhibiting Glu release is compromised (dashed green arrow). Rather, NAAG is broken down to NAA and Glu by GCPII (pink solid arrow). Excess Glu in the extracellular space can bind to NMDA receptors leading to an influx of calcium triggering apoptosis (red solid arrow). Note: not all of the glutamate receptors are included.

Both experimental groups displayed significant increases in light and heavy neurofilament chains compared to sham controls. The presence of neurofilament chains after brain injury has been identified in many different studies looking at fluid percussion (Pettus et al., 1994; Yaghmai and Povlishock, 1992), controlled cortical impact (Schuhmann et al., 2003; Dixon et al., 1991; Meaney et al., 1994; Chen et al., 2003), inertial rotation (Ross et al., 1994; Cecil et al., 1998; Smith et al., 1998; Smith et al., 1999; Smith et al., 2000; Browne et al., 2011), and weight-drop injuries (Foda et al., 1994; Povlishock et al., 1997; Stone et al., 2001). Neurofilaments are a common target for evaluating TBI. Specifically, neurofilament compaction was introduced over 20 years ago (Pettus et al., 1994; Povlishock et al., 1997; Pettus and Povlishock, 1996). This phenomenon involves disruption of the neurofilament sidearms, thereby misaligning the neurofilament chains by decreasing the inter-neurofilament spacing. As this disruption progresses, axoplasmic transport will become impaired, resulting in swelling and disconnection (Pettus and Povlishock, 1996). There were no other significant differences found

with any of the other immunohistochemical analyses. Further testing will help to quantify injury severity and to determine if neurofilament disruption is recoverable or develops in to axonal swelling.

Both injury devices produced responses that suggest glutamate excitotoxicity. These two impacts were also described by metabolic membrane disruption and immunostained axonal disruption. Some of the metabolite changes were similar between the devices, but some of them were different. There were 13 common significant metabolite changes (same trend and time point) compared to a total of 56 significant relationships between the two devices. The translation-input injury results displayed initial stages of glutamate excitotoxicity as an energy crisis (lack of ATP) characterized by an initial increase in glutamine and then subsequent increases in glutamate. The combined-input injury results produced a clearer response that outlines glutamate excitotoxicity. A potential pathway was identified with the breakdown of NAAG leading to the increase in glutamate. There are also relationships between this pathway and membrane disruption, which agrees with the axon cytoskeleton disruption observed with immunostaining of light and heavy neurofilaments. Importantly, there could be distinct metabolite pathways that characterize the same underlying changes.

Overall, the metabolite changes are useful because they can give insight in to the biochemical cascades involved in each impact. The interpretation of the metabolite ratios is difficult as some might be explained by individual metabolite changes alone. Some of the significant metabolite changes observed in this study might not have an important role in the impact response. There is not enough understanding of the biochemical processes to make definitive assessments. However, reporting these findings can help give insights in to potential pathways as future analyses add to the knowledge base. As ^{1}H-MRS becomes more commonly used, further connections can be made to clinical measurements.

These results differ slightly from Fievisohn et al. (2014) in that the current analyses use a stricter inclusion criterion for the metabolite data and the immunohistochemical analyses include additional animals. This is reflected in the number of animals used for each of the analyses. In addition, two animals were added to the metabolite analyses for each experimental group that survived 72 hours after impact. Fievisohn et al. (2014) also used a CRLB<100 and eliminated any extreme outliers. For the translation-input injury group, GABA was reported to be significantly increased at 24 h/b. An increase in GABA and an increase in glutamine (similar to

the current analyses) suggest that the energy crisis, describing the initial response to an increase in glutamate, involves the GABA shunt system (Figure 4.7). Increases in GABA and glutamine could be a systemic response to subdue increases in glutamate. For the combined-input injury group, the main differences between the two analyses were the significant decrease in NAAG and increase in NAA/NAAG at 1h/b. This further supported glutamate excitotoxicity and the pathway involved (Figure 4.6) However, despite the differences in the metabolite changes and immunohistochemical staining percentages, the conclusions remain largely unchanged.

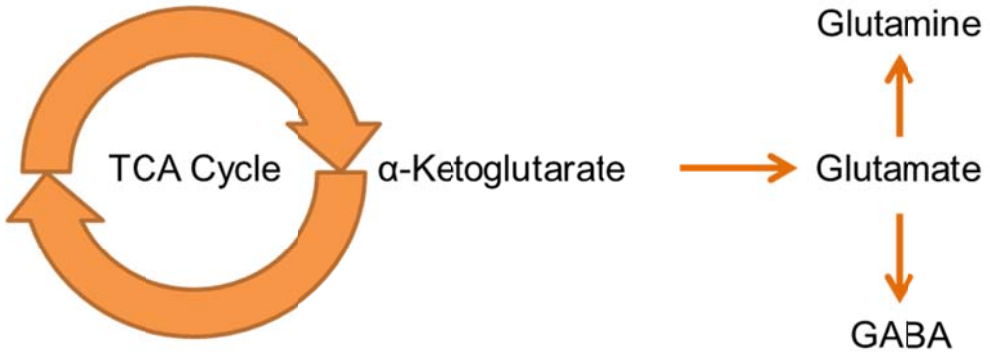

Figure 4.7: GABA shunt system.

4.4 LIMITATIONS AND FUTURE WORK

One limitation in this study is that a variety of different drop heights for each device were used, but the differences between the impact responses produced for each height was small. This might have introduced differences in the metabolite changes and immunohistochemical results that were not large enough to contribute to statistical significance, but instead increased variance in the findings. Conducting experiments at one level could produce further statistically significant results that would lead to a more comprehensive understanding of the response cascades. Alternately, investigating drop heights providing greater separation in the impact kinematics might lead to different injury levels.

The findings of this study represent initial steps to characterize minor TBI in the minipig. Further studies will look at longitudinal development of response cascades both with immunohistochemical staining and continued metabolite analyses with ^{1}H-MRS. Impact severity will be increased to better understand response cascades across a broader continuum of kinematics inputs. In addition, behavioral testing will be conducted to determine neurological

deficit. Understanding the functional neurological deficits in the animals will provide insight in to symptoms seen clinically, helping to connect the outcomes in the minipig to clinical pathologies in a more robust way. For example, identifying a common symptom of minor TBI such as memory deficit (Dean et al., 2013) in the minipig would be useful to make a clinical connection. This will facilitate appropriate interpretation of the injuries observed in the minipig within the context of human injury.

This study is also the first step toward developing a new, graded, head injury metric. High speed biplane x-ray experiments will be used with identical impacts to measure the relative brain/skull motion. These data will be used to develop and validate a finite element model of the minipig head that relates impact kinematics to underlying damage. This model will be compared to a human finite element model to determine an appropriate scaling factor, which can then be used to scale the minipig results to the human condition. This will lead to an injury metric that directly relates impact kinematics to underlying damage to produce more effective prevention strategies.

4.5 CONCLUSIONS

Overall, this study characterized impact response over the course of 24 hours in the Göttingen minipig using two impact modes. The translation-input injury device produced a response constellation exhibiting axon cytoskeletal disruption with significant increases in light and heavy neurofilament chains. The observed metabolite changes indicated membrane turnover and the beginning stages of glutamate excitotoxicity by exhibiting initial significant increases in glutamine. Similarly, the combined translation and rotation-input injury device showed significant increases in light and heavy neurofilament chains. The metabolite changes signified membrane turnover as well, but differed from the translation-input injury device results by showing clear signs of glutamate excitotoxicity and an associated potential pathway.

Two novel injury devices have been developed for use in a higher-order animal model. These injury devices replicate clinical occurrences of impact-induced TBI. There are still many unknowns associated with TBI, although this study has provided some insight in to some of the distinct biochemical pathways involved. For example, this study shows that two different injury modes can result in different metabolite changes, yet produce the same underlying axon cytoskeleton disruption. These devices and animal model can be used not only to contribute

further to the basic understanding of TBI, but also can help to identify possible drug targets for intervention strategies and to evaluate drug treatments before clinical trials.

CHAPTER 5: THE RELATIONSHIPS BETWEEN KINEMATICS, METABOLITES, AND UNDERLYING DISRUPTION WITHIN 24 HOURS OF IMPACT

5.1 RESULTS

Correlation analyses revealed 7 statistically significant correlations between metabolites, kinematics, and staining results for the translation-input injury group. The combined-input injury group displayed 37 significant correlations. There were relationships present between metabolites and kinematics, and metabolites and staining, but there were no significant relationships between kinematics and staining for either experimental group. All correlations with a Pearson Correlation Coefficient (R) greater than 0.5 are reported in Table 5.1 and Table 5.2 for the translation-input and combined-input injury groups, respectively.

Multiple linear regressions were performed based on metabolites that correlated to both a kinematics parameter and one of the staining parameters. The adjusted R^2 and corresponding p-values are shown in Table 5.3 and Table 5.4 for the translation-input and the combined-input injury groups, respectively.

Table 5.1: Correlations from the translation-input injury group[1].

Metabolite	Time Point	Kinematics/*Staining*	R	p-value	n
Cho	24h/1h	*HF*	0.529	0.116	10
Glu	24h/1h	Linear Speed	-0.517	0.085	12
Glu+Gln	24h/1h	CC	-0.543	0.068	12
		HIP	-0.531	0.076	12
		HIC	-0.520	0.083	12
		Linear Acceleration	-0.543	0.068	12
Glu/NAA	24h/1h	CC	-0.507	0.164	9
		HIP	-0.529	0.143	9
		HIC	-0.536	0.137	9
		Linear Acceleration	-0.507	0.164	9
		Linear Speed	-0.555	0.121	9
Glu/NAA+NAAG	24h/1h	CC	-0.661	0.027*	11
		HIP	-0.719#	0.013*	11
		HIC	-0.696	0.017*	11
		Linear Acceleration	-0.661	0.027*	11
		Linear Speed	-0.675	0.023*	11
NAA+NAAG/Glu+Gln	24h/1h	HIP	0.566	0.069	11
		HIC	0.524	0.098	11
Cho/NAA+NAAG	24h/1h	CC	-0.503	0.115	11
		HIP	-0.547	0.082	11
		Linear Acceleration	-0.503	0.115	11
NAA/Cho	1h/b	*HF*	-0.539	0.168	8
Cho/Glu+Gln	1h/b	*LF*	0.537	0.110	10
Scyllo	24h/1h	HIC	-0.500	0.141	10
		LF	0.685	0.061	8
		HF	0.733#	0.039*	8
NAAG/Scyllo	24h/1h	CC	0.669	0.069	8
		HIP	0.664	0.072	8
		HIC	0.674	0.067	8
		Linear Acceleration	0.669	0.069	8
		Linear Speed	0.749#	0.033*	8
		LF	-0.773#	0.071	6
		HF	-0.762#	0.078	6

[1]R is the Pearson correlation coefficient; *indicates p<0.05, # indicates R≥0.7.

Table 5.2: Correlations from the combined-input injury group[1].

Metabolite	Time Point	Kinematics/Staining	R	p-value	n
Cho	1h/b	*LF*	0.773[#]	0.041[*]	7
		HF	0.759[#]	0.048[*]	7
Glu	24h/1h	*LF*	0.546	0.204	7
Glu+Gln	24h/1h	CC	0.706[#]	0.034[*]	9
		HIP	0.612	0.080	9
		HIC	0.632	0.068	9
		BrIC	0.667	0.0497[*]	9
		Linear Acceleration	0.685	0.042[*]	9
		Linear Speed	0.590	0.094	9
		Angular Acceleration	0.696	0.037[*]	9
		Angular Speed	0.667	0.0497[*]	9
		HF	0.540	0.167	8
Glu/Glu+Gln	24h/b	*LF*	-0.547	0.204	7
		HF	-0.706[#]	0.076	7
Gln/Glu	24h/b	*HF*	0.714[#]	0.072	7
Gln/Glu+Gln	24h/b	*HF*	0.712[#]	0.073	7
NAA	1h/b	*LF*	0.751[#]	0.144	5
		HF	-0.545	0.342	5
NAAG/NAA+NAAG	1h/b	*LF*	-0.873[#]	0.053	5
NAA/NAAG	1h/b	*LF*	0.796[#]	0.107	5
NAA/NAA+NAAG	1h/b	*LF*	0.754[#]	0.141	5
		HF	-0.544	0.343	5
Glu/NAA	1h/b	*LF*	-0.970[#]	0.006[*]	5
Glu/NAA	24h/1h	CC	0.749[#]	0.032[*]	8
		HIP	0.663	0.073	8
		HIC	0.632	0.093	8
		BrIC	0.584	0.128	8
		Linear Acceleration	0.708[#]	0.0496[*]	8
		Linear Speed	0.650	0.081	8
		Angular Acceleration	0.809[#]	0.015[*]	8
		Angular Speed	0.584	0.128	8
Glu/NAAG	24h/b	Angular Acceleration	0.582	0.170	7
		LF	0.921[#]	0.026[*]	5
Gln/NAAG	24h/b	Angular Acceleration	0.598	0.156	7
		LF	0.953[#]	0.012[*]	5
Glu/NAA+NAAG	24h/1h	CC	0.729[#]	0.026[*]	9
		HIP	0.648	0.059	9
		HIC	0.685	0.042[*]	9
		BrIC	0.578	0.103	9
		Linear Acceleration	0.727[#]	0.027[*]	9
		Linear Speed	0.637	0.065	9
		Angular Acceleration	0.642	0.062	9
		Angular Speed	0.578	0.103	9
		LF	0.728[#]	0.063	7
		HF	0.532	0.219	7

Metabolite	Time Point	Kinematics/Staining	R	p-value	n
Glu/NAA+NAAG	24h/b	CC	0.596	0.091	9
		HIP	0.521	0.150	9
		Linear Acceleration	0.553	0.122	9
		Angular Acceleration	0.666	0.0501	9
NAA/Glu+Gln	1h/b	*LF*	0.872[#]	0.054	5
NAA/Glu+Gln	24h/1h	CC	-0.618	0.139	7
		HIP	-0.655	0.110	7
		HIC	-0.650	0.114	7
		BrIC	-0.613	0.143	7
		Linear Acceleration	-0.629	0.130	7
		Linear Speed	-0.714[#]	0.072	7
		Angular Speed	-0.613	0.143	7
		LF	-0.742[#]	0.091	6
NAAG/Glu+Gln	24h/b	Angular Acceleration	-0.542	0.266	6
		LF	-0.936[#]	0.019[*]	5
NAA+NAAG/Glu+Gln	24h/b	HIP	-0.557	0.151	8
		HIC	-0.509	0.198	8
		Linear Speed	-0.585	0.128	8
		LF	-0.757[#]	0.049[*]	7
Glu/Cre	24h/b	*LF*	-0.578	0.174	7
		HF	-0.886[#]	0.008[*]	7
Glu/Cre	24h/1h	*LF*	0.637	0.124	7
		HF	0.628	0.131	7
Gln/Cre	24h/b	CC	0.658	0.054	9
		HIP	0.503	0.167	9
		Linear Acceleration	0.591	0.093	9
		Angular Acceleration	0.806[#]	0.009[*]	9
Glu+Gln/Cre	24h/b	CC	0.545	0.206	7
		HIP	0.523	0.228	7
		BrIC	0.527	0.225	7
		Angular Acceleration	0.659	0.108	7
		Angular Speed	0.527	0.225	7
		HF	-0.878[#]	0.009[*]	7
Glu+Gln/Cre	24h/1h	CC	0.799	0.017[*]	8
		HIP	0.617	0.103	8
		HIC	0.718	0.045[*]	8
		BrIC	0.694	0.056	8
		Linear Acceleration	0.771	0.025[*]	8
		Linear Speed	0.595	0.120	8
		Angular Acceleration	0.768	0.026[*]	8
		Angular Speed	0.694	0.056	8
		HF	0.558	0.150	8
Glu/Scyllo	1h/b	CC	0.515	0.375	5
		Angular Acceleration	0.694	0.194	5
NAA/Cre	1h/b	*LF*	0.505	0.385	5
		HF	-0.681	0.206	5
NAAG/Cre	24h/1h	*HF*	-0.797[#]	0.058	6

Metabolite	Time Point	Kinematics/Staining	R	p-value	n
NAA/Cho	24h/1h	CC	-0.628	0.131	7
		HIP	-0.787[#]	0.036[*]	7
		HIC	-0.700[#]	0.080	7
		BrIC	-0.737[#]	0.059	7
		Linear Acceleration	-0.654	0.111	7
		Linear Speed	-0.826[#]	0.022[*]	7
		Angular Speed	-0.737[#]	0.059	7
NAAG/Cho	24h/b	*LF*	-0.925[#]	0.024[*]	5
NAA/Cho	1h/b	*HF*	-0.896[#]	0.039[*]	5
Cho/NAA+NAAG	1h/b	*LF*	0.815[#]	0.026[*]	7
		HF	0.823[#]	0.023[*]	7
Cho/NAA+NAAG	24h/1h	HIP	0.539	0.108	10
		HIC	0.528	0.117	10
		BrIC	0.504	0.137	10
		Linear Speed	0.569	0.086	10
		Angular Speed	0.504	0.137	10
Asp	24h/1h	Angular Acceleration	-0.790[#]	0.112	5
Asp/Ins	24h/1h	CC	-0.837[#]	0.077	5
		HIP	-0.915[#]	0.029[*]	5
		HIC	-0.884[#]	0.046[*]	5
		BrIC	-0.944[#]	0.016[*]	5
		Linear Acceleration	-0.902[#]	0.036[*]	5
		Linear Speed	-0.848[#]	0.069	5
		Angular Speed	-0.944[#]	0.016[*]	5
Asp/Cre	24h/1h	BrIC	0.500	0.391	5
		Angular Speed	0.500	0.391	5
		LF	-0.502	0.388	5
Ins/NAAG	1h/b	*HF*	-0.877[#]	0.051	5
Ins/NAAG	24h/b	*LF*	0.549	0.338	5
		HF	-0.714[#]	0.176	5
Ins/NAAG	24h/1h	HIC	0.530	0.176	8
Glu/Ins	24h/1h	*LF*	0.543	0.208	7
Gln/Ins	24h/b	*HF*	0.596	0.158	7
Asp/Gln	1h/b	Angular Acceleration	-0.666	0.219	5
		LF	-0.939[#]	0.061	4
		HF	-0.779[#]	0.221	4
Glu/Cho	1h/b	*HF*	-0.844[#]	0.017[*]	7
		LF	-0.663	0.104	7
Cho/Glu+Gln	24h/b	HIC	0.505	0.202	8
		Linear Acceleration	0.500	0.207	8

[1]R is the Pearson correlation coefficient; [*]indicates p<0.05, # indicates R≥0.7.

Table 5.3: Translation-input injury device multiple linear regression analyses.

Metabolite	Time point	Kinematic	Staining	Adjusted R^2	p-value	n
Scyllo	24h/1h	HIC	LF	0.347	0.149	8
Scyllo	24h/1h	HIC	HF	0.356	0.143	8
NAAG/Scyllo	24h/1h	CC	LF	0.350	0.244	6
		HIP	LF	0.368	0.234	6
		HIC	LF	0.350	0.243	6
		Linear Acceleration	LF	0.350	0.244	6
		Linear Speed	LF	0.457	0.186	6
NAAG/Scyllo	24h/1h	CC	HF	0.311	0.266	6
		HIP	HF	0.301	0.272	6
		HIC	HF	0.301	0.272	6
		Linear Acceleration	HF	0.311	0.266	6
		Linear Speed	HF	0.393	0.220	6

Table 5.4: Combined-input injury device multiple linear regression analyses.

Metabolite	Time point	Kinematic	Staining	Adjusted R^2	p-value	n
Glu/NAA+NAAG	24h/1h	CC	HF	0.166	0.309	7
		HIP	HF	0.197	0.286	7
		HIC	HF	0.127	0.339	7
		BrIC	HF	0.086	0.371	7
		Linear Acceleration	HF	0.119	0.345	7
		Linear Speed	HF	0.073	0.382	7
		Angular Acceleration	HF	0.184	0.296	7
		Angular Speed	HF	0.086	0.371	7
Glu/NAA+NAAG	24h/1h	CC	LF	0.297	0.219	7
		HIP	LF	0.303	0.216	7
		HIC	LF	0.300	0.218	7
		BrIC	LF	0.303	0.216	7
		Linear Acceleration	LF	0.298	0.219	7
		Linear Speed	LF	0.298	0.219	7
		Angular Acceleration	LF	0.407	0.156	7
		Angular Speed	LF	0.303	0.216	7
NAA/Glu+Gln	24h/1h	CC	LF	0.412	0.210	6
		HIP	LF	0.536#	0.147	6
		HIC	LF	0.566#	0.133	6
		BrIC	LF	0.571#	0.130	6
		Linear Acceleration	LF	0.538#	0.146	6
		Linear Speed	LF	0.540#	0.145	6
		Angular Speed	LF	0.571#	0.130	6
NAAG/Glu+Gln	24h/b	Angular Acceleration	LF	0.761#	0.120	5
Asp/Gln	1h/b	Angular Acceleration	LF	0.655#	0.339	4
Asp/Gln	1h/b	Angular Acceleration	HF	0	0.622	4
Gln/NAAG	24h/b	Angular Acceleration	LF	0.856#	0.072	5
Glu/NAAG	24h/b	Angular Acceleration	LF	0.703#	0.148	5

Metabolite	Time point	Kinematic	Staining	Adjusted R^2	p-value	n
NAA+NAAG/Glu+Gln	24h/b	HIP	LF	0.448	0.136	7
		HIC	LF	0.423	0.148	7
		Linear Speed	LF	0.402	0.159	7
Glu+Gln	24h/1h	CC	HF	0.321	0.164	8
		HIP	HF	0.216	0.235	8
		HIC	HF	0.193	0.252	8
		BrIC	HF	0.214	0.236	8
		Linear Acceleration	HF	0.246	0.213	8
		Linear Speed	HF	0.088	0.342	8
		Angular Acceleration	HF	0.321	0.164	8
		Angular Speed	HF	0.214	0.236	8
Glu+Gln/Cre	24h/b	CC	HF	$0.833^{\#}$	0.012^{*}	7
		HIP	HF	$0.807^{\#}$	0.017^{*}	7
		BrIC	HF	$0.847^{\#}$	0.010^{*}	7
		Angular Acceleration	HF	0.685	0.044^{*}	7
		Angular Speed	HF	$0.847^{\#}$	0.010^{*}	7
Glu+Gln/Cre	24h/1h	CC	HF	0.309	0.171	8
		HIP	HF	0.225	0.228	8
		HIC	HF	0.175	0.266	8
		BrIC	HF	0.254	0.207	8
		Linear Acceleration	HF	0.211	0.238	8
		Linear Speed	HF	0.123	0.310	8
		Angular Acceleration	HF	0.480	0.084	8
		Angular Speed	HF	0.254	0.207	8

$^{\#}$***indicates*** $R^2 \geq 0.49$, ****indicates*** $p<0.05$

5.2 DISCUSSION

Traumatic brain injury remains a persistent problem in society. The current automotive standard does not directly relate impact kinematics to the underlying injury response. However, BrIC (Takhounts et al., 2013) is an attempt to better relate kinematics to injury using historically available data, which are limited. This study is novel in that potential underlying disruption predictors were identified narrowing the range of useful noninvasive metabolic measures that should be considered in future studies. Regression analyses identified combinations of kinematics or injury metrics and metabolites that could potentially predict underlying disruption and should also be considered in future studies. This will allow improvement of an existing or development of a new, graded injury metric that relates impact parameters to underlying damage.

Animals were impacted using either the translation-input or the combined translation and rotation-input injury device. There were significant changes in both axon cytoskeleton proteins and neurochemicals in the genu of the corpus callosum. There were statistically significant

increases in both light and heavy neurofilament within both experimental groups 24 hours after impact compared to sham animals ($p<0.05$). There were no differences in any of the other stains (GFAP, cleaved caspase-3, Iba-1, β-APP). There were numerous metabolite differences found within each experimental group. For the translation-input injury group, metabolite changes suggest the beginning stages of glutamate excitotoxicity with a significant increase in glutamine both at 1 hour and 24 hours after impact compared to baseline. There were also significant increases in cholines at 24 hours compared to baseline and 24 hours compared to 1 hour, which suggest membrane turnover. For the combined-input injury group, metabolite changes indicate a clear pathway for glutamate excitotoxicity with relationships found between glutamate and NAA with NAAG pointing to the breakdown of NAAG as initiating glutamate excitotoxicity. Changes in cholines and in ratios between NAA, cholines, and Ins point to membrane disruption. These findings suggest that distinct metabolic pathways associated with each injury mode could lead to the same underlying disruption or that axon cytoskeleton disruption could lead to different response cascades.

Potential correlations between the significant metabolite changes, light and heavy neurofilament percent changes, and kinematics parameters were examined. When considering all correlations with a correlation coefficient greater than or equal to 0.5, only one relationship was common to the two devices. NAA/Cho at 1h/b negatively correlated to heavy neurofilament. This is reasonable because cholines and NAA are considered breakdown products of the cell membrane and can be identifiers of membrane disruption (Ross and Bluml, 2001; Chakraborty et al., 2001). This singular common finding suggests that the two devices produce different impact responses. This also agrees with the lack of common metabolite findings in the 24-hour impact response characterization. Further testing will improve comparison between the two injury methods.

There were no relationships between kinematics nor injury metrics and staining results. However, there were many relationships between kinematics or injury metrics and metabolite changes. There was no kinematics parameter nor injury metric that correlated to substantially more metabolite changes than the others. However, kinematics or injury metrics associated with the translation-input injuries (average of 5) correlated to less metabolite relationships than those observed for the combined-input injuries (average of 11). The meaning of this finding is unclear.

5.2.1 TRANSLATION-INPUT INJURY

The important metabolite changes described as part of the 24-hour impact response characterization for the translation-input injury device were the significant increases in glutamine and cholines post-impact. However, glutamine did not correlate with the staining results or with any kinematics parameters. Cholines at 24h/1h did correlate with HF, but did not have a particularly high R value (0.529) and was also not statistically significant. There were correlations found within ratios between choline and NAA and/or NAAG compounds, which individually are considered indicators of underlying membrane disruption. Ratios that can be interpreted as related to membrane turnover correlate to kinematics and staining parameters as shown in Table 5.5.

The ratio Glu/NAA+NAAG at 24h/1h correlated with HIP with the lowest p-value (R: -0.719; p-value: 0.013). The ratios between glutamate and NAA and/or NAAG have been identified as an important relationship in the 24-hour impact response characterization. The correlation with the highest R value was NAAG/Scyllo at 24h/1h and light neurofilament (R: -0.773; p-value: 0.071). Scyllo has been shown to be elevated in patients with different neuropathologies including Alzheimer's disease (Griffith et al., 2007). The exact role of NAAG remains unclear, but as discussed previously, inhibiting NAAG breakdown can reduce levels of glutamate present after ischemic injury (Slusher et al., 1999). The meaning of the relationship between NAAG and Scyllo is unclear.

The multiple linear regression analyses did not produce many strong relationships between a metabolite, kinematics, or staining parameters. The best underlying disruption predictor combination was NAAG/Scyllo at 24h/1h and linear speed for predicting light neurofilament underlying disruption (Adjusted R^2: 0.457; p-value: 0.186). Further testing is needed to establish this ratio as an important aspect of the impact response. Clinically, non-invasive measurements that can correlate to underlying impact response or give insight in to the severity of the impact can be potentially useful for immediate treatment strategies (once adequate treatment strategies are developed).

Table 5.5: Translation-input injury group correlations related to membrane disruption.

Metabolite	Time Point	Kinematics/Staining	R	p-value	n
Cho	24h/1h	*HF*	0.529	0.116	10
NAA/Cho	1h/b	*HF*	-0.539	0.168	8
Cho/NAA+NAAG	24h/1h	CC	-0.503	0.115	11
		HIP	-0.547	0.082	11
		Linear Acceleration	-0.503	0.115	11

5.2.2 COMBINED-INPUT INJURY

The important metabolite changes described as part of the 24-hour impact response characterization for the combined-input injury device were significant increases in glutamate, NAA, ratios between these, aspartate, and also changes in choline and the ratios between choline, NAA, and Ins. All correlate to staining and/or kinematics parameters. Importantly, choline, and the ratios between choline, NAA, and Ins are thought to be related to a membrane disruption or turnover. Ratios that can be interpreted as membrane disruption correlate to kinematics and staining parameters as shown in Table 5.6.

There were many correlations found with an R>0.7. Glu/NAA at 1h/b correlated with light neurofilament with the highest R value and lowest p-value (R: -0.970; p-value: 0.006). This suggests that the degradation of NAAG leading to glutamate excitoxicity is related to the underlying axon cytoskeleton disruption. With further testing, metabolite ratios or combinations of them could be used as a noninvasive measurement to predict the underlying response.

The multiple linear regression analyses showed that the metabolites having the best potential for predicting underlying disruption within the combined-input injury group are ratios of glutamate to NAA and/or NAAG, including aspartate, a breakdown product of NAA, and the ratios between glutamate and total creatine (Table 5.4). The strongest predictor combination with the highest adjusted R^2 was Gln/NAAG at 24h/b and angular acceleration for predicting underlying light neurofilament disruption (Adjusted R^2: 0.856; p-value: 0.072). There were statistically significant predictors with the ratio of Glu+Gln/Cre at 24h/b and HIP, BrIC, CC, angular acceleration, and angular speed for predicting underlying heavy neurofilament disruption. Overall, these groups of metabolite ratios correlate to both staining and kinematics parameters. The ratios between glutamate and NAA and/or NAAG have been identified as an important relationship in the 24-hour impact response characterization. In addition, ratios between glutamate and total creatine compounds point to an energy crisis (not enough ATP) caused by excess glutamate and the inability to convert to glutamine. Phosphocreatine is an

important metabolite in the brain because it is a storage form of ATP (Moore and Galloway, 2002). Since converting glutamate to glutamine to prevent excitotoxicity requires ATP (Mark et al., 2001), observing an increase in Glu+Gln relative to total creatine further supports excess glutamate in the extracellular space. However, further testing is needed. The underlying disruption predictors identified by multiple linear regressions should be investigated in further testing.

Table 5.6: Combined-input injury group correlations related to membrane disruption.

Metabolite	Time Point	Kinematics/Staining	R	p-value	n
Cho	1h/b	*LF*	0.773#	0.041*	7
	1h/b	*HF*	0.759#	0.048*	7
Cho/NAA+NAAG	24h/1h	HIP	0.539	0.108	10
		HIC	0.528	0.117	10
		BrIC	0.504	0.137	10
		Linear Speed	0.569	0.086	10
		Angular Speed	0.504	0.137	10
NAAG/Cho	24h/b	*LF*	-0.925#	0.024*	5
Cho/NAA+NAAG	1h/b	*LF*	0.815#	0.026*	7
		HF	0.823#	0.023*	7
NAA/Cho	1h/b	*HF*	-0.896#	0.039*	5
NAA/Cho	24h/1h	CC	-0.628	0.131	7
		HIP	-0.787#	0.036	7
		HIC	-0.700#	0.080	7
		BrIC	-0.737#	0.059	7
		Linear Acceleration	-0.654	0.111	7
		Linear Speed	-0.826#	0.022*	7
		Angular Speed	-0.737#	0.059	7
Asp	24h/1h	Angular Acceleration	-0.790#	0.112	5
Asp/Ins	24h/1h	CC	-0.837#	0.077	5
		HIP	-0.915#	0.029	5
		HIC	-0.884#	0.046*	5
		BrIC	-0.944#	0.016*	5
		Linear Acceleration	-0.902#	0.036*	5
		Linear Speed	-0.848#	0.069	5
		Angular Speed	-0.944#	0.016*	5
NAA/NAAG	1h/b	*LF*	0.796#	0.107	5

****indicates p<0.05, # indicates R≥0.7***

5.3 LIMITATIONS AND FUTURE WORK

The multiple linear regression analyses identified potential underlying disruption predictors when combining a non-invasive measure such as ^{1}H-MRS with a kinematics parameters or injury metric. The multiple regression analyses support some potential underlying disruption predictors and rule out others. For the correlation analyses, there were more animals included in the data set. However, if an animal had a missing metabolite concentration or staining result it could not be included in the regression analysis, which reduced the number of possible comparisons. This reduction in comparisons could be why there were potential predictors identified, yet no correlations between staining and a kinematics parameter or injury metric. Also, some of the correlation and regression comparisons did not involve many data points. The exclusion or inclusion of a single animal can change the results substantially, further emphasizing the need for more testing.

There were no correlations found between the kinematics and staining results for either injury device. This could result from several factors. From an overall understanding of the problem, the current standard injury metric HIC and the proposed metrics HIP, BrIC, and CC are not directly related to underlying damage. Therefore, it is possible that there might be a more appropriate injury metric that has yet to be discovered. Also, the inputs studied here do not include a wide range of linear and angular speeds (translation: 2.7-3.5 m/s; combined: 2.6-4.4 m/s, 7.2-10.8 rad/s). Hardy et al. (2007) found that cadaveric brain motion patterns can best be interpreted with respect to angular speed. Using a larger range that could produce both minor and moderate TBI might result in better correlation between kinematics and underlying damage.

The practical aspects of injury severity for these tests are unknown without longitudinal evaluation and behavioral testing. Further studies will help illuminate stronger relationships between metabolic changes, staining results, kinematics, and current injury metrics. Adding a behavioral component in to these relationships will produce more robust connections that can be related to clinical symptoms. Knowing the structural damage will give insight in to the underlying impact response and progression/recovery over time. More experiments investigating different immunohistochemical staining, different time points, and a wider range of impacts will also improve the understanding of the correlations and regression results.

5.4 CONCLUSIONS

Preliminary findings in terms of correlations and potential underlying disruption predictors for minor TBI were identified. More insight is needed to determine the best predictors for underlying disuption and the most promising metabolites that best describe the impact response. Knowing the metabolites that give the best indication of injury severity will translate to a valuable non-invasive measurement technique. This is useful for *in vivo* studies, reducing the number of animals used to characterize the impact, and could potentially be used clinically for diagnosis.

CHAPTER 6: 72-HOUR PILOT STUDY

6.1 RESULTS

Gross damage was observed in one of the translation-input injury group animals after 72 hours. This animal developed hemorrhaging along the dorsal sagittal sinus (Figure 6.1). This animal was subjected to 66 g linear acceleration and 3.4 m/s linear speed.

Figure 6.1: Dorsal sagittal sinus hemorrhaging in a translation-input injury animal.

For metabolite and staining analyses, two animals were survived until the 72-hour time point for each injury device. Therefore, statistical analyses were not conducted between the 72-hour and the other time points.

Both light and heavy neurofilament chains were present in the 72-hour survival animals impacted using each device (Figure 6.2). There were no β-APP accumulations in any animals at 72 hours.

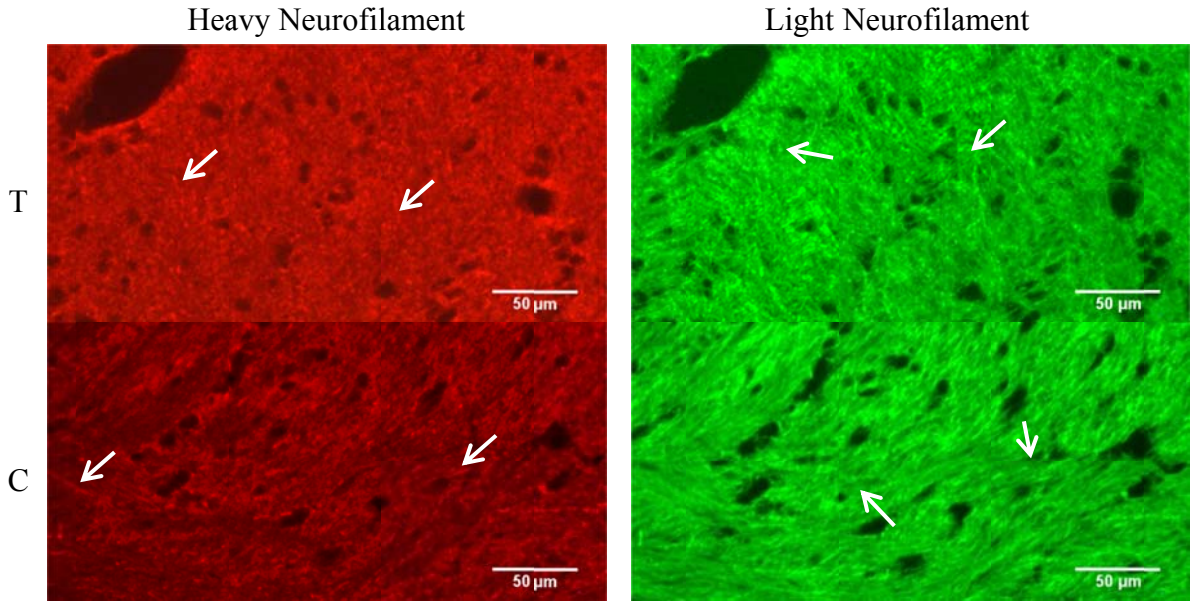

Figure 6.2: Immunostained translation-input (T) and a combined-input injurygroup animal (C). A few of the highlighted NF chains are shown by arrows.

6.1.1 Translation-Input Injury

Metabolite relationships that persisted through the 72-hour time point are cataloged in Figure 6.3. These include:

- Increase in Gln, Cho, Cho/NA+NAAG, and Gln/Cre compared to baseline,
- Increase in Glu and Glu+Gln compared to baseline, but decreased compared to 24-h time point,
- Decrease in NAA/Cho compared to baseline and 24-h time point,
- Decrease in NAA/Glu+Gln and NAA+NAAG/Glu+Gln compared to baseline, but increased compared to 24-h time point.

6.1.2 Combined-Input Injury

Metabolite changes that persisted through the 72-hour time point are cataloged in Figure 6.4. These include:

- Increase in Glu and Cho/NAA+NAAG compared to baseline,
- Increase in Cho compared to baseline and 24-h time point,
- Increase in Glu/NAA, Glu/NAAG, Glu/NAA+NAAG, and Glu/Cre compared to baseline, but decreased compared to 24-h time point,

- Decrease in Gln/Glu, NAA/Cho, NAA/Glu+Gln, NAA+NAAG/Glu+Gln, NAAG/Cho, and Ins/Cho compared to baseline.

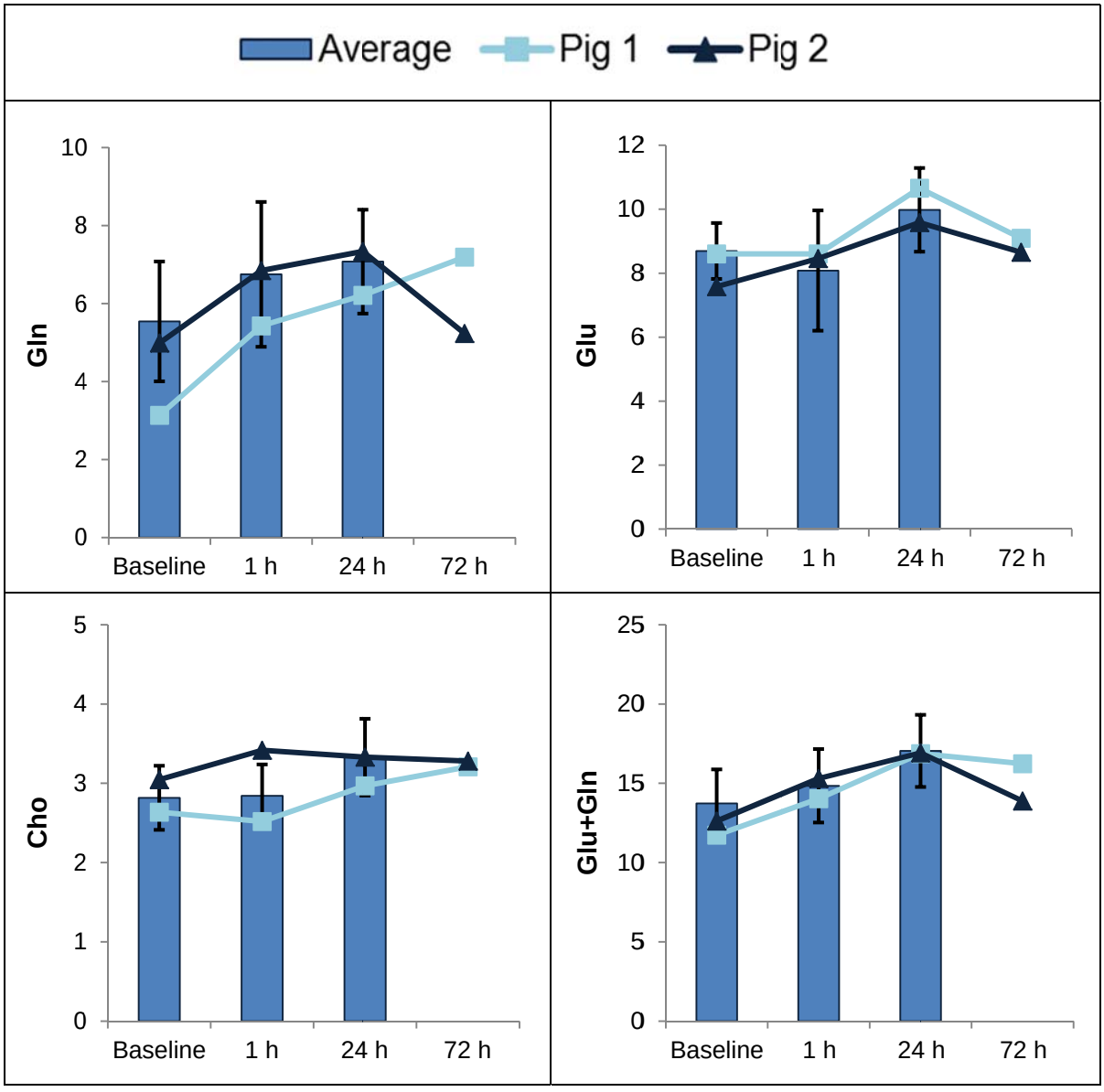

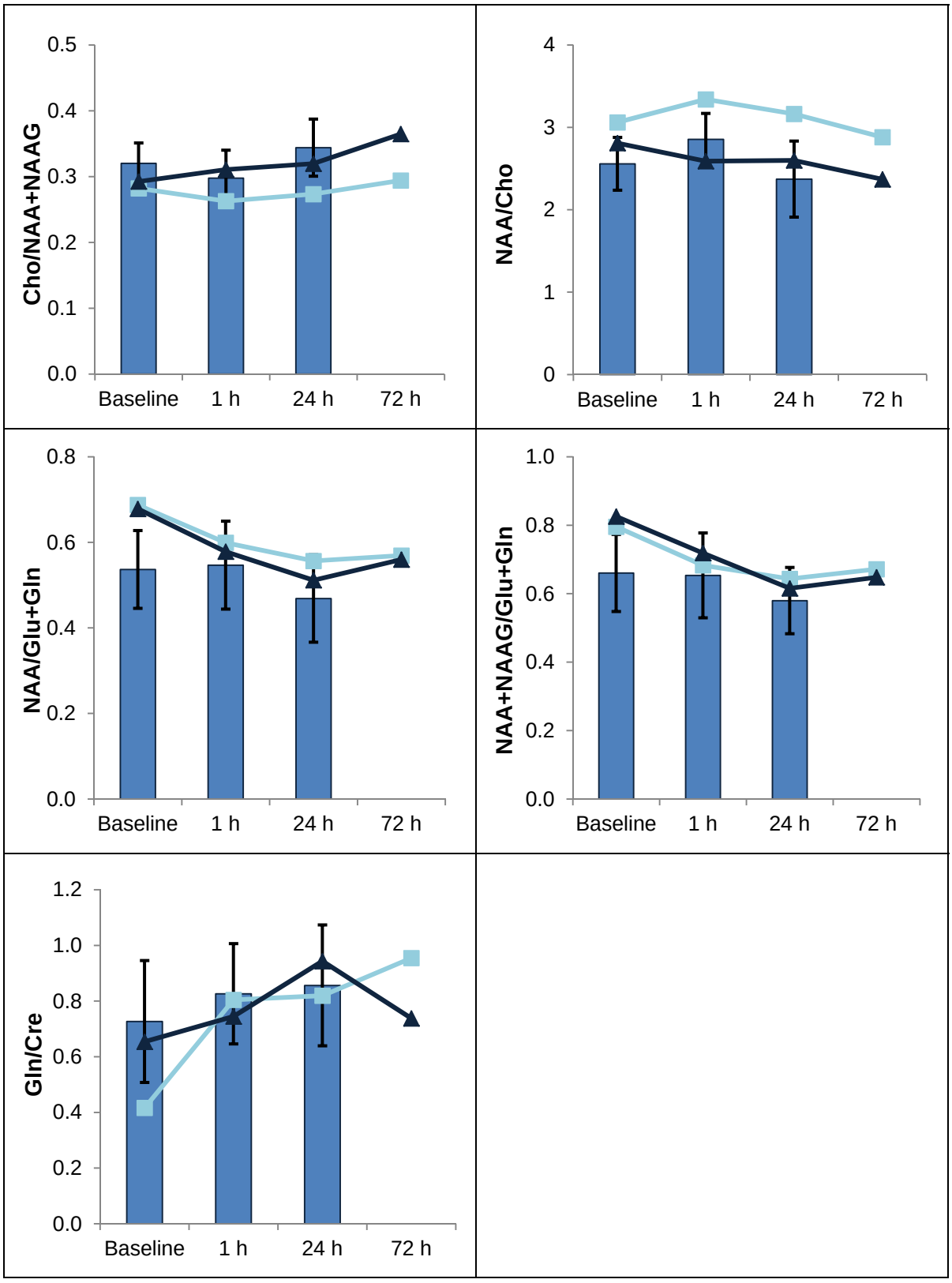

Figure 6.3: Trends for the two translation-input 72-h survival animal metabolite concentrations.

The average metabolite concentrations from all animals for the baseline, 1-h, and 24-h time points are shown by an average ± standard deviation and the two 72-h survival animal concentrations are shown by individual points.

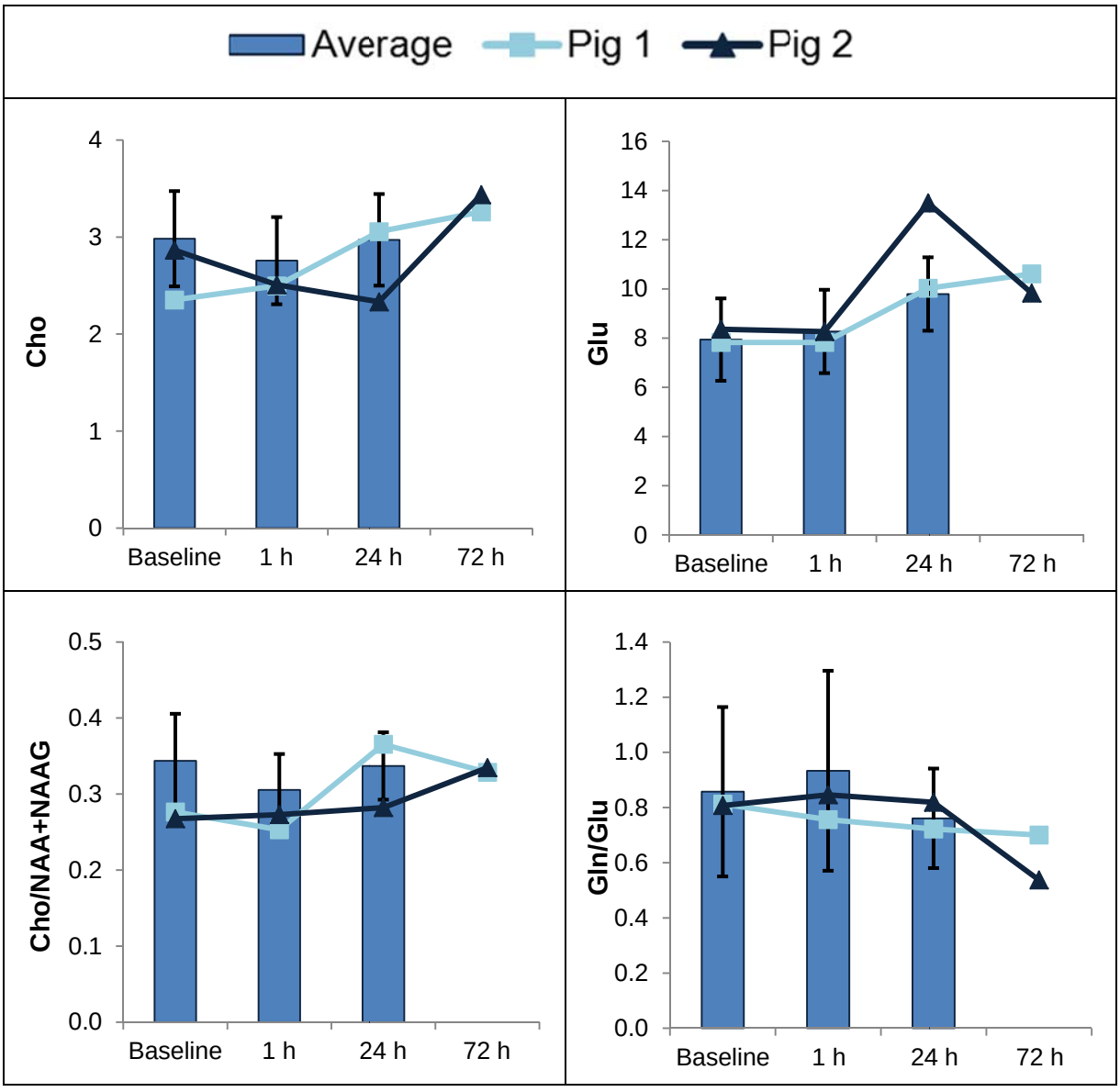

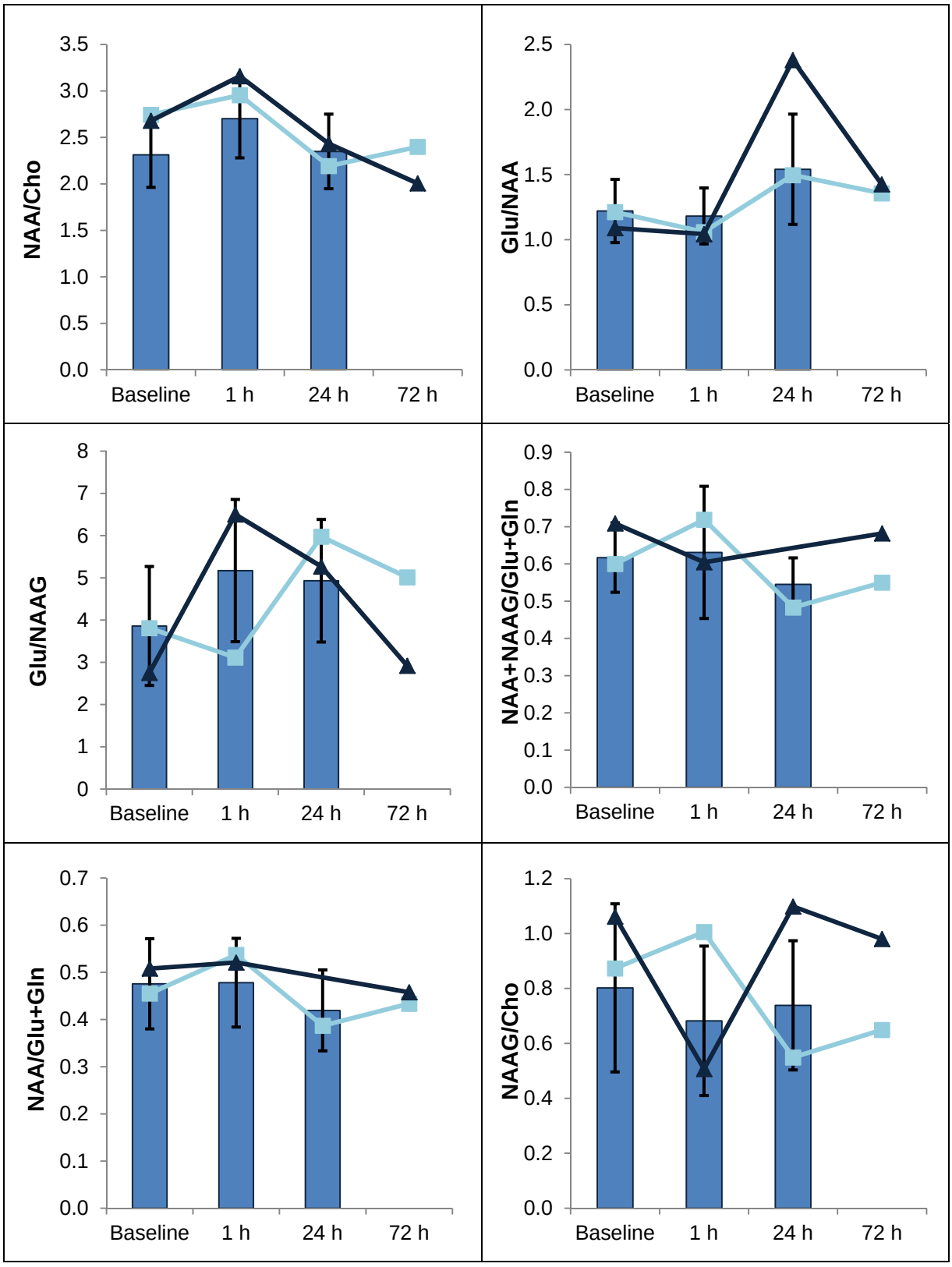
NAA/Cho
3.5
3.0
2.5
2.0
1.5
1.0
0.5
0.0
Baseline
1 h
24 h
72 h
Glu/NAA
2.5
2.0
1.5
1.0
0.5
0.0
Baseline
1 h
24 h
72 h
Glu/NAAG
8
7
6
5
4
3
2
1
0
Baseline
1 h
24 h
72 h
NAA+NAAG/Glu+Gln
0.9
0.8
0.7
0.6
0.5
0.4
0.3
0.2
0.1
0.0
Baseline
1 h
24 h
72 h
NAA/Glu+Gln
0.7
0.6
0.5
0.4
0.3
0.2
0.1
0.0
Baseline
1 h
24 h
72 h
NAAG/Cho
1.2
1.0
0.8
0.6
0.4
0.2
0.0
Baseline
1 h
24 h
72 h

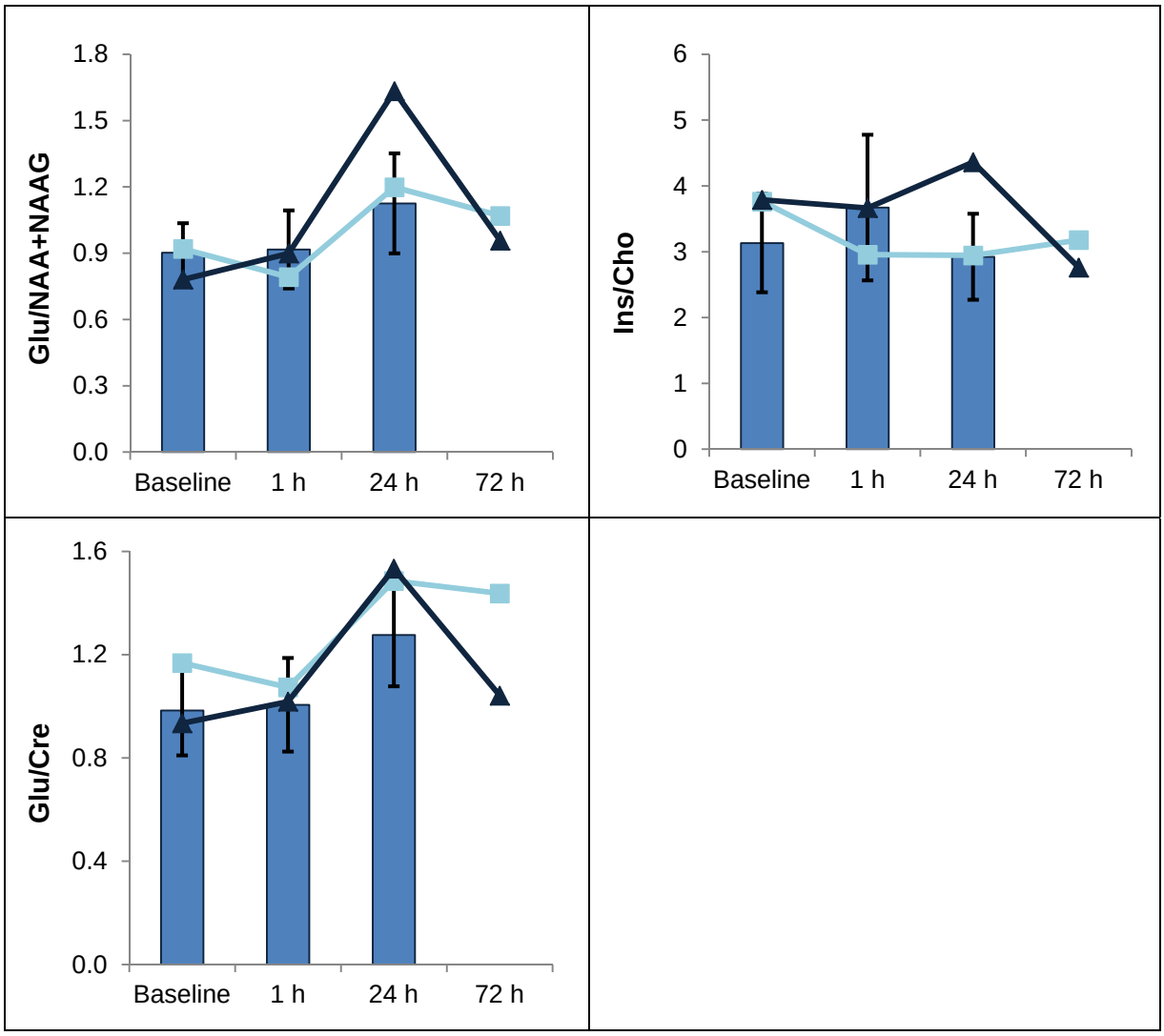

Figure 6.4: Trends for the two combined-input 72-h survival animal metabolite concentrations.

The average metabolite concentrations from all animals for the baseline, 1-h, and 24-h time points are shown by an average ± standard deviation and the two 72-h survival animal concentrations are shown by individual points.

6.2 DISCUSSION

There were persistent metabolite changes and light and heavy neurofilament chains present in the genu of the corpus callosum 72 hours after impact. Many trends are similar for both injury devices at 72-hours. Continuing changes in Cho and in ratios between Cho, NAA and/or NAAG, and Ins point to continued membrane disruption. This agrees with the presence of light and heavy neurofilament chains in the 72-hour survival animals. However, β-amyloid

precursor protein accumulation was not observed at this longer time point, nor earlier time points.

There are important differences in the outcomes produced by the two injury devices as well. For the translation-input injury group, the initial stages of glutamate excitotoxicity are still present at 72 hours. There is a persistent increase in both glutamine and glutamate showing that these perturbations have not subsided. In addition, a continuing increase in Gln/Cre still supports an energy crisis. For the combined-input injury group, glutamate excitotoxicity persists as indicated by further increases in Glu, decreases in Gln/Glu, and changes in the ratios between Glu and NAA and/or NAAG. A continuing increase in Glu/Cre also supports a systemic energy crisis because of the increase in glutamate. It is unclear whether the translation-input impact response has advanced to similar response cascades as the combined-input injury group without further testing.

The goal with these two injury devices was to study minor TBI. This level of injury is not well understood and has not been generated in clinically relevant ways using previous *in vivo* models. Impact characterization at the 24-hour mark showed that the only underlying disruption was that reflected by significant increases in light and heavy neurofilament chains. There were no changes in GFAP, Iba-1, cleaved caspase-3, or β-APP. The structural damage is unknown without closer investigation such as using electron microscopy. This technique would help define the neurofilament disruption (i.e. if there is misalignment or sidearm compaction and if this persists or recovers longitudinally). However, axonal damage has not progressed to a more severe state (no β-APP accumulations). The gross damage found along the sagittal sinus in one of the translation-input injury group animals suggests that these methods might hold promise for the study of subdural hematoma.

Previous studies have shown an axolemma perturbation and initial organelle swelling and pooling that progressed over time to form swollen and bulbous structures, which ultimately led to disconnection within 24-72 hours (Povlishock et al., 1983; Povlishock and Kontos, 1985; Yaghmai and Povlishock, 1992). The current analyses did not observe axonal swellings or disconnection 72 hours after impact. There are persistent metabolite and structural perturbations, but these could be recoverable in these minor injuries. Additional testing will help to make these determinations. Electron microscopy could help evaluate the extent of the structural damage to the axon. Axon pathologies found in other studies such as axolemma perturbation (Povlishock et

al., 1983; Povlishock and Kontos, 1985; Yaghmai and Povlishock, 1992; Povlishock, 1993; Pettus et al., 1994; Pettus and Povlishock, 1996; Okonkwo et al., 1998; Povlishock et al., 1997; Stone et al., 2004; Creed et al., 2011), neurofilament compaction (Pettus et al., 1994; Pettus and Povlishock, 1996; Povlishock et al., 1997; Okonkwo et al., 1998; Buki et al., 1999; Stone et al., 2001; Marmarou et al., 2005; Kallakuri et al., 2012; Zakaria et al., 2012), impaired axonal transport, both anterograde (Povlishock et al., 1983; Povlishock and Kontos, 1985; Yaghmai and Povlishock, 1992; Povlishock, 1993; Pettus et al., 1994; Pettus and Povlishock, 1996; Povlishock et al., 1997; Okonkwo et al., 1998; Stone et al., 2001; Stone et al., 2004; Marmarou et al., 2005; Kallakuri et al., 2012; Zakaria et al., 2012) and retrograde (Creed et al., 2011), and other structural changes such as mitochondrial swelling (Pettus et al., 1994; Pettus and Povlishock, 1996; Povlishock et al., 1997; Buki et al., 1999; Stone et al., 2001) or axolemma infoldings (Povlishock, 1993; Pettus and Povlishock, 1996; Buki et al., 1999; Stone et al., 2001; Stone et al., 2004; Marmarou et al., 2005) should be investigated longitudinally. These phenomena described previously for axon pathology need to be reevaluated using the two novel injury devices and a new animal model used in this study.

6.3 SUMMARY

A preliminary study was conducted to observe the longitudinal effects of translation-input and combined translation and rotation-input injury devices. There was a persistent presence of both light and heavy neurofilament chains in both experimental groups, and there were continuing metabolite changes that did not return to baseline. The underlying disruption and metabolite changes caused from these two devices might not be recoverable within 72 hours. Although further testing is needed, sustaining a minor impact might be more serious than is currently thought. Extrapolating these ideas, sustaining more than one minor impact might lead to a more severe injury response if the system does not recover from the initial insult. Longitudinal testing over the course of 1-2 weeks would determine if these perturbations persevere or if there is recovery. Behavioral testing in combination with the longitudinal testing would evaluate the neurological deficits caused by these persistent changes to allow for comparisons between *in vivo* injury and clinical symptoms of TBI.

CHAPTER 7: SUMMARY

This research presents preliminary steps toward the development of an improved injury metric. The outcomes of this research are:

- Two novel injury devices have been developed and repeatability has been established.
- A Göttingen minipig animal model has been developed for neurotrauma research.
- The observed translation-input impact response is defined by:
  - Bilateral cortical contusions,
  - Initial stages of glutamate excitoxicity,
  - Axonal disruption supported by increases in light and heavy neurofilament and metabolite changes,
  - Relationships between metabolite, kinematics, and staining and potential underlying disruption predictors,
  - Immunohistochemical and metabolite changes that persist to 72 hours after impact.
- The observed combined translation and rotation-input impact response is defined by:
  - A clear pathway for glutamate excitoxicity,
  - Axonal disruption supported by increases in light and heavy neurofilament and metabolite changes,
  - Relationships between metabolite, kinematics, and staining and potential underlying disruption predictors,
  - Immunohistochemical and metabolite changes that persist to 72 hours after impact.

This study developed two clinically-relevant injury devices to be used in a gyrencephalic animal model. This research provides the foundation for many potential follow-up studies to gain a more comprehensive understanding of traumatic brain injury. Understanding injury cascades in a relevant model might lead to new drug therapy targets. In addition, these devices can be used as another stage of pre-clinical drug testing as a more robust assessment of potential drug treatments where the currently used models fall short.

More immediately, this research will support the development of an improved injury metric. Companion high-speed biplane x-ray experiments will measure the relative brain/skull motion during identical head impacts as the ones described for the *in vivo* experiments. These data will be used to develop and validate a finite element model of the minipig head that relates impact kinematics to underlying damage. This model will be compared to a human finite element model to determine an appropriate scaling factor, which can then be used to scale the minipig impacts. The size and shape of the Göttingen minipig brain will result in much smaller scaling factors than would other animal models (e.g. rodents), substantially reducing errors associated with scaling estimations. This will lead to an injury metric that directly relates impact kinematics to underlying damage. This research has the potential to lead to safer vehicles, sporting equipment and military protective gear, and can be used to design work and play environments to minimize head injuries.

7.1 CONTRIBUTIONS TO THE FIELD

Intended publications from this dissertation are summarized in Table 7.1.

Table 7.1: Intended publications from this dissertation research.

Ch.	Title	Publication
2	Develop and Demonstrate the Repeatability of Two Unique Traumatic Brain Injury Devices	*Journal of Transportation Safety*
3	Techniques for the Investigation of Traumatic Brain Injury Mechanisms Characterized by Magnetic Resonance Spectroscopy	*Biomedical Sciences Instrumentation* 48, 126-133 (2012)
4	Injury Characterization Over the Course of 24 hours Using Two Novel Injury Devices	*Journal of Neurotrauma*
4	Evaluation of Impact-Induced Traumatic Brain Injury in the Göttingen Minipig Using Two Input Modes	*Traffic Injury Prevention*. 15, S81-87 (2014)
5	Mapping Biochemical Changes and Kinematics to Immunohistochemical Staining	*Journal of Neurotrauma or Journal of Neurochemistry or NMR in Biomedicine*
6	Injury Characterization Over the Course of 72 hours Using Two Novel Injury Devices	*Journal of Neurotrauma or Neuroscience letters*

REFERENCES

49CFR571.208 (2011) Standard No. 208; Occupant Crash Protection.

49CFR571.213 (2008) Standard No. 213; Child Restraint Systems.

49CFR571.214 (2008) Standard No. 214; Side Impact Protection.

Adams, J. H., Graham, D. I., Murray, L. S., and Scott, G. (1982). Diffuse Axonal Injury Due to Nonmissile Head Injury in Humans: an Analysis of 45 cases. *Annals of Neurology*, *12*(6), 557-563.

Adams, J. H., Graham, D. I., and Gennarelli, T. A. (1983). Head Injury in Man and Experimental Animals: Neuropathology. *Acta Neurochirurgica. Supplementum*, *32*, 15-30.

Alessandri, B., Heimann, A., Filippi, R., Kopacz, L., and Kempski, O. (2003). Moderate Controlled Cortical Contusion in Pigs: Effects on Multi-Parametric Neuromonitoring and Clinical Relevance. *Journal of Neurotrauma*, *20*(12), 1293-1305.

Arfanakis, K., Haughton, V. M., Carew, J. D., Rogers, B. P., Dempsey, R. J., and Meyer, M. E. (2002). Diffusion Tensor MR Imaging in Diffuse Axonal Injury. *American Journal of Neuroradiology*, *23*(5), 794-802.

Arroyo, E. J., and Scherer, S. S. (2000). On the Molecular Architecture of Myelinated Fibers. *Histochemistry and Cell Biology*, *113*(1), 1-18.

Bandak, F. A., and Eppinger, R. H. (1994). A Three-Dimensional Finite Element Analysis of the Human Brain Under Combined Rotational and Translational Accelerations. *SAE Technical Pape*r. No. 942215

Basser, P. J., Mattiello, J., and LeBihan, D. (1994). MR Diffusion Tensor Spectroscopy and Imaging. *Biophysical Journal*, *66*(1), 259-267.

Basser, P. J., and Pierpaoli, C. (1996). Microstructural and Physiological Features of Tissues Elucidated by Quantitative-Diffusion-Tensor MRI. *Journal of Magnetic Resonance. Series B*, *111*(3), 209-219.

Bigler, E. D., and Maxwell, W. L. (2011). Neuroimaging and Neuropathology of TBI. *NeuroRehabilitation*, *28*(2), 63-74.

Brooks, W. M., Friedman, S. D., and Gasparovic, C. (2001). Magnetic Resonance Spectroscopy in Traumatic Brain Injury. *The Journal of Head Trauma Rehabilitation*, *16*(2), 149-164.

Browne, K. D., Chen, X. H., Meaney, D. F., and Smith, D. H. (2011). Mild Traumatic Brain Injury and Diffuse Axonal Injury in Swine. *Journal of Neurotrauma*, *28*(9), 1747-1755.

Büki, A., Siman, R., Trojanowski, J. Q., and Povlishock, J. T. (1999). The Role of Calpain-Mediated Spectrin Proteolysis in Traumatically Induced Axonal Injury. *Journal of Neuropathology and Experimental Neurology*, *58*(4), 365-375.

Carbonell, W. S., Maris, D. O., McCall, T. O. D. D., and Grady, M. S. (1998). Adaptation of the Fluid Percussion Injury Model to the Mouse. *Journal of Neurotrauma*, *15*(3), 217-229.

Cazalis, F., Feydy, A., Valabrègue, R., Pélégrini-Issac, M., Pierot, L., and Azouvi, P. (2006). fMRI Study of Problem-Solving After Severe Traumatic Brain Injury. *Brain Injury*, *20*(10), 1019-1028.

Cecil, K. M., Lenkinski, R. E., Meaney, D. F., McIntosh, T. K., and Smith, D. H. (1998). High-Field Proton Magnetic Resonance Spectroscopy of a Swine Model for Axonal Injury. *Journal of Neurochemistry*, *70*(5), 2038-2044.

Cernak, I. (2005). Animal Models of Head Trauma. *NeuroRx*, *2*(3), 410-422.

Chakraborty, G., Mekala, P., Yahya, D., Wu, G., and Ledeen, R. W. (2001). Intraneuronal N-acetylaspartate Supplies Acetyl Groups for Myelin Lipid Synthesis: Evidence for Myelin-Associated Aspartoacylase. *Journal of Neurochemistry*, *78*(4), 736-745.

Chen, S., Pickard, J. D., and Harris, N. G. (2003). Time Course of Cellular Pathology After Controlled Cortical Impact Injury. *Experimental Neurology*, *182*(1), 87-102.

Chen, Y., Constantini, S., Trembovler, V., Weinstock, M., and Shohami, E. (1996). An Experimental Model of Closed Head Injury in Mice: Pathophysiology, Histopathology, and Cognitive Deficits. *Journal of Neurotrauma*, *13*(10), 557-568.

Corrigan, J. D., Selassie, A. W., and Orman, J. A. L. (2010). The Epidemiology of Traumatic Brain Injury. *The Journal of Head Trauma Rehabilitation*, *25*(2), 72-80.

Creed, J. A., DiLeonardi, A. M., Fox, D. P., Tessler, A. R., and Raghupathi, R. (2011). Concussive Brain Trauma in the Mouse Results in Acute Cognitive Deficits and Sustained Impairment of Axonal Function. *Journal of Neurotrauma*, *28*(4), 547-563.

Dean, P. J. A., and Sterr, A. (2013). Long-Term Effects of Mild Traumatic Brain Injury on Cognitive Performance. *Frontiers in Human Neuroscience*, *7*(30), 1-11.

Denny-Brown, D., and Russell, W. R. (1941). Experimental Cerebral Concussion. *Brain*, *64*(2-3), 93-164.

Dixon, C. E., Lyeth, B. G., Povlishock, J. T., Findling, R. L., Hamm, R. J., Marmarou, A., Young, H. F., and Hayes, R. L. (1987). A Fluid Percussion Model of Experimental Brain Injury in the Rat. *Journal of Neurosurgery*, *67*(1), 110-119.

Dixon, C. E., Clifton, G. L., Lighthall, J. W., Yaghmai, A. A., and Hayes, R. L. (1991). A Controlled Cortical Impact Model of Traumatic Brain Injury in the Rat. *Journal of Neuroscience Methods*, *39*(3), 253-262.

Eppinger, R. H. (1981, March). Discussion of Injury Criteria. In *Head and Neck Injury Criteria: a Consensus Workshop. Washington, DC: US Department of Transportation* (pp. 204-249).

Faul, M., Xu, L., Wald, M. M., and Coronado, V. G. (2010). Traumatic Brain Injury in the United States. *Atlanta, GA: Centers for Disease Control and Prevention, National Center for Injury Prevention and Control*.

Feeney, D. M., Boyeson, M. G., Linn, R. T., Murray, H. M., and Dail, W. G. (1981). Responses to Cortical Injury: I. Methodology and Local Effects of Contusions in the Rat. *Brain Research*, *211*(1), 67-77.

Fievisohn, E. M., Vaughn, B. M., and Hardy, W. N. (2012). Techniques for the Investigation of Traumatic Brain Injury Mechanisms Characterized by Magnetic Resonance Spectroscopy. *Biomedical Sciences Instrumentation*, *48*, 126-133.

Fievisohn, E. M., Sajja, V. S. S. S., VandeVord, P. J., and Hardy, W. N. (2014). Evaluation of Impact-Induced Traumatic Brain Injury in the Göttingen Minipig Using Two Input Modes. *Traffic Injury Prevention*, *15*(sup1), S81-S87.

Fletcher, D. A., and Mullins, R. D. (2010). Cell Mechanics and the Cytoskeleton. *Nature*, *463*(7280), 485-492.

Floyd, C. L., Golden, K. M., Black, R. T., Hamm, R. J., and Lyeth, B. G. (2002). Craniectomy Position Affects Morris Water Maze Performance and Hippocampal Cell Loss After Parasagittal Fluid Percussion. *Journal of Neurotrauma*, *19*(3), 303-316.

Foda, M. A., and Marmarou, A. (1994). A New Model of Diffuse Brain Injury in Rats. Part II: Morphological Characterization. *Journal of Neurosurgery*, *80*(2), 301-313.

Fox, G. B., Fan, L. E. I., Levasseur, R. A., and Faden, A. I. (1998). Sustained Sensory/Motor and Cognitive Deficits With Neuronal Apoptosis Following Controlled Cortical Impact Brain Injury in the Mouse. *Journal of Neurotrauma*, *15*(8), 599-614.

Gadd, C. W. (1966). Use of a Weighted-Impulse Criterion for Estimating Injury Hazard. *SAE Technical Paper*. No. 660793

Gehre, C., Gades, H., and Wernicke, P. (2009). Objective Rating of Signals Using Test and Simulation Responses. In *21st International Technical Conference on the Enhanced Safety of Vehicles, Stuttgart, Germany*.

Gennarelli, T. A., Abel, J. M., Adams, H., and Graham, D. (1979). Differential Tolerance of Frontal and Temporal Lobes to Contusion Induced by Angular Acceleration. *SAE Technical Paper*. No. 791022.

Gennarelli, T. A., Spielman, G. M., Langfitt, T. W., Gildenberg, P. L., Harrington, T., Jane, J. A., Marshall, L. F., Miller, J. D., and Pitts, L. H. (1982). Influence of the Type of Intracranial Lesion on Outcome from Severe Head Injury: A Multicenter Study Using a New Classification System. *Journal of Neurosurgery*, *56*(1), 26-32.

Gennarelli, T. A., Thibault, L. E., Adams, J. H., Graham, D. I., Thompson, C. J., and Marcincin, R. P. (1982). Diffuse Axonal Injury and Traumatic Coma in the Primate. *Annals of Neurology*, *12*(6), 564-574.

Gennarelli, T. A. (1983). Head Injury in Man and Experimental Animals: Clinical Aspects. *Acta Neurochirurgica Supplementum*, *32*, 1.

Gennarelli, T. A. (1994). Animate Models of Human Head Injury. *Journal of Neurotrauma*, *11*(4), 357-368.

Gennarelli, T. A. (1996). The Spectrum of Traumatic Axonal Injury. *Neuropathology and Applied Neurobiology*, *22*(6), 509-513.

Gennarelli, T. A., Thibault, L. E., and Graham, D. I. (1998). Diffuse Axonal Injury: An Important Form of Traumatic Brain Damage. *The Neuroscientist*, *4*(3), 202-215.

Gennarelli, T. A. and Wodzin, E. (Eds.) (2005). Abbreviated Injury Scale 2005, Update 2008. Barrington, IL: Association for the Advancement of Automotive Medicine.

Gerberding, J. L., and Binder, S. (2003). Report to Congress on Mild Traumatic Brain Injury in the United States: Steps to Prevent a Serious Public Health Problem. *Atlanta, GA: National Center for Injury Prevention and Control, Centers for Disease Control and Prevention*.

Griffith, H. R., den Hollander, J. A., Stewart, C. C., Evanochko, W. T., Buchthal, S. D., Harrell, L. E., Zamrini, E. Y., Brockington, J. C., and Marson, D. C. (2007). Elevated Brain Scyllo-

inositol Concentrations in Patients with Alzheimer's Disease. *NMR in Biomedicine*, *20*(8), 709-716.

Groat, R. A., Windle, W. F., and Magoun, H. W. (1945). Functional and Structural Changes in the Monkey's Brain During and After Concussion*. *Journal of Neurosurgery*, *2*(1), 26-35.

Gurdjian, E. S., Lissner, H. R., Evans, F. G., Patrick, L. M., and Hardy, W. G. (1961). Intracranial Pressure and Acceleration Accompanying Head Impacts in Human Cadavers. *Surgery, Gynecology & Obstetrics*, *113*, 185.

Gurdjian, E. S., Hodgson, V. R., Hardy, W. G., Patrick, L. M., and Lissner, H. R. (1964). Evaluation of The Protective Characteristics Of Helmets In Sports. *Journal of Trauma and Acute Care Surgery*, *4*(3), 309-324.

Gurdjian, E. S., Roberts, V. L., and Thomas, L. M. (1966). Tolerance Curves of Acceleration and Intracranial Pressure and Protective Index in Experimental Head Injury. *Journal of Trauma and Acute Care Surgery*, *6*(5), 600-604.

Hamm, R. J., Dixon, C. E., Gbadebo, D. M., Singha, A. K., Jenkins, L. W., Lyeth, B. G., and Hayes, R. L. (1992). Cognitive Deficits Following Traumatic Brain Injury Produced by Controlled Cortical Impact. *Journal of Neurotrauma*, *9*(1), 11-20.

Hannay, H. J., Feldman, Z., Phan, P., Keyani, A., Panwar, N., Goodman, J. C., and Robertson, C. S. (1999). Validation of a Controlled Cortical Impact Model of Head Injury in Mice. *Journal of Neurotrauma*, *16*(11), 1103-1114.

Hardy, W. N., Khalil, T. B., & King, A. I. (1994). Literature Review of Head Injury Biomechanics. *International Journal of Impact Engineering*, *15*(4), 561-586.

Hardy, W. N., Mason, M. J., Foster, C. D., Shah, C. S., Kopacz, J. M., Yang, K. H., King, S. I., Bishop, J., Bey, M., Anderst, W., and Tashman, S. (2007). A Study of the Response of the Human Cadaver Head to Impact. *Stapp Car Crash Journal*, *51*, 17-80.

Harris, J. L., Yeh, H. W., Choi, I. Y., Lee, P., Berman, N. E., Swerdlow, R. H., Craciunas, S. C., and Brooks, W. M. (2012). Altered Neurochemical Profile After Traumatic Brain Injury: ^{1}H-MRS Biomarkers of Pathological Mechanisms. *Journal of Cerebral Blood Flow and Metabolism*, *32*(12), 2122-2134.

Heath, D. L., and Vink, R. (1995). Impact Acceleration-Induced Severe Diffuse Axonal Injury in Rats: Characterization of Phosphate Metabolism and Neurologic Outcome. *Journal of Neurotrauma*, *12*(6), 1027-1034.

Herculano-Houzel, S. (2009). The Human Brain in Numbers: a Linearly Scaled-Up Primate Brain. *Frontiers in human neuroscience*, *3*, 1-11.

Higgins, L. S., and Schmall, R. A. (1967). A Device for the Investigation of Head Injury Effected by Non-Deforming Head Accelerations. *SAE Technical Paper*. No. 670905.

Hinkley, L. B., Marco, E. J., Findlay, A. M., Honma, S., Jeremy, R. J., Strominger, Z., Bukshpun, P., Wakahire, M., Brown, W. S., Paul, L. K., Barkovich, J., Mukherjee, P., Nagarajan, S. S., and Sherr, E. H. (2012). The Role of Corpus Callosum Development in Functional Connectivity and Cognitive Processing. *PLoS One*, *7*(8), e39804.

Holbourn, A. H. S. (1945). The Mechanics of Brain Injuries. *British Medical Bulletin*, *3*(6), 147-149.

Hunter, J. V., Wilde, E. A., Tong, K. A., and Holshouser, B. A. (2012). Emerging Imaging Tools for Use with Traumatic Brain Injury Research. *Journal of Neurotrauma*, *29*(4), 654-671.

Kabadi, S. V., Hilton, G. D., Stoica, B. A., Zapple, D. N., and Faden, A. I. (2010). Fluid-Percussion-Induced Traumatic Brain Injury Model in Rats. *Nature Protocols*, *5*(9), 1552-1563.

Kallakuri, S., Li, Y., Zhou, R., Bandaru, S., Zakaria, N., Zhang, L., and Cavanaugh, J. M. (2012). Impaired Axoplasmic Transport is the Dominant Injury Induced by an Impact Acceleration Injury Device: an Analysis of Traumatic Axonal Injury in Pyramidal Tract and Corpus Callosum of Rats. *Brain Research*, *1452*, 29-38.

Kandel, E. R., Schwartz, J. H., and Jessel, T. M. (2000). *Principles of Neural Science (4th ed.)*. New York: McGraw-Hill.

Kettenmann, H., Hanisch, U. K., Noda, M., and Verkhratsky, A. (2011). Physiology of Microglia. *Physiological Reviews*, *91*(2), 461-553.

Kimura, H., Meaney, D. F., McGowan, J. C., Grossman, R. I., Lenkinski, R. E., Ross, D. T., McIntosh, T. K., Gennarelli, T. A., and Smith, D. H. (1996). Magnetization Transfer Imaging of Diffuse Axonal Injury Following Experimental Brain Injury in the Pig: Characterization by Magnetization Transfer Ratio with Histopathologic Correlation. *Journal of Computer Assisted Tomography*, *20*(4), 540-546.

King, A. I., Yang, K. H., Zhang, L., Hardy, W., and Viano, D. C. (2003). Is Head Injury Caused by Linear or Angular Acceleration? In *Proceedings of the IRCOBI Conference*.

Kou, Z., and VandeVord, P. J. (2014). Traumatic White Matter Injury and Glial Activation: From Basic Science to Clinics. *Glia*, *62*(11), 1831-1855.

Laituri, T. R., El-Jawahri, R. E., Henry, S., and Sullivan, K. (2015). Field-Based Assessments of Various AIS2+ Head Risk Curves for Frontal Impact. *SAE Technical Paper*. No. 2015-01-1437.

Lee, H., Wintermark, M., Gean, A. D., Ghajar, J., Manley, G. T., and Mukherjee, P. (2008). Focal Lesions in Acute Mild Traumatic Brain Injury and Neurocognitive Outcome: CT Versus 3T MRI. *Journal of Neurotrauma*, *25*(9), 1049-1056.

Lei, H., Berthet, C., Hirt, L., and Gruetter, R. (2009). Evolution of the Neurochemical Profile After Transient Focal Cerebral Ischemia in the Mouse Brain. *Journal of Cerebral Blood Flow and Metabolism*, *29*(4), 811-819.

Li, Y., Zhang, L., Kallakuri, S., Zhou, R., and Cavanaugh, J. M. (2011). Quantitative Relationship Between Axonal Injury and Mechanical Response in a Rodent Head Impact Acceleration Model. *Journal of Neurotrauma*, *28*(9), 1767-1782.

Li, Y., Zhang, L., Kallakuri, S., Zhou, R., and Cavanaugh, J. M. (2011). Injury Predictors for Traumatic Axonal Injury in a Rodent Head Impact Acceleration Model. *Stapp Car Crash Journal*, *55*, 25.

Lighthall, J. W. (1988). Controlled Cortical Impact: a New Experimental Brain Injury Model. *Journal of Neurotrauma*, *5*(1), 1-15.

Lighthall, J. W., Dixon, C. E., and Anderson, T. E. (1989). Experimental Models of Brain Injury. *Journal of Neurotrauma*, *6*(2), 83-97.

Lighthall, J. W., Goshgarian, H. G., and Pinderski, C. R. (1990). Characterization of Axonal Injury Produced by Controlled Cortical Impact. *Journal of Neurotrauma*, *7*(2), 65-76.

Lindgren, S., and Rinder, L. (1966). Experimental Studies in Head Injury. *Biophysik*, *3*(2), 174-180.

Lindgren, S., and Rinder, L. (1969). Production and Distribution of Intracranial and Intraspinal Pressure Changes at Sudden Extradural Fluid Volume Input in Rabbits. *Acta Physiologica Scandinavica*, *76*(3), 340-351.

Maas, A. I., Stocchetti, N., and Bullock, R. (2008). Moderate and Severe Traumatic Brain Injury in Adults. *The Lancet Neurology*, *7*(8), 728-741.

Mao, H., Zhang, L., Jiang, B., Genthikatti, V. V., Jin, X., Zhu, F., Makwana, R., Gill, A., Jandir, G., Singh, A., and Yang, K. H. (2013). Development of a Finite Element Human Head Model Partially Validated With Thirty Five Experimental Cases. *Journal of Biomechanical Engineering*, *135*(11), 111002.

Manley, G. T., Rosenthal, G., Lam, M., Morabito, D., Yan, D., Derugin, N., Bollen, A., Knudsen, M. M., and Panter, S. S. (2006). Controlled Cortical Impact in Swine: Pathophysiology and Biomechanics. *Journal of Neurotrauma*, *23*(2), 128-139.

Margulies, S., and Hicks, R. (2009). Combination Therapies for Traumatic Brain Injury: Prospective Considerations. *Journal of Neurotrauma*, *26*(6), 925-939.

Mark, L. P., Prost, R. W., Ulmer, J. L., Smith, M. M., Daniels, D. L., Strottmann, J. M., Brown, W. D., and Hacein-Bey, L. (2001). Pictorial Review of Glutamate Excitotoxicity: Fundamental Concepts for Neuroimaging. *American Journal of Neuroradiology*, *22*(10), 1813-1824.

Marklund, N., Bakshi, A., Castelbuono, D. J., Conte, V., and McIntosh, T. K. (2006). Evaluation of Pharmacological Treatment Strategies in Traumatic Brain Injury. *Current Pharmaceutical Design*, *12*(13), 1645-1680.

Marmarou, A., Foda, M. A. A. E., Brink, W. V. D., Campbell, J., Kita, H., and Demetriadou, K. (1994). A New Model of Diffuse Brain Injury in Rats: Part I: Pathophysiology and Biomechanics. *Journal of Neurosurgery*, *80*(2), 291-300.

Marmarou, C. R., Walker, S. A., Davis, C. L., and Povlishock, J. T. (2005). Quantitative Analysis of the Relationship Between Intra-Axonal Neurofilament Compaction and Impaired Axonal Transport Following Diffuse Traumatic Brain Injury. *Journal of Neurotrauma*, *22*(10), 1066-1080.

Martin, J. H. (1996). *Neuroanatomy – Text and Atlas (2nd ed.).* New York: McGraw-Hill.

Matis, G., and Birbilis, T. (2008). The Glasgow Coma Scale—a Brief Review. Past, Present, Future. *Acta Neurol Belg*, *108*(3), 75-89.

Maxwell, W. L., Povlishock, J. T., and Graham, D. L. (1997). A Mechanistic Analysis of Nondisruptive Axonal Injury: A Review. *Journal of Neurotrauma*, *14*(7), 419-440.

McIntosh, T. K., Noble, L., Andrews, B., and Faden, A. I. (1987). Traumatic Brain Injury in the Rat: Characterization of a Midline Fluid-Percussion Model. *Central Nervous System Trauma*, *4*(2), 119-134.

McIntosh, T. K., Vink, R., Noble, L., Yamakami, I., Fernyak, S., Soares, H., and Faden, A. L. (1989). Traumatic Brain Injury in the Rat: Characterization of a Lateral Fluid-Percussion Model. *Neuroscience*, *28*(1), 233-244.

McLean, A. J. (1995). Brain Injury Without Head Impact?. *Journal of Neurotrauma*, *12*(4), 621-625.

Mehta, A., Prabhakar, M., Kumar, P., Deshmukh, R., and Sharma, P. L. (2013). Excitotoxicity: Bridge to Various Triggers in Neurodegenerative Disorders. *European Journal of Pharmacology*, *698*(1), 6-18.

Mertz, H. J., Irwin, A. L., and Prasad, P. (2003). Biomechanical and Scaling Bases for Frontal and Side Impact Injury Assessment Reference Values. *Stapp Car Crash Journal*, *47*, 155-188.

Mittl, R. L., Grossman, R. I., Hiehle, J. F., Hurst, R. W., Kauder, D. R., Gennarelli, T. A., and Alburger, G. W. (1994). Prevalence of MR Evidence of Diffuse Axonal Injury in Patients with Mild Head Injury and Normal Head CT Findings. *American Journal of Neuroradiology*, *15*(8), 1583-1589.

Moffett, J. R., Ross, B., Arun, P., Madhavarao, C. N., and Namboodiri, A. M. (2007). N-Acetylaspartate in the CNS: From Neurodiagnostics to Neurobiology. *Progress in Neurobiology*, *81*(2), 89-131.

Moore, G. J., and Galloway, M. P. (2001). Magnetic Resonance Spectroscopy: Neurochemistry and Treatment Effects in Affective Disorders. *Psychopharmacology Bulletin*, *36*(2), 5-23.

Narayan, R. K., Michel, M. E., Ansell, B., Baethmann, A., Biegon, A., Bracken, M. B., et al. (2002). Clinical Trials in Head Injury. *Journal of Neurotrauma*, *19*(5), 503-557.

Neale, J. H., Olszewski, R. T., Gehl, L. M., Wroblewska, B., and Bzdega, T. (2005). The Neurotransmitter N-acetylaspartylglutamate in Models of Pain, ALS, Diabetic Neuropathy, CNS Injury and Schizophrenia. *Trends in Pharmacological Sciences*, *26*(9), 477-484.

Netter, F. H. (2011). *Atlas of Human Anatomy (5th ed.)*. Philadelphia, PA: Saunders/Elsevier.

Newman, J. A., Shewchenko, N., and Welbourne, E. (2000). A Proposed New Biomechanical Head Injury Assessment Function-the Maximum Power Index. *Stapp Car Crash Journal*, *44*, 215-247.

Nucifora, P. G., Verma, R., Lee, S. K., and Melhem, E. R. (2007). Diffusion-Tensor MR Imaging and Tractography: Exploring Brain Microstructure and Connectivity 1. *Radiology*, *245*(2), 367-384.

Okonkwo, D. O., Pettus, E. H., Moroi, J., and Povlishock, J. T. (1998). Alteration of the Neurofilament Sidearm and its Relation to Neurofilament Compaction Occurring with Traumatic Axonal Injury. *Brain Research*, *784*(1), 1-6.

Ommaya, A. K., and Hirsch, A. E. (1971). Tolerances for Cerebral Concussion from Head Impact and Whiplash in Primates. *Journal of Biomechanics*, *4*(1), 13-21.

Ono, K., Kikuchi, A., Nakamura, M., Kobayashi, H., and Nakamura, N. (1980). Human Head Tolerance to Sagittal Impact Reliable Estimation Deduced from Experimental Head Injury Using Subhuman Primates and Human Cadaver Skulls. *SAE Technical Paper*. No. 801303

Palmer, A. M., Marion, D. W., Botscheller, M. L., Swedlow, P. E., Styren, S. D., and DeKosky, S. T. (1993). Traumatic Brain Injury-Induced Excitotoxicity Assessed in a Controlled Cortical Impact Model. *Journal of Neurochemistry*, *61*(6), 2015-2024.

Paniak, C., Reynolds, S., Phillips, K., Toller-Lobe, G., Melnyk, A., and Nagy, J. (2002). Patient Complaints Within 1 Month of Mild Traumatic Brain Injury: A Controlled Study. *Archives of Clinical Neuropsychology*, *17*(4), 319-334.

Parnaik, Y., Beillas, P., Demetropoulos, C. K., Hardy, W. N., Yang, K. H., and King, A. I. (2004). The Influence of Surrogate Blood Vessels on the Impact Response of a Physical Model of the Brain. *Stapp Car Crash Journal*, *48*, 259-277.

Pascual, J. M., Solivera, J., Prieto, R., Barrios, L., López-Larrubia, P., Cerdán, S., and Roda, J. M. (2007). Time Course of Early Metabolic Changes Following Diffuse Traumatic Brain Injury in Rats as Detected by ^{1}H NMR Spectroscopy. *Journal of Neurotrauma*, *24*(6), 944-959.

Peles, E., and Salzer, J. L. (2000). Molecular Domains of Myelinated Axons. *Current Opinion in Neurobiology*, *10*(5), 558-565.

Pettus, E. H., Christman, C. W., Giebel, M. L., and Povlishock, J. T. (1994). Traumatically Induced Altered Membrane Permeability: Its Relationship to Traumatically Induced Reactive Axonal Change. *Journal of Neurotrauma*, *11*(5), 507-522.

Pettus, E. H., and Povlishock, J. T. (1996). Characterization of a Distinct Set of Intra-Axonal Ultrastructural Changes Associated with Traumatically Induced Alteration in Axolemmal Permeability. *Brain Research*, *722*(1), 1-11.

Podell, K., Gifford, K., Bougakov, D., and Goldberg, E. (2010). Neuropsychological Assessment in Traumatic Brain Injury. *Psychiatric Clinics of North America*, *33*(4), 855-876.

Poliak, S., and Peles, E. (2003). The Local Differentiation of Myelinated Axons at Nodes of Ranvier. *Nature Reviews Neuroscience*, *4*(12), 968-980.

Polikov, V. S., Tresco, P. A., and Reichert, W. M. (2005). Response of Brain Tissue to Chronically Implanted Neural Electrodes. *Journal of Neuroscience Methods*, *148*(1), 1-18.

Porter, A. G., and Jänicke, R. U. (1999). Emerging Roles of Caspase-3 in Apoptosis. *Cell Death and Differentiation*, *6*(2), 99-104.

Povlishock, J. T., Becker, D. P., Sullivan, H. G., and Miller, J. D. (1978). Vascular Permeability Alterations to Horseradish Peroxidase in Experimental Brain Injury. *Brain Research*, *153*(2), 223-239.

Povlishock, J. T., Becker, D. P., Cheng, C. L. Y., and Vaughan, G. W. (1983). Axonal Change in Minor Head Injury. *Journal of Neuropathology and Experimental Neurology*, *42*(3), 225-242.

Povlishock, J. T., and Kontos, H. A. (1985). Continuing Axonal and Vascular Change Following Experimental Brain Trauma. *Central Nervous System Trauma*, *2*(4), 285-298.

Povlishock, J. T. (1993). Pathobiology of Traumatically Induced Axonal Injury in Animals and Man. *Annals of Emergency Medicine*, *22*(6), 980-986.

Povlishock, J. T., Hayes, R. L., Michel, M. E., and McIntosh, T. K. (1994). Workshop on Animal Models of Traumatic Brain Injury. *Journal of Neurotrauma*, *11*(6), 723-732.

Povlishock, J. T., Marmarou, A., McIntosh, T., Trojanowski, J. Q., and Moroi, J. (1997). Impact Acceleration Injury in the Rat: Evidence for Focal Axolemmal Change and Related Neurofilament Sidearm Alteration. *Journal of Neuropathology and Experimental Neurology*, *56*(4), 347-359.

Prasad, P., and Mertz, H. J. (1985). The Position of the United States Delegation to the ISO Working Group 6 on the Use of HIC in the Automotive Environment. *SAE Technical Paper*. No. 851246.

Rae, C. D. (2014). A Guide to the Metabolic Pathways and Function of Metabolites Observed in Human Brain ^{1}H Magnetic Resonance Spectra. *Neurochemical Research*, *39*(1), 1-36.

Ramonet, D., Rodriguez, M. J., Fredriksson, K., Bernal, F., and Mahy, N. (2004). In Vivo Neuroprotective Adaptation of the Glutamate/Glutamine Cycle to Neuronal Death. *Hippocampus*, *14*(5), 586-594.

Ross, B., and Bluml, S. (2001). Magnetic Resonance Spectroscopy of the Human Brain. *The Anatomical Record*, *265*(2), 54-84.

Ross, D. T., Meaney, D. F., Sabol, M. K., Smith, D. H., and Gennarelli, T. A. (1994). Distribution of Forebrain Diffuse Axonal Injury Following Inertial Closed Head Injury in Miniature Swine. *Experimental Neurology*, *126*(2), 291-299.

Rowson, S., and Duma, S. M. (2013). Brain Injury Prediction: Assessing the Combined Probability of Concussion Using Linear and Rotational Head Acceleration. *Annals of Biomedical Engineering*, *41*(5), 873-882.

Sajja, V. S. S. S., Galloway, M. P., Ghoddoussi, F., Thiruthalinathan, D., Kepsel, A., Hay, K., Bir, C. A., and VandeVord, P. J. (2012). Blast-Induced Neurotrauma Leads to Neurochemical Changes and Neuronal Degeneration in the Rat Hippocampus. *NMR in Biomedicine*, *25*(12), 1331-1339.

Sanchez-Carrion, R., Fernandez-Espejo, D., Junque, C., Falcon, C., Bargallo, N., Roig, T., Bernabeu, M., Tormos, J. M., and Vendrell, P. (2008). A Longitudinal fMRI Study of Working Memory in Severe TBI Patients with Diffuse Axonal Injury. *Neuroimage*, *43*(3), 421-429.

Schuhmann, M. U., Stiller, D., Skardelly, M., Bernarding, J., Klinge, P. M., Samii, A., Samii, M., and Brinker, T. (2003). Metabolic Changes in the Vicinity of Brain Contusions: A Proton Magnetic Resonance Spectroscopy and Histology Study. *Journal of Neurotrauma*, *20*(8), 725-743.

Shutter, L., Tong, K. A., and Holshouser, B. A. (2004). Proton MRS in Acute Traumatic Brain Injury: Role for Glutamate/Glutamine and Choline for Outcome Prediction. *Journal of Neurotrauma*, *21*(12), 1693-1705.

Sidaros, A., Engberg, A. W., Sidaros, K., Liptrot, M. G., Herning, M., Petersen, P., Paulson, O.B., Jernigan, T. L., and Rostrup, E. (2008). Diffusion Tensor Imaging During Recovery

from Severe Traumatic Brain Injury and Relation to Clinical Outcome: a Longitudinal Study. *Brain*, *131*(2), 559-572.

Siegel, G. J., Agranoff, B. W., Albers, R. W., Fisher, S. K., Uhler, M. D. (1999). *Basic Neurochemistry – Molecular, Cellular and Medical Aspects (6th ed.)*. Philadelphia, PA: Lippincott-Raven.

Slusher, B. S., Vornov, J. J., Thomas, A. G., Hurn, P. D., Harukuni, I., Bhardwaj, A., Traystman, R. J., Robinson, M. B., Britton, P., May Lu, X.-C., Tortella, F. C., Wozniak, K. M., Yudkoff, M., Potter, B. M., and Jackson, P. F. (1999). Selective Inhibition of NAALADase, which Converts NAAG to Glutamate, Reduces Ischemic Brain Injury. *Nature Medicine*, *5*(12), 1396-1402.

Smith, D. H., Soares, H. D., Pierce, J. S., Perlman, K. G., Saatman, K. E., Meaney, D. F., Dixon, C. E., and McIntosh, T. K. (1995). A Model of Parasagittal Controlled Cortical Impact in the Mouse: Cognitive and Histopathologic Effects. *Journal of Neurotrauma*, *12*(2), 169-178.

Smith, D. H., Cecil, K. M., Meaney, D. F., Chen, X. H., McIntosh, T. K., Gennarelli, T. A., and Lenkinski, R. E. (1998). Magnetic Resonance Spectroscopy of Diffuse Brain Trauma in the Pig. *Journal of Neurotrauma*, *15*(9), 665-674.

Smith, D. H., Chen, X. H., Nonaka, M., Trojanowski, J. Q., Lee, V. Y., Saatman, K. E., Meaney, D. F., Dixon, C. E., and Meaney, D. F. (1999). Accumulation of Amyloid β and Tau and the Formation of Neurofilament Inclusions Following Diffuse Brain Injury in the Pig. *Journal of Neuropathology and Experimental Neurology*, *58*(9), 982-992.

Smith, D. H., and Meaney, D. F. (2000). Axonal Damage in Traumatic Brain Injury. *The Neuroscientist*, *6*(6), 483-495.

Society of Automotive Engineers. (2007). Standard J211/1 Instrumentation for Impact Test - Part 1 - Electronic Instrumentation. Warrendale, PA.

Spain, A., Daumas, S., Lifshitz, J., Rhodes, J., Andrews, P. J., Horsburgh, K., and Fowler, J. H. (2010). Mild Fluid Percussion Injury in Mice Produces Evolving Selective Axonal Pathology and Cognitive Deficits Relevant to Human Brain Injury. *Journal of Neurotrauma*, *27*(8), 1429-1438.

Squire, L., Berg, D., Bloom, F., du Lac, S., Ghosh, A., Spitzer, N. (2008). Fundamental Neuroscience (3rd ed.). Massachusetts: Academic Press/Elsevier.

Stalhammar, D., Galinat, B. J., Allen, A. M., Becker, D. P., Stonnington, H. H., and Hayes, R. L. (1987). A New Model of Concussive Brain Injury in the Cat Produced by Extradural Fluid Volume Loading: I. Biomechanical Properties. *Brain Injury*, *1*(1), 73-91.

Stone, J. R., Singleton, R. H., and Povlishock, J. T. (2001). Intra-Axonal Neurofilament Compaction Does Not Evoke Local Axonal Swelling in All Traumatically Injured Axons. *Experimental Neurology*, *172*(2), 320-331.

Stone, J. R., Okonkwo, D. O., Dialo, A. O., Rubin, D. G., Mutlu, L. K., Povlishock, J. T., and Helm, G. A. (2004). Impaired Axonal Transport and Altered Axolemmal Permeability Occur in Distinct Populations of Damaged Axons Following Traumatic Brain Injury. *Experimental Neurology*, *190*(1), 59-69.

Sullivan, H. G., Martinez, J., Becker, D. P., Miller, J. D., Griffith, R., and Wist, A. O. (1976). Fluid-Percussion Model of Mechanical Brain Injury in the Cat. *Journal of Neurosurgery*, *45*(5), 520-534.

Swanson, L. W. (1995). Mapping the Human Brain: Past, Present, and Future. *Trends in Neurosciences*, *18*(11), 471-474.

Takhounts, E. G., Hasija, V., Ridella, S. A., Rowson, S., and Duma, S. M. (2011). Kinematic Rotational Brain Injury Criterion (BRIC). In *Proceedings of the 22nd Enhanced Safety of Vehicles Conference. Paper* (No. 11-0263).

Takhounts, E. G., Craig, M. J., Moorhouse, K., McFadden, J., and Hasija, V. (2013). Development of Brain Injury Criteria (BrIC). *Stapp Car Crash Journal*, *57*, 243-266.

Teasdale, G., and Jennett, B. (1974). Assessment of Coma and Impaired Consciousness. A Practical Scale. *Lancet*, *2*(7872), 81-83.

Teasdale, G., and Jennett, B. (1976). Assessment and Prognosis of Coma After Head Injury. *Acta Neurochirurgica*, *34*(1-4), 45-55.

Tsaousides, T., and Gordon, W. A. (2009). Cognitive Rehabilitation Following Traumatic Brain Injury: Assessment to Treatment. *Mount Sinai Journal of Medicine: A Journal of Translational and Personalized Medicine*, *76*(2), 173-181.

Ucar, T., Tanriover, G., Gurer, I., Onal, M. Z., and Kazan, S. (2006). Modified Experimental Mild Traumatic Brain Injury Model. *Journal of Trauma and Acute Care Surgery*, *60*(3), 558-565.

Unterharnscheidt, F., and Higgins, L. S. (1969). Pathomorphology of Experimental Head Injury Due to Rotational Acceleration. *Acta Neuropathologica*, *12*(2), 200-204.

Versace, J. (1971). A Review of the Severity Index. *SAE Technical Paper*. No. 710881

Vink, R., Mullins, P. G., Temple, M. D., Bao, W., and Faden, A. I. (2001). Small Shifts in Craniotomy Position in the Lateral Fluid Percussion Injury Model are Associated with Differential Lesion Development. *Journal of Neurotrauma*, *18*(8), 839-847.

Walker, A. E., Kollros, J. J., and Case, T. J. (1944). The Physiological Basis of Concussion*. *Journal of Neurosurgery*, *1*(2), 103-116.

Waxman, S. G., Docsis, J. D., Stys, P. K. (1995). *The Axon – Structure, Function and Pathophysiology*. New York: Oxford University Press.

Yaghmai, A., and Povlishock, J. (1992). Traumatically Induced Reactive Change as Visualized Through the Use of Monoclonal Antibodies Targeted to Neurofilament Subunits. *Journal of Neuropathology and Experimental Neurology*, *51*(2), 158-176.

Yamaki, T., Murakami, N., Iwamoto, Y., Yoshino, E., Nakagawa, Y., Ueda, S., Horikawa, J., and Tsujii, T. (1994). A Modified Fluid Percussion Device. *Journal of Neurotrauma*, *11*(5), 613-622.

Yoganandan, N., Fitzharris, M., Pintar, F. A., Stemper, B. D., Rinaldi, J., Maiman, D. J., and Fildes, B. N. (2011). Demographics, Velocity Distributions, and Impact Type as Predictors of AIS 4+ Head Injuries in Motor Vehicle Crashes. *Annals of Advances in Automotive Medicine, 55*, 267-280.

Xiong, Y., Mahmood, A., and Chopp, M. (2013). Animal Models of Traumatic Brain Injury. *Nature Reviews Neuroscience*, *14*(2), 128-142.

Zakaria, N., Kallakuri, S., Bandaru, S., and Cavanaugh, J. M. (2012). Temporal Assessment of Traumatic Axonal Injury in the Rat Corpus Callosum and Optic Chiasm. *Brain Research*, *1467*, 81-90.

APPENDIX A: TECHNICAL DRAWINGS OF SELECTED PARTS

TRANSLATION-INPUT INJURY DEVICE

Aluminum block/brass tubing:

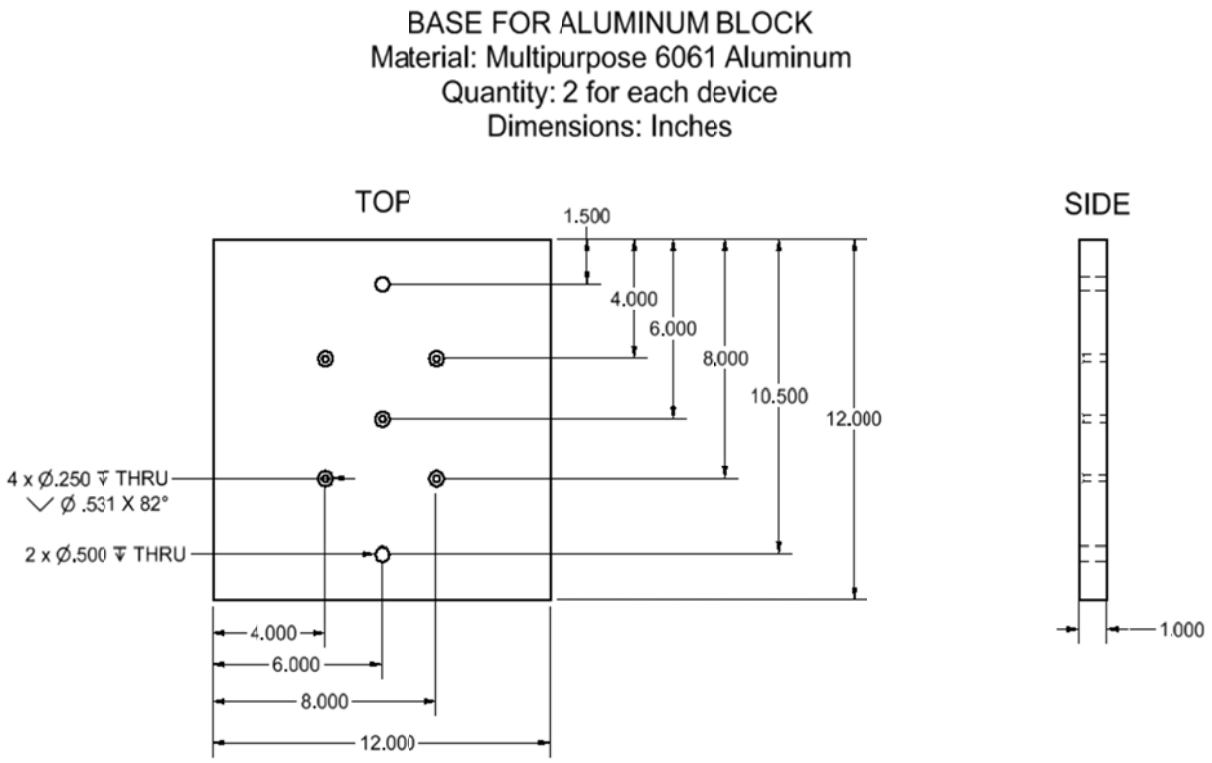

ALUMINUM BLOCK: TRANSLATIONAL-INPUT DEVICE
Material: Multipurpose 6061 Aluminum
Quantity: 2
Dimensions: Inches

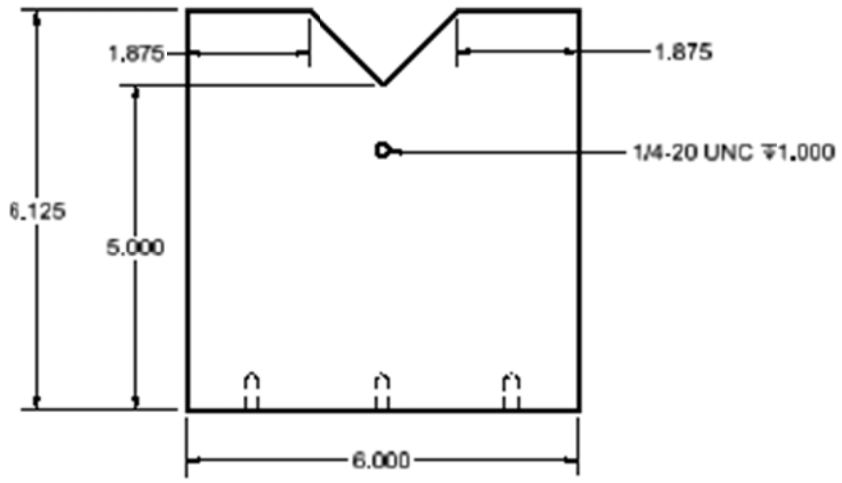

SIDE

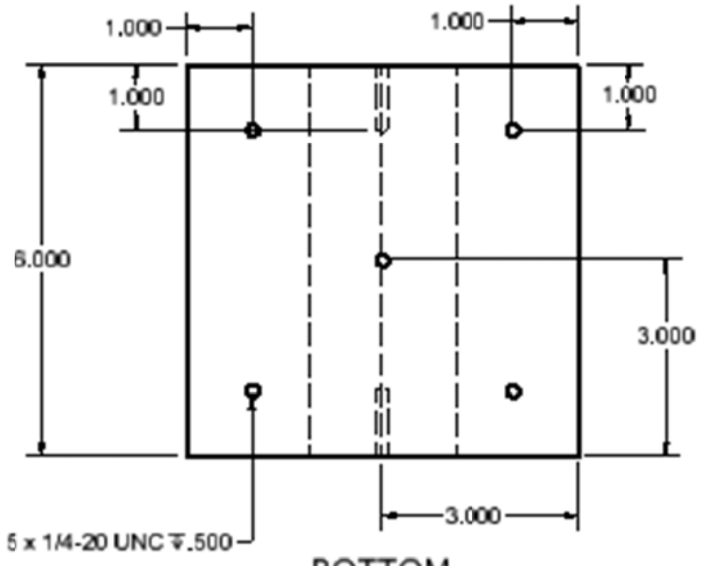

BOTTOM

Animal Platform:

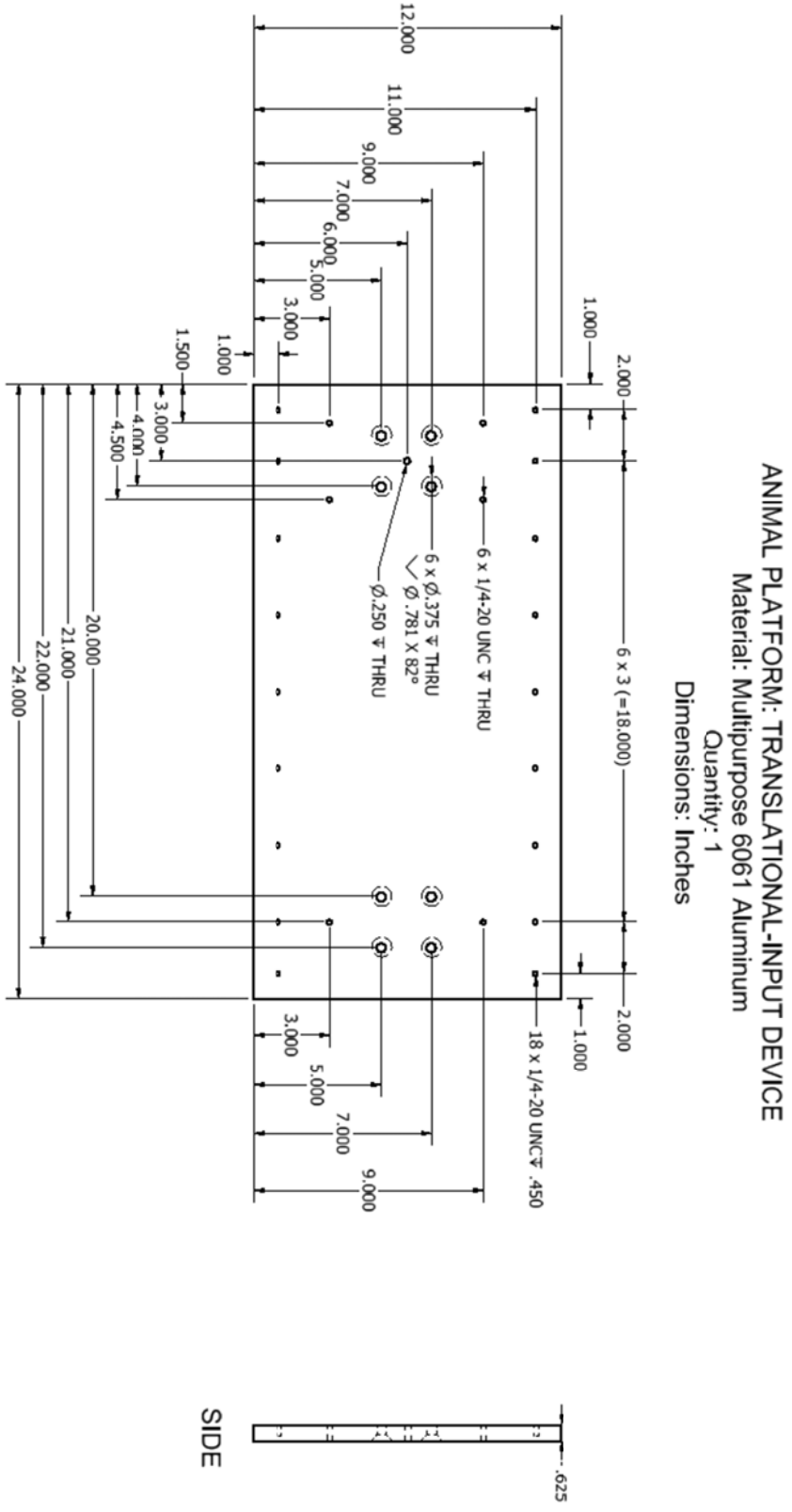

COMBINED TRANSLATION AND ROTATION-INPUT INJURY DEVICE

Aluminum hinges:

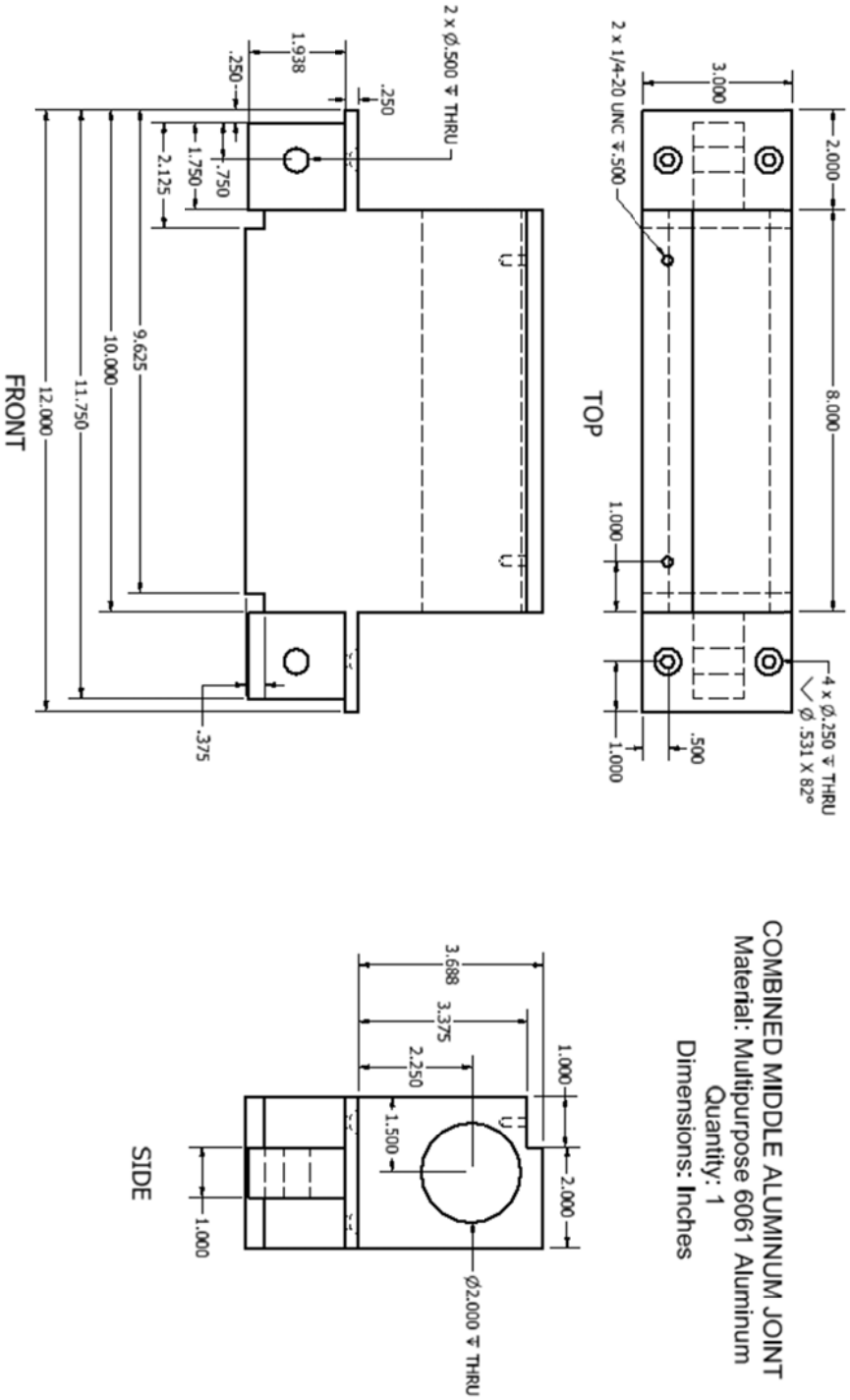

STEEL SHAFT FOR BASE PLATFORM: COMBINED-INPUT DEVICE
Material: Type 303 Stainless Steel
Quantity: 1
Dimensions: Inches

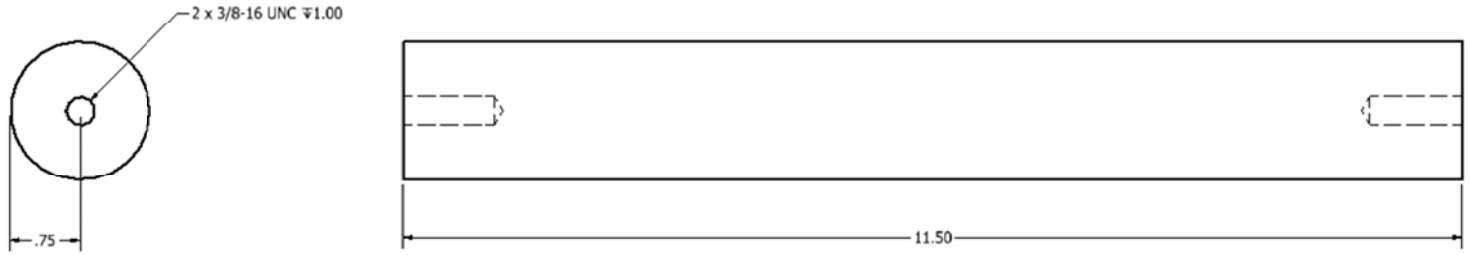

SIDE

TOP

STEEL SHAFT FOR MIDDLE JOINT: COMBINED-INPUT DEVICE
Material: Type 303 Stainless Steel
Quantity: 1
Dimensions: Inches

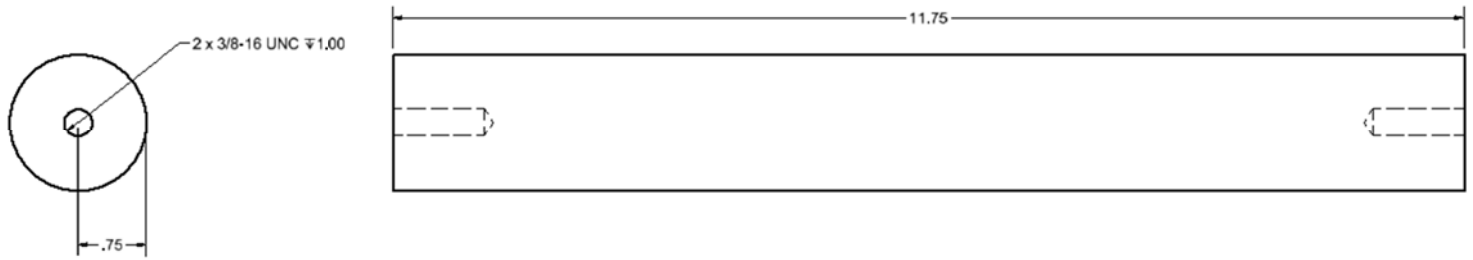

SIDE

TOP

TOP OF BASE HINGE: COMBINED-INPUT DEVICE
Material: Multipurpose 6061 Aluminum
Quantity: 1
Dimensions: Inches

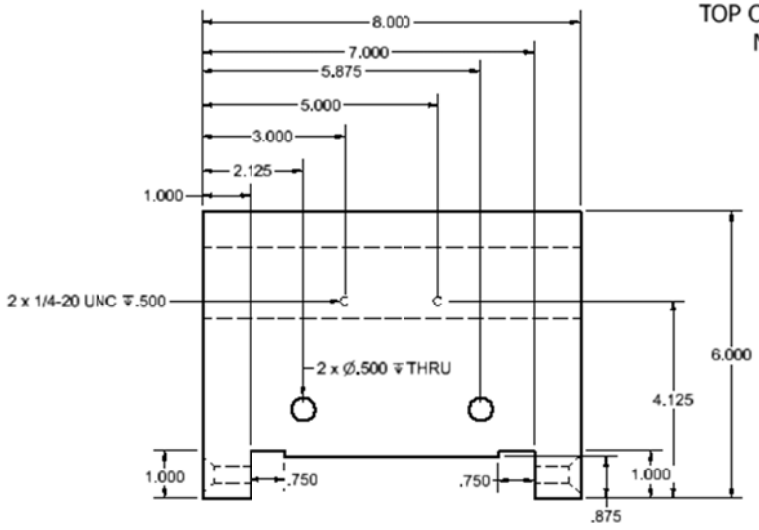

FRONT

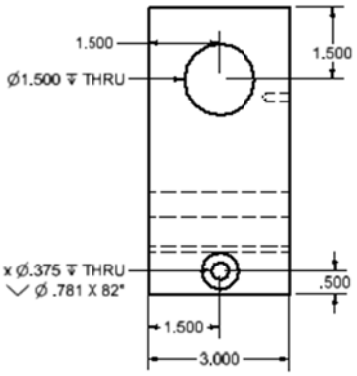

SIDE

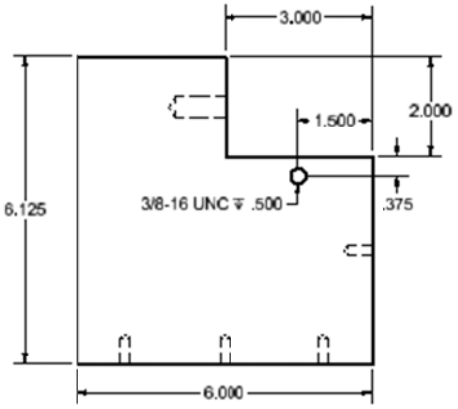

SIDE

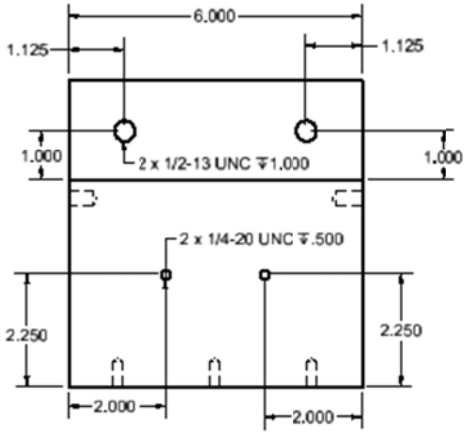

FRONT

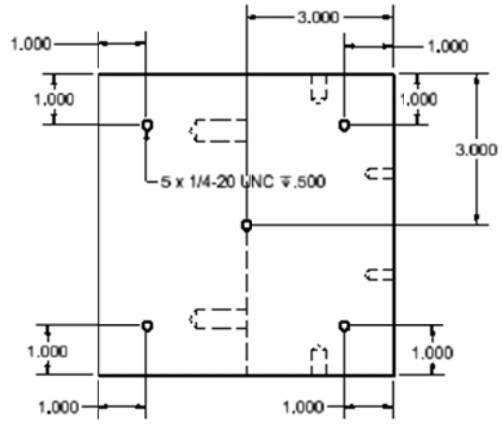

BOTTOM

BOTTOM OF BASE HINGE: COMBINED-INPUT DEVICE
Material: Multipurpose 6061 Aluminum
Quantity: 1
Dimensions: Inches

Plate that bolts to both the base hinge and the aluminum block/brass tubing:

BASE FOR ALUMINUM BLOCK
Material: Multipurpose 6061 Aluminum
Quantity: 2 for each device
Dimensions: Inches

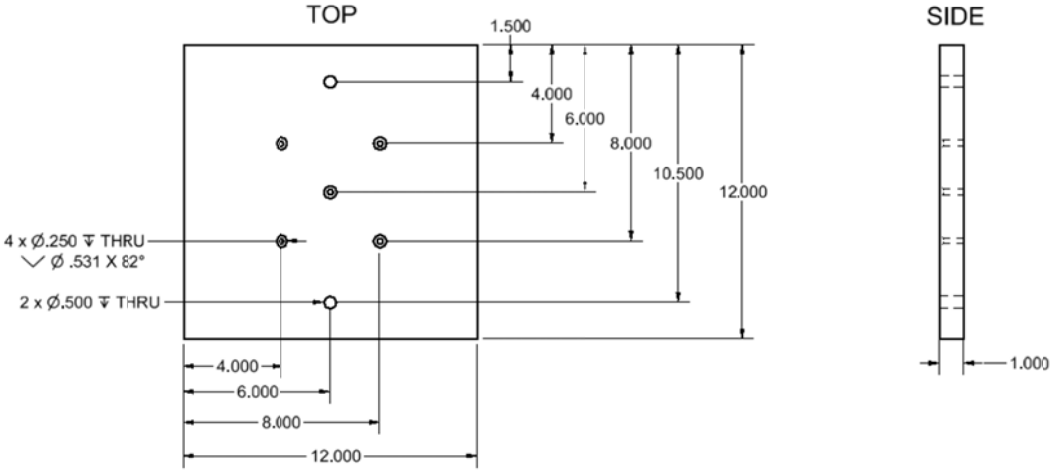

Aluminum block/brass tubing:

ALUMINUM BLOCK: COMBINED-INPUT DEVICE
Material: Multipurpose 6061 Aluminum
Quantity: 1
Dimensions: Inches

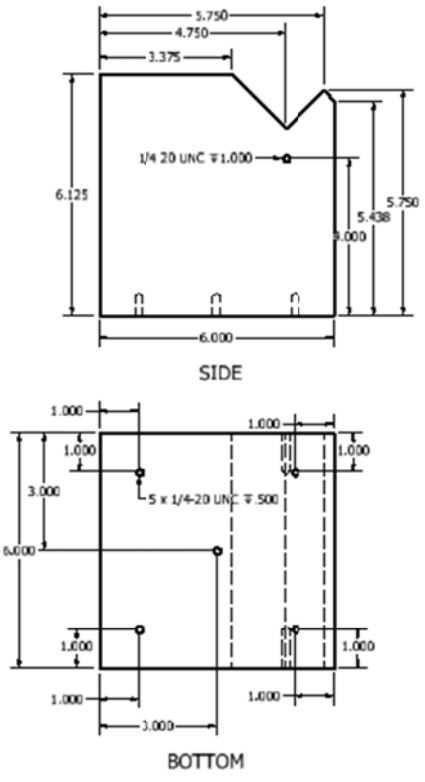

ALUMINUM PLUG FOR ALUMINUM PLATFORMS: COMBINED-INPUT DEVICE
Material: Multipurpose 6061 Aluminum
Quantity: 4
Dimensions: Inches

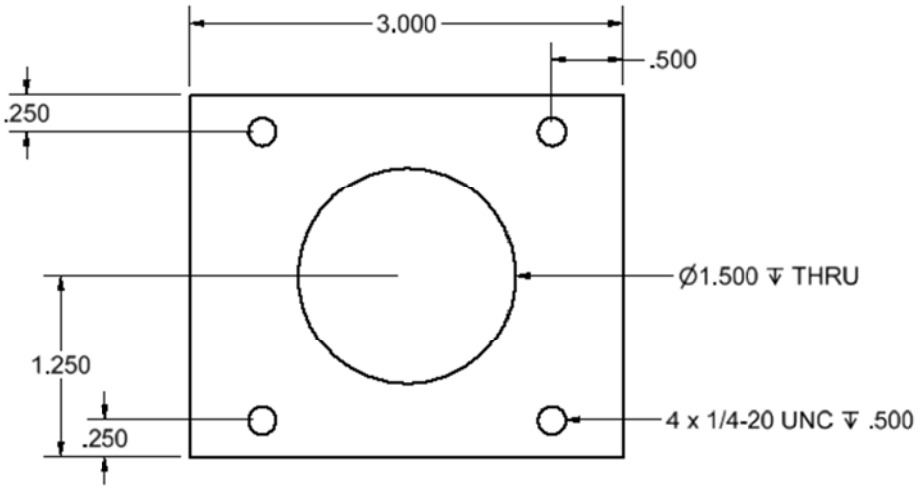

FRONT

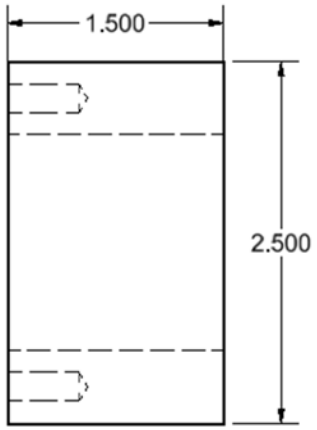

SIDE

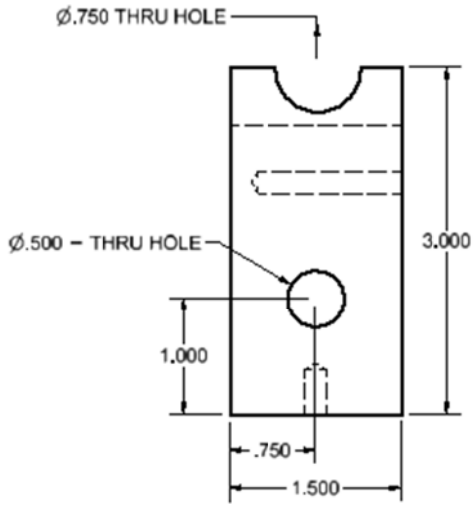

TOP

ALUMINUM BLOCK FOR BOTTOM PLATFORM: COMBINED-INPUT DEVICE
Material: Multipurpose 6061 Aluminum
Quantity: 2
Dimensions: Inches

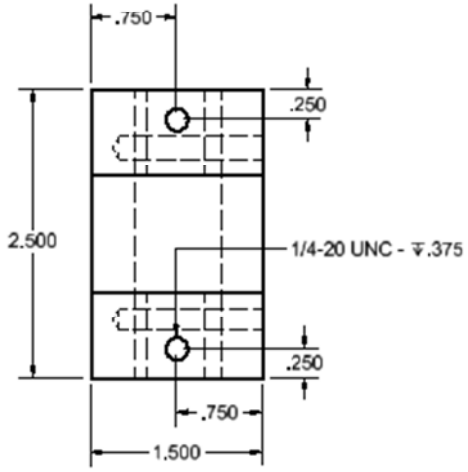

SIDE

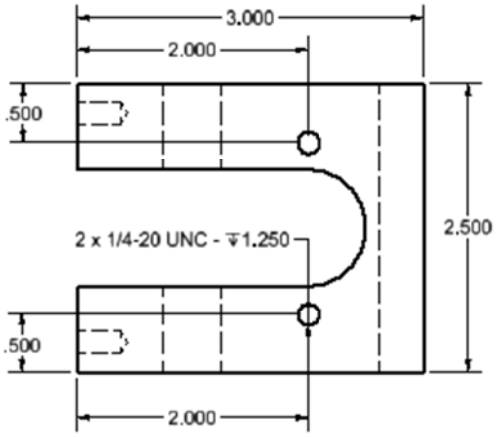

FRONT

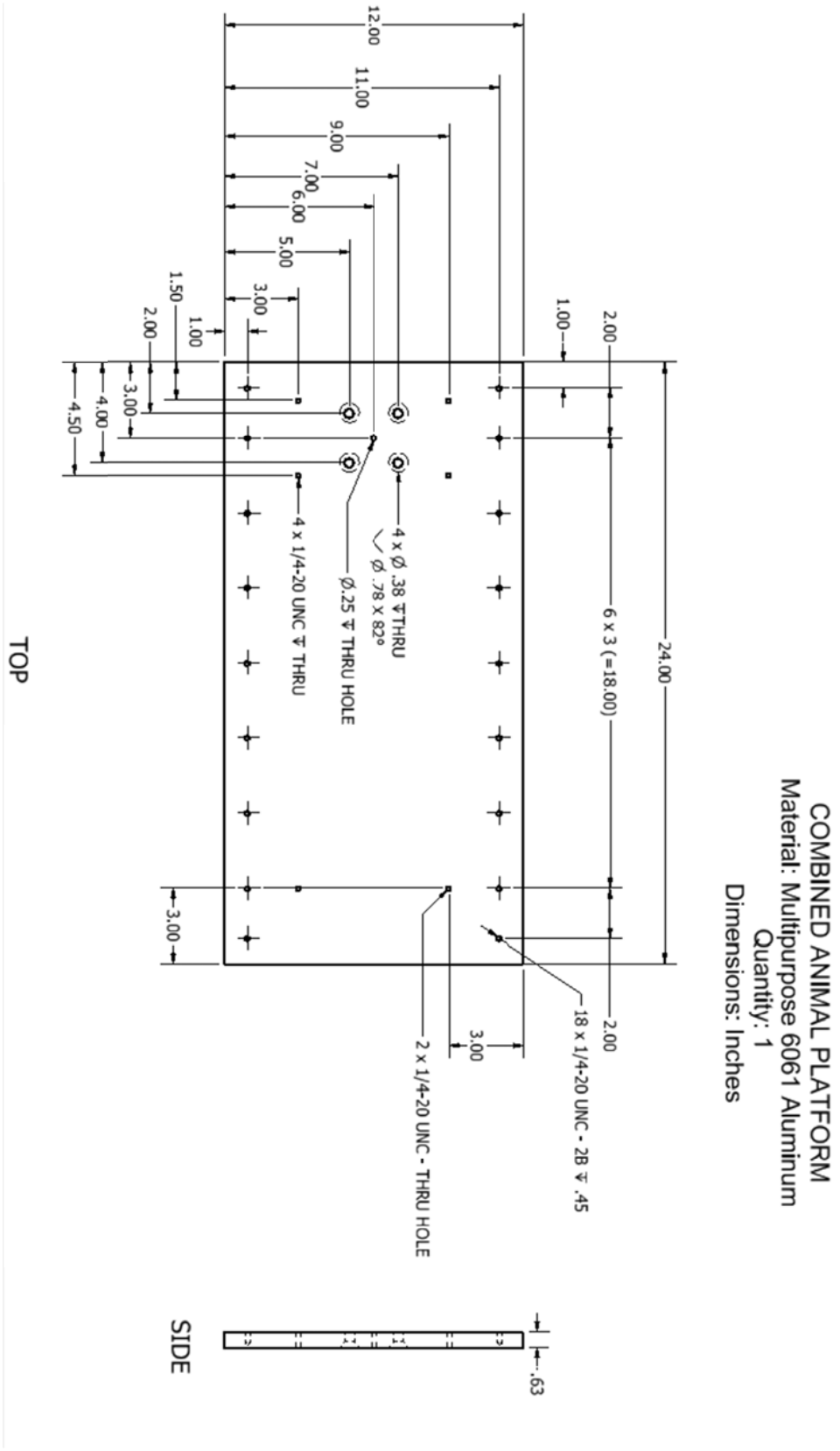

(The base platform is similar, but only has the 18 outer holes)

APPENDIX B: MATERIALS AND DIMENSIONS

Al=aluminum, SS=stainless steel

Dimensions reflect those of device, not purchased part. Some parts were cut to size. * indicates that there is a technical drawing for that part.

TRANSLATION-INPUT INJURY DEVICE

	Name	Material	Dimensions (Inches)	#
Linear Rail Frame	Baseplate	6061 Al	24 x 24 x 1/2	1
	I-beams	6061 Al	3 x 2.5 x 0.35; 60 long	4
	90° angle	6061 Al	3 x 3 x 0.5; 48 long	4
	U-channel	6061 Al	4 x 1.58 x 0.18; 24 long	2
	Threaded rods	316 SS	1/2-13 thread; 36 long	2
	Support Rail	6061 Al	48 long	4
	Hardened precision shaft	1566 steel	1 D; 48 long	4
Steel Support Blocks	Steel blocks	Steel	2 x 8 x 12	8
	Leather sheet	Cow Leather	12 x 12 x 5/64	8
	Vibration damping pad	nitrile	12 x 12 x 1/4	2
	Threaded rods	316 SS	1/2-13 thread; 4@12 long	2
	Delrin®	Delrin®	3 x 12 x 0.5	2
Al block/brass tubing	Block*	6061 Al	6 x 6 x 6	2
	Plate*	6061Al	12 x 12 x 1	2
	Brass tubing	260 Brass	2D, 0.065 thickness	
	Brass tubing	260 Brass	2D, 0.032 thickness	
	Brass tubing	260 Brass	1.5D, 0.032 thickness	
Winch Attachment	U-channel	6061 Al	4 x 1.58 x 0.18; 17 long	2
	U-channel	6061 Al	4 x 1.58 x 0.18; 32 long	1
	Winch with nylon strap			1
Animal Platform	Platform*	6061 Al	12 x 24 x 5/8	1
	Pillow block open bushings	Al with PTFE lining		8
	Al mounts for pillow blocks	6061 Al	12 x 4 x 1/2	4
	Rectangular tube	6061 Al	2 x 3 x 0.25; 36 long	2
	Steel cube	304 SS	3 x 3 x 3	2

COMBINED TRANSLATION AND ROTATION-INPUT INJURY DEVICE

	Name	Material	Dimensions (Inches)	#
Support structure	Steel blocks	Steel	2 x 8 x 12	8
	Leather sheet	Cow Leather	12 x 12 x 5/64	10
	Vibration damping pad	Nitrile	12 x 12 x 1/4	2
	Threaded rods	316 SS	1/2-13 thread; 4@12 long	2
	Steel plate	Steel	12 x 72 x 1/2	
	Heavy duty shock absorber			
Al block/brass tubing	Block*	6061 Al	6 x 6 x 6	2
	Plate*	6061 Al	12 x 12 x 1	1
	Brass tubing	260 Brass	2D, 0.065 thickness	
	Brass tubing	260 Brass	2D, 0.032 thickness	
	Brass tubing	260 Brass	1.5D, 0.032 thickness	
Al Hinges	Middle aluminum hinge*	6061 Al	overall 12 x 5.938 x 3	1
	Steel bolted to middle hinge	304 SS	overall 1 x 1 x 8	1
	Top of Al hinge at base*	6061 Al	overall 6 x 8 x 3	1
	Bottom of Al hinge at base*	6061 Al	6 x 6 x 6	1
	Al plate bolted to base hinge*	6061 Al	12 x 12 x 1	1
	Steel shaft for base platform*	303 SS	overall 1.5 D x 11.75 long	1
	Steel shaft for between platforms*	303 SS	overall 1.5 D x 11.5 long	1
	Bronze sleeves	932 Bronze	for 1.5 D shaft, 2 OD, 4 long	4
Al platforms	Platform*	6061 Al	12 x 24 x 5/8	2
	Rectangular tube for platforms	6061 Al	2 x 3 x 0.25; 2 (animal platform) were 27 long, 2 were 27.5 long (base platform)	4
	Steel cube	304 SS	3 x 3 x 3	1
	Al pieces that fit in rectangular tubes*	6061 Al	3 x 2.5 x 1.5	6
Winch attachment	Al angle	6061 Al	1.5 x 1 x 1/8; 48 long	2
	Al double t-slotted framing	Al alloy	3 x 1.5; one piece 17 long and one 42 long piece	2

APPENDIX C: KINEMATICS TRACES FROM *IN VIVO* TESTS

TRANSLATION-INPUT INJURY DEVICE

Measure kinematics from the *in vivo* tests are plotted below. For animals 1, 3, 10, and 11 there is a 10-ms offset and for animals 4, 8, 9, 12, and 13 there is a 20-ms offset.

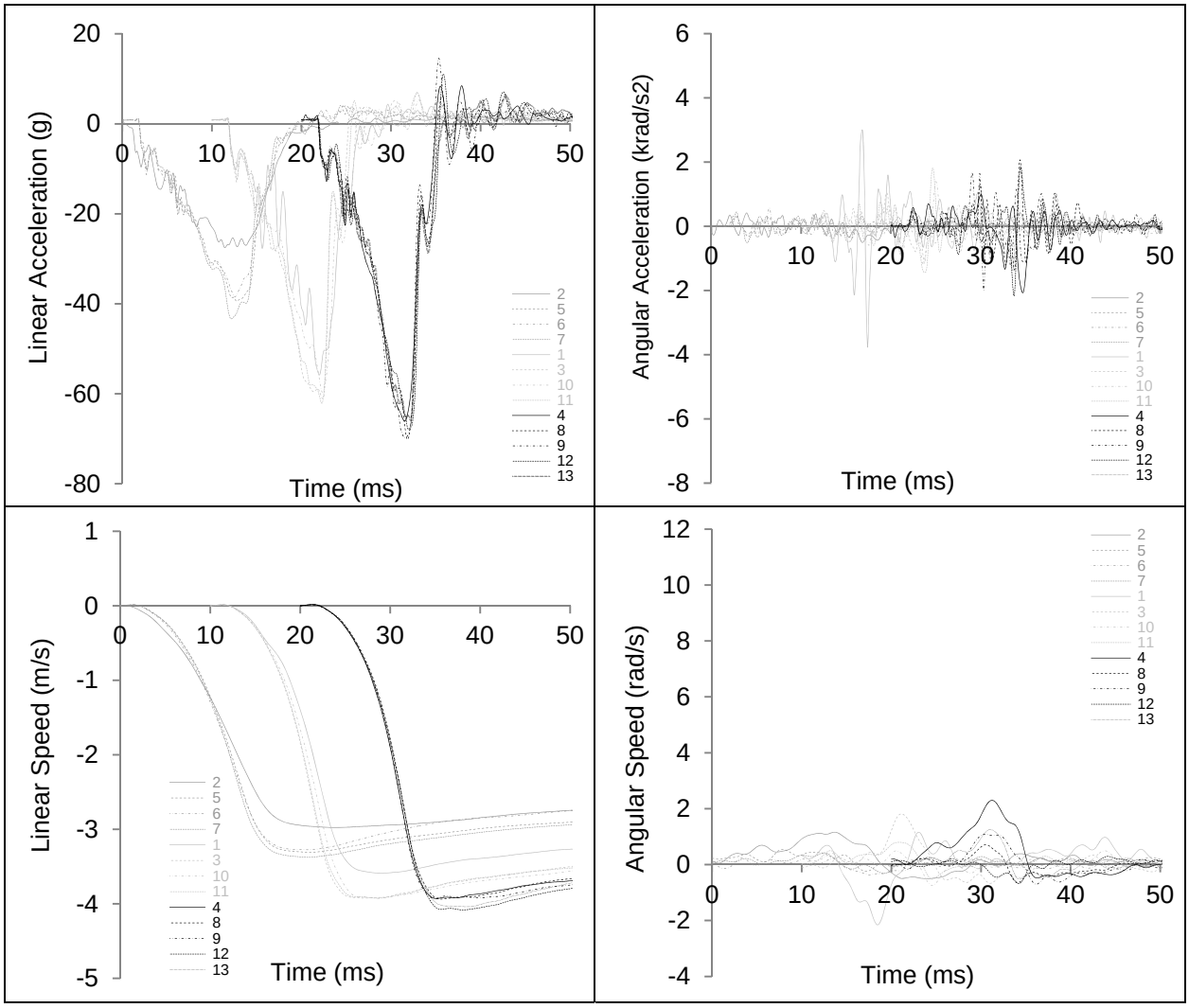

COMBINED-INPUT INJURY DEVICE

Measure kinematics from the *in vivo* tests are plotted below. For animals 5, 7, 8, 11, and 13 there is a 10-ms offset and for animals 2, 3, 4, 6, 9, 14, and 15 there is a 20-ms offset.

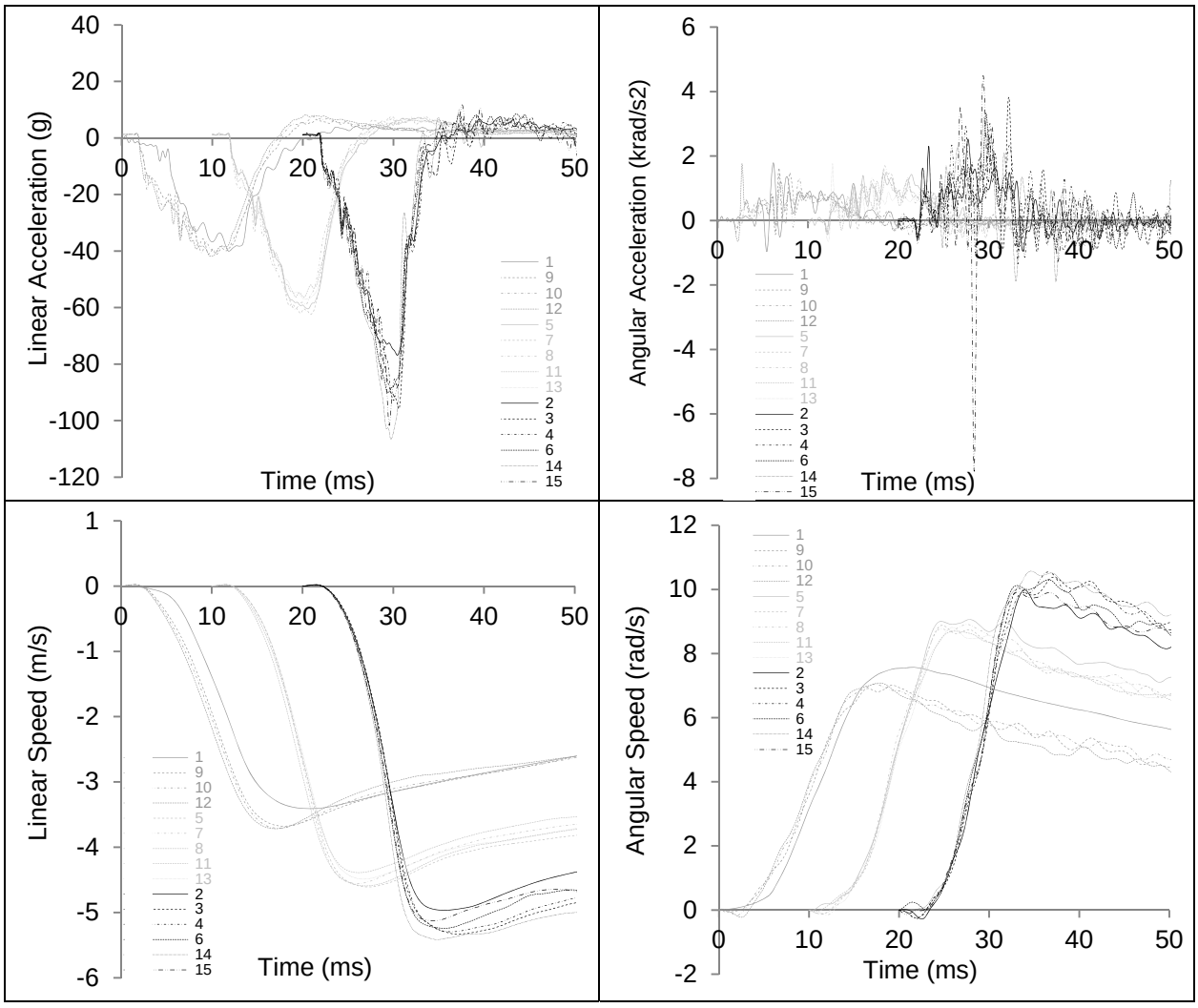

APPENDIX D: RAW DATA FROM *IN VIVO* TESTS

TRANSLATION-INPUT INJURY DEVICE

The italicized values were not included in the analyses and are not part of the mean, SEM, etc. that are described in the tables.

Pig #	Survival Time (h)	Gln								Glu							
		b		1h		24h		72h		b		1h		24h		72h	
		C	CRLB	C	CRLB	C	CRLB	C	CRLB	C	CRLB	C	CRLB	C	CRLB	C	CRLB
1	24	*3.54*	*65*	8.12	18	6.80	15			*1.45*	*140*	9.14	14	10.90	8		
2	24	4.70	22	5.13	18	7.29	14			10.07	9	7.63	11	10.86	8		
3	24	6.31	16	7.24	16					8.61	11	4.66	22				
4	24	7.97	16	7.87	15	6.85	17			9.29	11	10.81	9	10.12	10		
5	24	5.87	17	7.53	14	7.82	18			8.26	10	8.41	11	10.95	11		
6	24	6.26	17	10.42	16	9.58	13			*2.58*	*37*	4.23	34	10.86	10		
7	24	4.67	24	5.97	16	6.94	13			8.26	11	8.31	9	7.04	11		
8	24	4.39	18	3.45	28	5.57	15			9.93	7	8.36	10	9.00	8		
9	24	4.53	26	6.41	21	5.87	22			8.46	12	10.37	11	10.42	10		
10	24	8.51	12	8.65	16	9.29	13			7.33	12	8.80	13	11.25	10		
11	24	5.18	16	4.66	19	5.33	17			9.24	7	7.29	10	8.12	10		
12	72	3.13	40	5.43	20	6.21	17	7.19	16	8.61	13	8.61	11	10.66	9	9.09	11
13	72	4.99	22	6.85	16	7.33	13	5.23	19	7.58	12	8.46	11	9.58	8	8.65	10
	Mean	5.54		6.75		7.07				8.69		8.08		9.98			
	SEM	0.44		0.52		0.38				0.26		0.52		0.38			
	%SEM	0.08		0.08		0.05				0.03		0.06		0.04			
	/Cre	0.69		0.83		0.84				1.09		1.00		1.19			

		Ins								NAA							
Pig	Survival	b		1h		24h		72h		b		1h		24h		72h	
#	Time (h)	C	CRLB	C	CRLB	C	CRLB	C	CRLB	C	CRLB	C	CRLB	C	CRLB	C	CRLB
1	24	15.60	12	11.25	8	11.83	5			*3.31*	*19*	7.24	8	8.12	5		
2	24	10.81	6	9.09	6	11.39	5			8.26	6	7.24	5	8.65	5		
3	24	11.05	6	11.39	6					6.99	6	5.38	8				
4	24	13.15	6	13.84	5	16.43	4			6.75	8	8.26	5	8.12	5		
5	24	11.05	5	10.12	6	14.91	5			7.29	6	8.70	5	*9.34*	*5*		
6	24	10.46	7	12.27	9	4.21	18			*2.68*	*15*	*3.77*	*16*	4.94	9		
7	24	10.81	6	11.98	5	11.20	5			6.94	9	8.17	5	4.87	8		
8	24	10.71	5	9.68	6	9.58	5			7.63	4	8.80	4	8.90	4		
9	24	12.32	6	8.85	9	15.30	5			7.58	6	*7.73*	*7*	8.65	7		
10	24	9.34	6	8.85	9	11.93	7			6.89	5	7.58	7	8.65	5		
11	24	9.19	6	10.32	5	9.73	6			7.38	5	7.87	5	6.94	6		
12	72	9.44	9	10.76	6	10.42	6	12.03	6	8.07	5	8.41	5	9.39	5	9.24	5
13	72	7.92	8	12.66	5	9.14	6	7.63	7	8.56	6	8.85	5	8.65	4	7.77	5
	Mean	10.91		10.85		11.34				7.49		7.86		7.81			
	SEM	0.54		0.43		0.94				0.18		0.30		0.47			
	%SEM	0.05		0.04		0.08				0.02		0.04		0.06			
	/Cre	1.37		1.34		1.35				0.94		0.97		0.93			

Pig #	Survival Time (h)	NAAG								Scyllo							
		b		1h		24h		72h		b		1h		24h		72h	
		C	CRLB	C	CRLB	C	CRLB	C	CRLB	C	CRLB	C	CRLB	C	CRLB	C	CRLB
1	24	2.91	20	2.10	23	2.17	18			*1.76*	*16*	0.74	30	1.35	13		
2	24	1.38	28	1.62	16	1.79	18			0.49	30	0.40	29	0.85	17		
3	24	1.12	31	2.32	16					0.46	31	0.67	21				
4	24	1.62	29	1.64	20	1.21	26			0.78	22	0.82	17	0.75	19		
5	24	1.96	16	1.42	23	*0.27*	*171*			0.66	21	0.82	17	0.56	32		
6	24	1.25	30	*0.00*	*999*	2.70	15			0.59	24	*0.00*	*999*	0.40	38		
7	24	3.10	16	2.04	16	2.36	13			0.65	27	0.50	27	0.76	17		
8	24	1.37	17	2.11	15	1.77	14			0.83	13	0.78	17	0.71	16		
9	24	2.10	18	*0.66*	*75*	1.64	33			0.72	22	0.85	22	1.17	16		
10	24	1.77	17	1.21	39	1.88	19			0.50	26	0.73	24	1.02	16		
11	24	1.39	22	1.20	25	2.47	15			0.41	29	0.51	24	*0.27*	*51*		
12	72	1.28	28	1.16	27	1.48	22	1.67	20	0.79	19	0.80	17	0.89	16	0.77	19
13	72	1.85	23	2.13	17	1.75	16	1.25	26	0.55	28	0.50	31	0.49	26	0.35	37
	Mean	1.78		1.72		1.93				0.62		0.68		0.81			
	SEM	0.17		0.13		0.14				0.04		0.05		0.09			
	%SEM	0.10		0.08		0.07				0.06		0.07		0.11			
	/Cre	0.22		0.21		0.23				0.08		0.08		0.10			

Pig #	Survival Time (h)	GPC+PCh								NAA+NAAG							
		b		1h		24h		72h		b		1h		24h		72h	
		C	CRLB	C	CRLB	C	CRLB	C	CRLB	C	CRLB	C	CRLB	C	CRLB	C	CRLB
1	24	1.90	13	2.91	6	3.45	4			6.21	15	9.34	6	10.27	4		
2	24	2.89	5	2.44	5	3.46	4			9.68	4	8.85	4	10.46	4		
3	24	2.72	5	1.96	8					8.12	6	7.68	6				
4	24	2.80	6	2.68	5	3.48	4			8.36	6	9.88	5	9.34	5		
5	24	2.86	5	2.77	5	3.54	5			9.24	5	10.12	5	9.63	6		
6	24	2.27	6	3.22	7	2.97	5			*3.94*	*12*	*3.77*	*16*	7.63	7		
7	24	3.31	5	2.97	4	2.46	6			10.02	5	10.17	4	7.24	5		
8	24	2.71	4	2.75	4	2.86	4			9.00	4	10.90	4	10.71	3		
9	24	2.96	5	3.23	6	3.78	5			9.68	5	8.36	7	10.32	5		
10	24	3.42	4	3.20	5	4.36	4			8.70	5	8.80	6	10.51	5		
11	24	3.10	3	2.89	4	3.29	4			8.75	4	9.09	4	9.44	4		
12	72	2.64	5	2.52	6	2.97	5	3.21	4	9.34	6	9.58	5	10.86	4	10.90	4
13	72	3.05	5	3.42	4	3.33	4	3.28	4	10.42	5	11.00	4	10.42	4	9.00	4
	Mean	2.82		2.84		3.33				8.96		9.48		9.73			
	SEM	0.11		0.11		0.14				0.32		0.29		0.34			
	%SEM	0.04		0.04		0.04				0.04		0.03		0.04			
	/Cre	0.35		0.35		0.40				1.12		1.17		1.16			

Pig #	Survival Time (h)	Cr+PCr								Glu+Gln							
		b		1h		24h		72h		b		1h		24h		72h	
		C	CRLB	C	CRLB	C	CRLB	C	CRLB	C	CRLB	C	CRLB	C	CRLB	C	CRLB
1	24	11.05	10	8.61	6	8.02	5			*4.99*	*57*	17.26	9	17.70	7		
2	24	8.36	5	6.60	5	8.65	4			14.82	8	12.76	9	18.09	7		
3	24	8.02	5	7.19	6					14.91	8	11.93	11				
4	24	7.87	6	7.92	5	8.61	5			17.26	9	18.73	7	16.92	8		
5	24	7.33	5	8.41	5	10.51	5			14.13	7	15.94	8	18.78	9		
6	24	5.67	7	9.54	7	6.60	6			8.85	14	14.67	14	20.44	8		
7	24	9.44	5	8.21	4	7.92	5			12.96	10	14.28	8	13.98	7		
8	24	7.24	4	7.24	5	7.82	4			14.28	7	11.83	10	14.57	6		
9	24	7.87	6	9.54	5	10.02	5			12.96	11	16.82	9	16.33	10		
10	24	8.51	4	8.70	5	9.54	4			15.84	7	17.46	8	20.49	8		
11	24	7.33	5	7.63	4	7.82	5			14.42	7	11.93	9	13.45	9		
12	72	7.53	6	6.75	6	7.58	5	7.53	6	11.74	13	14.03	9	16.87	7	16.23	7
13	72	7.63	6	9.19	5	7.77	4	7.09	5	12.62	10	15.30	9	16.92	6	13.89	8
	Mean	7.99		8.12		8.41				13.73		14.84		17.04			
	SEM	0.35		0.28		0.32				0.62		0.64		0.66			
	%SEM	0.04		0.03		0.04				0.05		0.04		0.04			
	/Cre	-----		-----		-----				1.72		1.83		2.03			

Pig #	Survival Time (h)	HIP (W)	HIC	Linear Acceleration Magnitude (g)	Linear Acceleration Duration (ms)	Linear Speed (m/s)	LF (%)	HF (%)
1	24	92.59	66.33	55.82	17.5	3.00	25.52	15.38
2	24	46.57	24.60	27.53	23.0	2.86	26.71	20.88
3	24	112.49	95.10	61.09	13.1	3.47	7.13	7.66
4	24	116.70	104.82	66.06	13.1	3.44	14.86	11.13
5	24	62.06	42.66	39.43	19.4	2.75	10.67	2.70
6	24	59.24	40.61	38.42	17.9	2.70	10.97	6.58
7	24	66.70	45.98	43.35	17.5	2.82	9.72	3.35
8	24	119.23	102.99	70.16	13.4	3.42	16.36	5.04
9	24	134.82	113.89	69.82	13.0	3.47	20.53	7.54
10	24	100.23	80.42	59.65	14.2	3.32	11.77	6.21
11	24	109.79	91.02	62.09	13.7	3.35	28.50	5.33
12	72	122.34	104.64	67.90	13.7	3.54		
13	72	119.59	100.65	65.99	14.1	3.43		

COMBINED TRANSLATION AND ROTATION-INPUT INJURY DEVICE

The italicized values were not included in the analyses and are not part of the mean, SEM, etc. that are described in the tables.

		Asp								Gln							
Pig	Survival	b		1h		24h		72h		b		1h		24h		72h	
#	Time (h)	C	CRLB	C	CRLB	C	CRLB	C	CRLB	C	CRLB	C	CRLB	C	CRLB	C	CRLB
1	24	*1.93*	*74*	2.77	46	3.64	32			10.14	23	11.37	18	9.70	14		
2	24	*2.48*	*55*	*1.93*	*60*	*1.90*	*61*			5.42	44	6.68	28	5.60	29		
3	24	*1.96*	*67*	*1.62*	*88*	*0.00*	*999*			*0.00*	*999*	*4.88*	*64*	7.97	19		
4	1	3.30	42	*1.55*	*77*					7.19	29	8.26	18				
5	24																
6	24																
7	24	1.89	47	2.20	46	3.02	38			4.85	26	9.19	16	8.21	16		
8	1	*0.37*	*302*	*1.00*	*133*					7.58	16	6.16	24				
9	1	2.88	45	3.72	36					6.16	27	9.14	19				
10	24	2.26	43	2.57	35	2.83	35			4.76	25	7.14	14	4.84	24		
11	24	3.91	28	2.80	40	2.53	39			4.89	25	4.81	23	5.33	19		
12	24	*2.03*	*51*	2.38	38	*0.66*	*132*			7.87	17	6.85	16	7.58	16		
13	24	2.30	43	2.42	37	3.66	32			6.01	18	5.97	17	6.55	21		
14	72	*1.52*	*55*	*0.96*	*106*	2.60	38	*1.78*	*62*	6.36	14	5.92	21	7.24	15	7.43	15
15	72	*1.21*	*95*	2.25	39	*1.91*	*51*	2.99	38	6.75	19	6.99	13	11.05	21	5.28	23
	Mean	2.76		2.64		3.04				6.50		7.37		7.41			
	SEM	0.31		0.17		0.20				0.45		0.52		0.62			
	%SEM	0.11		0.07		0.07				0.07		0.07		0.08			
	/Cre	0.34		0.32		0.39				0.79		0.88		0.95			

Pig #	Survival Time (h)	Glu								Ins							
		b		1h		24h		72h		b		1h		24h		72h	
		C	CRLB	C	CRLB	C	CRLB	C	CRLB	C	CRLB	C	CRLB	C	CRLB	C	CRLB
1	24	6.00	33	9.99	18	9.92	12			11.95	11	9.49	13	8.25	9		
2	24	7.05	28	8.69	19	10.50	13			6.17	23	12.31	9	8.98	10		
3	24	*5.48*	*45*	*3.82*	*72*	8.21	15			*8.61*	*21*	18.24	11	9.29	9		
4	1	9.88	18	8.75	15					4.61	27	6.11	14				
5	24																
6	24																
7	24	4.20	27	4.62	28	8.95	13			6.94	10	6.36	13	6.80	11		
8	1	9.34	11	7.48	17					13.45	5	*19.36*	*5*				
9	1	10.12	14	11.59	13					10.86	9	10.95	9				
10	24	7.63	13	7.19	12	10.12	10			9.39	7	11.10	5	7.43	9		
11	24	8.95	12	8.85	11	9.00	10			11.05	6	11.25	6	7.09	8		
12	24	8.41	14	8.85	11	8.75	11			8.12	9	8.90	7	7.09	10		
13	24	7.53	13	7.14	12	8.95	13			8.80	7	9.63	6	10.90	7		
14	72	7.82	10	7.82	14	10.02	9	10.61	9	8.85	6	7.38	10	9.00	8	10.37	6
15	72	8.36	14	8.26	9	13.50	15	9.83	11	10.86	7	9.19	6	10.17	13	9.49	7
	Mean	7.94		8.27		9.79				9.25		10.08		8.5			
	SEM	0.48		0.49		0.47				0.73		0.93		0.44			
	%SEM	0.06		0.06		0.05				0.08		0.09		0.05			
	/Cre	0.97		0.99		1.26				1.13		1.21		1.10			

Pig #	Survival Time (h)	NAA								NAAG							
		b		1h		24h		72h		b		1h		24h		72h	
		C	CRLB	C	CRLB	C	CRLB	C	CRLB	C	CRLB	C	CRLB	C	CRLB	C	CRLB
1	24	*0.84*	*170*	6.00	12	7.07	8			*6.51*	*17*	1.69	35	2.22	20		
2	24	4.94	26	7.01	12	5.27	18			3.27	32	1.76	39	2.99	25		
3	24	*4.78*	*32*	*7.77*	*13*	8.51	7			*6.31*	*22*	*1.75*	*53*	1.96	28		
4	1	7.97	14	8.02	7					1.88	48	1.09	46				
5	24																
6	24																
7	24	6.26	8	*6.16*	*9*	*8.51*	*7*			1.09	40	*1.02*	*52*	*0.40*	*157*		
8	1	8.02	6	8.07	7					1.35	30	2.44	23				
9	1	*8.56*	*10*	8.46	8					*0.88*	*80*	1.95	30				
10	24	6.45	10	7.33	6	7.33	6			1.68	32	1.15	29	1.32	28		
11	24	6.75	11	8.46	6	7.77	5			2.69	43	1.64	26	1.55	21		
12	24	5.23	16	7.09	6	5.77	8			3.23	20	1.68	18	1.87	21		
13	24	5.87	8	5.38	7	5.67	14			2.23	17	2.90	11	3.20	20		
14	72	6.45	5	7.38	7	6.70	6	7.82	6	2.05	13	2.51	16	1.68	20	2.12	17
15	72	7.68	9	7.92	4	5.67	13	6.89	12	3.04	19	1.27	20	2.56	25	3.37	19
	Mean	6.56		7.38		6.64				2.25		1.83		2.15			
	SEM	0.34		0.30		0.37				0.25		0.18		0.22			
	%SEM	0.05		0.04		0.06				0.11		0.10		0.10			
	/Cre	0.80		0.88		0.86				0.28		0.22		0.28			

Pig #	Survival Time (h)	Scyllo								Cho (GPC+PCh)							
		b		1h		24h		72h		b		1h		24h		72h	
		C	CRLB	C	CRLB	C	CRLB	C	CRLB	C	CRLB	C	CRLB	C	CRLB	C	CRLB
1	24	*0.39*	*99*	1.16	24	0.82	25			3.68	10	3.12	8	3.22	5		
2	24	*0.48*	*80*	0.65	43	1.11	25			3.04	11	2.51	10	3.46	7		
3	24	*0.00*	*999*	1.71	23	0.86	27			*3.79*	*10*	3.02	12	3.42	6		
4	1	*0.19*	*129*	0.58	33					3.43	9	3.19	6				
5	24																
6	24																
7	24	0.51	29	*0.29*	*60*	0.65	28			2.37	6	2.33	8	2.97	6		
8	1	1.02	16	1.50	14					3.55	4	2.52	8				
9	1	0.45	48	0.59	37					3.46	7	3.71	6				
10	24	0.36	45	0.41	33	*0.05*	*319*			2.56	7	2.46	5	2.87	5		
11	24	0.62	30	0.66	25	0.65	21			3.25	6	3.28	5	3.11	4		
12	24	*0.25*	*71*	0.61	22	0.38	37			2.37	9	2.30	6	1.99	7		
13	24	*0.15*	*103*	0.30	44	*0.04*	*522*			2.89	5	2.39	5	3.28	7		
14	72	0.70	17	0.65	24	0.70	21	0.43	37	2.35	5	2.50	7	3.06	5	3.26	4
15	72	*0.33*	*57*	0.50	23	*0.21*	*88*	0.46	43	2.87	6	2.51	4	2.33	11	3.44	5
	Mean	0.61		0.78		0.74				2.98		2.76		2.97			
	SEM	0.10		0.13		0.08				0.14		0.12		0.15			
	%SEM	0.16		0.16		0.12				0.05		0.05		0.05			
	/Cre	0.07		0.09		0.10				0.36		0.33		0.38			

Pig #	Survival Time (h)	NAA+NAAG								Cre (Cr+PCr)							
		b		1h		24h		72h		b		1h		24h		72h	
		C	CRLB	C	CRLB	C	CRLB	C	CRLB	C	CRLB	C	CRLB	C	CRLB	C	CRLB
1	24	7.39	15	7.68	11	9.27	6			9.49	12	9.27	7	8.47	6		
2	24	8.18	12	8.76	9	8.25	8			9.27	11	8.62	8	8.33	9		
3	24	*11.10*	*11*	9.54	14	10.46	6			*6.99*	*14*	9.34	10	9.63	6		
4	1	9.83	9	9.09	7					11.54	8	8.41	6				
5	24																
6	24																
7	24	7.33	8	7.14	9	8.90	7			4.94	8	7.58	8	8.07	6		
8	1	9.39	5	10.51	6					8.36	5	9.63	5				
9	1	9.44	8	10.42	7					9.24	7	10.37	6				
10	24	8.12	6	8.51	5	8.65	6			6.50	8	6.75	6	7.14	6		
11	24	9.44	6	10.12	5	9.34	5			8.36	6	9.88	5	7.14	5		
12	24	8.46	7	8.80	5	7.63	7			7.68	8	6.60	6	6.45	7		
13	24	8.12	6	8.31	5	8.90	7			7.14	6	6.85	5	6.80	9		
14	72	8.51	5	9.88	5	8.36	6	9.93	5	6.70	5	7.29	7	6.75	6	7.38	5
15	72	10.71	5	9.19	4	8.26	11	10.27	5	8.95	6	8.12	4	8.80	8	9.44	6
	Mean	8.74		9.07		8.80				8.18		8.36		7.76			
	SEM	0.29		0.28		0.25				0.50		0.35		0.33			
	%SEM	0.03		0.03		0.03				0.06		0.04		0.04			
	/Cre	1.07		1.09		1.13				-----		-----		-----			

Pig #	Survival Time (h)	Glu+Gln							
		b		1h		24h		72h	
		C	CRLB	C	CRLB	C	CRLB	C	CRLB
1	24	16.15	14	21.36	10	19.62	7		
2	24	12.45	21	15.35	12	16.08	10		
3	24	*5.48*	*45*	8.70	43	16.19	11		
4	1	17.07	13	16.97	9				
5	24								
6	24								
7	24	9.05	15	13.84	12	17.16	9		
8	1	16.92	8	13.64	14				
9	1	16.23	11	20.78	8				
10	24	12.37	10	14.33	8	14.96	8		
11	24	13.84	10	13.69	9	14.33	8		
12	24	16.28	9	15.70	7	16.28	8		
13	24	13.54	9	13.10	9	15.50	10		
14	72	14.18	7	13.74	10	17.31	8	18.04	8
15	72	15.11	9	15.21	6	*24.55*	*9*	15.06	9
	Mean	14.43		15.11		16.38			
	SEM	0.68		0.91		0.52			
	%SEM	0.05		0.06		0.03			
	/Cre	1.76		1.81		2.11			

Pig #	Survival Time (h)	HIP (W)	BrIC	HIC	Linear Acceleration		Linear Speed (m/s)	Angular Acceleration (rad/s^2)	Angular Speed		LF (%)	HF (%)
					Magnitude (g)	Duration (ms)			Magnitude (rad/s)	Duration (ms)		
1	24	88.16	0.05	50.27	40.08	19.9	2.63	1783.75	7.61	145.0	4.24	1.82
2	24	212.55	0.06	189.71	76.87	13.9	4.32	2524.03	10.28	122.2	13.93	0.19
3	24	213.05	0.07	229.71	95.86	13.6	4.19	3814.87	10.79	124.7	18.87	30.77
4	1	210.54	0.07	218.93	90.48	13.7	4.11	3005.65	10.81	106.4		
5	24	136.98	0.06	128.22	60.45	16.2	3.56	1443.10	9.11	105.0	6.01	13.41
6	24	239.53	0.06	237.74	90.07	13.2	4.37	3324.86	10.46	111.6	16.51	20.13
7	24	153.07	0.06	135.61	62.41	14.6	3.67	1584.35	9.00	113.8	24.71	32.44
8	1	139.18	0.06	124.71	60.61	14.8	3.54	1699.72	9.12	112.6		
9	1	83.46	0.04	57.75	41.24	16.2	2.75	1630.77	7.27	143.3		
10	24	86.76	0.04	59.28	40.59	16.0	2.80	1474.83	7.20	133.5	14.22	22.96
11	24	134.35	0.05	111.53	56.39	14.5	3.50	2134.64	8.74	115.5	18.18	28.99
12	24	86.87	0.05	61.56	41.85	15.7	2.80	1760.46	7.39	146.0	18.83	19.61
13	24	136.67	0.05	119.01	57.08	15.2	3.54	1014.53	8.98	120.4	8.14	22.62
14	72	222.49	0.07	286.67	106.50	12.7	4.17	3180.91	10.63	116.1		
15	72	209.56	0.06	228.82	101.64	13.4	4.13	4492.64	10.16	116.8		

APPENDIX E: ERROR ESTIMATES FROM INTEGRATION

Error estimates from integrating linear acceleration to obtain linear speed are calculated below. Transducer drift over 15 ms (approximate duration of the impact) and 50 ms (approximate duration of the pulse shown in the plots) of baseline data were calculated. The data are presented from each test and were calculated as a percentage of the peak linear speed (before filtering).

TRANSLATION-INPUT INJURY DEVICE

Pig #	Survival Time (h)	Peak Linear Speed (m/s)	15 ms (m/s)	15 ms % peak	50 ms (m/s)	50 ms % peak
1	24	3.00	9.04E-05	3.01E-05	1.19E-03	3.95E-04
2	24	2.87	3.71E-04	1.29E-04	-2.90E-04	-1.01E-04
3	24	3.47	2.51E-03	7.24E-04	7.12E-03	2.05E-03
4	24	3.44	7.87E-04	2.29E-04	3.52E-03	1.02E-03
5	24	2.75	-5.76E-04	-2.10E-04	-1.16E-03	-4.20E-04
6	24	2.70	-5.21E-04	-1.93E-04	-1.49E-03	-5.54E-04
7	24	2.82	1.19E-03	4.21E-04	2.24E-03	7.92E-04
8	24	3.42	-4.58E-04	-1.34E-04	-2.37E-03	-6.92E-04
9	24	3.47	2.11E-04	6.10E-05	-1.94E-03	-5.61E-04
10	24	3.32	-8.28E-04	-2.50E-04	-1.26E-03	-3.79E-04
11	24	3.36	-2.98E-04	-8.89E-05	-1.54E-03	-4.58E-04
12	72	3.53	-7.03E-05	-1.99E-05	1.02E-03	2.88E-04
13	72	3.43	-1.62E-04	-4.71E-05	5.45E-04	1.59E-04
Average		3.20	1.73E-04	5.02E-05	4.28E-04	1.18E-04
Standard Deviation		0.32	9.02E-04	2.76E-04	2.67E-03	7.95E-04

COMBINED TRANSLATION AND ROTATION-INPUT INJURY DEVICE

Pig	Survival	Peak Linear Speed	15 ms		50 ms	
#	Time (h)	(m/s)	(m/s)	% peak	(m/s)	% peak
1	24	2.64	-2.76E-03	-1.05E-03	-2.08E-02	-7.90E-03
2	24	4.32	1.27E-02	2.94E-03	3.73E-02	8.64E-03
3	24	4.20	2.21E-03	5.26E-04	6.87E-03	1.64E-03
4	1	2.80	1.72E-04	6.15E-05	2.18E-03	7.77E-04
5	24	3.54	-3.76E-05	-1.06E-05	-2.01E-03	-5.68E-04
6	24	4.11	3.50E-04	8.50E-05	1.43E-03	3.49E-04
7	24	3.57	1.50E-03	4.20E-04	-3.50E-03	-9.81E-04
8	1	4.37	2.52E-03	5.76E-04	3.00E-03	6.87E-04
9	1	3.67	7.42E-04	2.02E-04	2.67E-03	7.27E-04
10	24	3.54	-1.58E-03	-4.46E-04	-3.83E-03	-1.08E-03
11	24	2.75	-7.40E-04	-2.69E-04	-2.67E-03	-9.71E-04
12	24	2.80	1.30E-03	4.66E-04	5.40E-03	1.93E-03
13	24	3.50	2.16E-05	6.17E-06	-8.56E-04	-2.45E-04
14	72	4.17	-1.72E-04	-4.12E-05	-2.05E-03	-4.92E-04
15	72	4.13	4.18E-04	1.01E-04	7.72E-04	1.87E-04
Average		3.61	1.11E-03	2.38E-04	1.59E-03	1.79E-04
Standard Deviation		0.61	3.48E-03	8.54E-04	1.17E-02	3.26E-03

APPENDIX F: COPYRIGHT PERMISSION

ELSEVIER LICENSE
TERMS AND CONDITIONS

Oct 27, 2015

This is a License Agreement between Elizabeth M Fievisohn ("You") and Elsevier ("Elsevier") provided by Copyright Clearance Center ("CCC"). The license consists of your order details, the terms and conditions provided by Elsevier, and the payment terms and conditions.

All payments must be made in full to CCC. For payment instructions, please see information listed at the bottom of this form.

Supplier	Elsevier Limited The Boulevard,Langford Lane Kidlington,Oxford,OX5 1GB,UK
Registered Company Number	1982084
Customer name	Elizabeth M Fievisohn
Customer address	Center for Injury Biomechanics Blacksburg, VA 24061
License number	3737021165905
License date	Oct 27, 2015
Licensed content publisher	Elsevier
Licensed content publication	Trends in Pharmacological Sciences
Licensed content title	The neurotransmitter N-acetylaspartylglutamate in models of pain, ALS, diabetic neuropathy, CNS injury and schizophrenia
Licensed content author	Joseph H. Neale,Rafal T. Olszewski,Laura M. Gehl,Barbara Wroblewska,Tomasz Bzdega
Licensed content date	September 2005
Licensed content volume number	26
Licensed content issue number	9
Number of pages	8
Start Page	477
End Page	484
Type of Use	reuse in a thesis/dissertation
Portion	figures/tables/illustrations
Number of figures/tables/illustrations	1
Format	both print and electronic
Are you the author of this Elsevier article?	No
Will you be translating?	No

Original figure numbers	figure 1
Title of your thesis/dissertation	TRAUMATIC BRAIN INJURY MECHANISMS IN THE GÖTTINGEN MINIPIG IN RESPONSE TO TWO UNIQUE INPUT MODES
Expected completion date	Oct 2015
Estimated size (number of pages)	140
Elsevier VAT number	GB 494 6272 12
Permissions price	0.00 USD
VAT/Local Sales Tax	0.00 USD / 0.00 GBP
Total	0.00 USD
Terms and Conditions	

INTRODUCTION

1. The publisher for this copyrighted material is Elsevier. By clicking "accept" in connection with completing this licensing transaction, you agree that the following terms and conditions apply to this transaction (along with the Billing and Payment terms and conditions established by Copyright Clearance Center, Inc. ("CCC"), at the time that you opened your Rightslink account and that are available at any time at http://myaccount.copyright.com).

GENERAL TERMS

2. Elsevier hereby grants you permission to reproduce the aforementioned material subject to the terms and conditions indicated.
3. Acknowledgement: If any part of the material to be used (for example, figures) has appeared in our publication with credit or acknowledgement to another source, permission must also be sought from that source. If such permission is not obtained then that material may not be included in your publication/copies. Suitable acknowledgement to the source must be made, either as a footnote or in a reference list at the end of your publication, as follows:
"Reprinted from Publication title, Vol /edition number, Author(s), Title of article / title of chapter, Pages No., Copyright (Year), with permission from Elsevier [OR APPLICABLE SOCIETY COPYRIGHT OWNER]." Also Lancet special credit - "Reprinted from The Lancet, Vol. number, Author(s), Title of article, Pages No., Copyright (Year), with permission from Elsevier."
4. Reproduction of this material is confined to the purpose and/or media for which permission is hereby given.
5. Altering/Modifying Material: Not Permitted. However figures and illustrations may be altered/adapted minimally to serve your work. Any other abbreviations, additions, deletions and/or any other alterations shall be made only with prior written authorization of Elsevier Ltd. (Please contact Elsevier at permissions@elsevier.com)
6. If the permission fee for the requested use of our material is waived in this instance, please be advised that your future requests for Elsevier materials may attract a fee.
7. Reservation of Rights: Publisher reserves all rights not specifically granted in the combination of (i) the license details provided by you and accepted in the course of this licensing transaction, (ii) these terms and conditions and (iii) CCC's Billing and Payment terms and conditions.
8. License Contingent Upon Payment: While you may exercise the rights licensed immediately upon issuance of the license at the end of the licensing process for the transaction, provided that you have disclosed complete and accurate details of your proposed use, no license is finally effective unless and until full payment is received from you (either